LOCATIONS AND TRAFFICKING OF GLUTAMATE RECEPTORS

by

Shuo Li

A dissertation submitted to Johns Hopkins University in conformity with the requirements for the degree of Doctor of Philosophy

Baltimore, Maryland

April 2021

Abstract

Neurotransmission occurs at the specialized structure termed the synapse, which consists of the pre-synapse, synaptic cleft, and the post-synapse. Within the presynaptic terminal, there are many synaptic vesicles filled with neurotransmitters. When an action potential reaches the presynaptic terminal, calcium influx via activated voltage-gated calcium channels leads to synaptic vesicle fusion with the presynaptic membrane. Released neurotransmitters diffuse across a synaptic cleft and bind to neurotransmitter receptors that reside on the postsynaptic membrane, resulting in activation of receptors and eventual signal transduction.

To ensure efficient neurotransmission between neurons, the pre-and postsynaptic compartments must align structurally and coordinate functionally. In the mammalian central nervous system, ionotropic glutamate receptors, α-amino-3-hydroxy-5-methyl-4-isoxazoleproionic acid (AMPA) receptors and N-methyl-D-aspartate (NMDA) receptors are two major types of glutamate receptors. AMPA receptors mediate the majority of fast excitatory neurotransmission. The trans-synaptic alignment between neurotransmitter release sites and receptors is one of the important determinants in the activation of receptors and therefore the efficacy of neurotransmission. Our recent study indicates that release sites are segregated within an active zone, with synchronous release uniformly distributed and asynchronous release sites enriched near the center of an active zone. Moreover, synchronous and asynchronous release sites are aligned with AMPA receptor and NMDA receptor clusters, respectively. Computational simulations indicate that this trans-synaptic organization of release sites and AMPA receptors and NMDA receptors are likely to contribute to better activation of NMDA receptors.

In addition to the trans-synaptic alignment, the number of AMPA receptors also plays an important role in determining the strength of neurotransmission. Currently, clathrin-mediated

endocytosis at postsynaptic terminals is thought to be the major pathway in regulating the number of the glutamate receptors, especially AMPA receptors. Endocytosis typically occurs at a specific region termed the endocytic zone (EZ) adjacent to the postsynaptic density (PSD). However, in our present study, we identified a clathrin-independent endocytosis that occurs directly within the PSD on a millisecond time scale. To further understand this novel endocytic pathway, we have to investigate how this pathway is triggered, what cargos are internalized, and what proteins mediate this pathway in future.

Advisor:

Dr. Shigeki Watanabe

Primary Readers:

Dr. Shigeki Watanabe, Dr. Michael J. Matunis, Dr. Alan L. Scott, Dr. Jiou Wang

Secondary Readers:

Dr. Paul Worley, Dr. Philip Jordan

Acknowledgements

I would like to thank my mentor Dr. Shigeki Watanabe for all the guidance, help, and support that he provided in the past four years. Without his efforts, this thesis would not have been possible. I have learned a lot from him both in science and in daily life. The most valuable lesson I learned from him is always being positive and never give up. It will have a far-reaching influence in every aspects of my life.

I would like to thank all the members of the Watanabe lab: Dr. Sumana Raychaudhuri, Dr. Kie Itoh, Dr. Alfred Gan, Dr.Yuuta Imoto, Dr. Sebastian Markert, Grant Kusick, Tyler Ogunmowo, Chelsy Eddings, Brady Goulden, Jackie Griswold, Sarah Syed, and all other undergraduates. It is wonderful to work with you guys in the lab.

I would also like to thank all the staff working in the Microscopy facility, Michael Delannoy, Dr. LaToya Roker, Barbara Smith, Dr. Hoku West-Foyle, and Loza Lee. Without your help, none of the experiments in the thesis could have been done.

I appreciate the knowledge and insights provided by members of my thesis committee: Dr. Paul F. Worley, Dr. Douglas N. Robinson, Dr. Michael J. Matunis, and Dr. Scot Kuo.

I would like to thank my friends Dr. Tianlu Ma, Dr. Emmanuel Datan, and Samantha Tienda for their friendship and moral support.

I would like to thank my father Weiming Li and my mother Xiujuan Kang. Thank you for the support, care, understanding, and unconditional love. I would like to thank my cousin Wei Wang. As my only family member in the United States, you help me throughout the hardships and made my life abroad less lonely. I would also like to thank my grandmother who raised me up. It is very sad that you cannot see me finish my Ph.D. training and open a new chapter of my life. But I will never forget the love you gave me in my life. I would like to thank all other family members for their love and support.

Finally, I would like to thank my cat, Euler Li. Thank you for waiting for me in front of the door every late night. Thank you for the joy and happiness you bring to my life. Thank you for loving me all the time. I love you more than ever – you mean the world to me. This dissertation is for all we shared together.

Table of Contents

List of tables

List of figures

List of abbreviations

AMPA	α-amino-3-hydroxy-5-methyl-4-isoxazole propionic acid
ATD	amino-terminal domain
BDMA	benzyl dimethylamine
CAMKII	calcium/calmodulin-dependent protein kinase II
CLEM	correlative light and electron microscopy
CNS	central nervous system
CPG2	candidate plasticity gene 2
CTD	carboxyl-terminal domain
DDSA	dodecenyl succinic anhydride
Dlg1	Drosophila disc large tumor suppressor
ER	endoplasmic reticulum
ERES	endoplasmic reticulum exit sites
GIPC	GAIP-interacting protein, C terminus
GPCR	G-protein coupled receptor
GRIP1	glutamate receptor interacting protein
HFS	high frequency stimulation
iGluR	ionotropic glutamate receptor
LBD	ligand-binding domain
LFS	low frequency stimulation
LRRTM2	Leucine-rich-repeat transmembrane protein 2
MAGUK	membrane-associated guanylate kinase
mGluR	metabotropic glutamate receptor
mPin	mammalian homologue of *Drosophila melanogaster* partner of inscuteable
NTD	N-terminal domain
NMDA	N-methyl-D-aspartate
PDZ	PSD95/Dlg1/zo-1
PICK1	protein interacting with C kinase-1
PKA	protein kinase A
PKC	protein kinase C

PNS	periphery nervous system
PP1	protein phosphatase I
PSD	postsynaptic density
SAP97	synapse-associated protein 97
SAP102	synapse-associated protein 102
STORM	stochastic optical reconstruction microscopy
TARP	transmembrane AMPA receptor regulatory protein
TBS	theta-burst stimulation
TEM	transmission electron microscopy
TMD	transmembrane domain
TGN	trans-Golgi network
VGCC	voltage-gated calcium channel
ZO1	zonula occludens-1

Chapter 1

Introduction

Synaptic transmission

Chemically-mediated synaptic transmission involves a series of processes: fusion of synaptic vesicles with the presynaptic membrane after an action potential, release of neurotransmitter to the synaptic cleft, and activation of receptors upon neurotransmitter binding(Purves et al. 2001). When the presynaptic neuron is stimulated and depolarized sufficiently, it fires an action potential that propagates along the axon into the presynaptic terminals (Hodgkin and Huxley 1939). Depolarization leads to the opening of voltage-gated Ca^{2+} channels (VGCC) at the presynaptic terminals, allowing influx of Ca^{2+} into the terminal (Catterall 2011). In response to Ca^{2+} entry, synaptic vesicles fuse with the presynaptic membrane and release their content-neurotransmitters into the synaptic cleft (Südhof 2013). The diffused neurotransmitters interact with receptors, which are often ligand-gated ion channels, on the postsynaptic membrane, resulting in the opening of the receptors (Purves et al. 2001). The ions flow into and out of the postsynaptic neurons, further propagating the signal. Although the detailed process varies, the general sequence of synaptic transmission is conserved throughout the central nervous system (CNS) and peripheral nervous system (PNS) in a variety of organisms ranging from nematodes to humans.

Ionotropic glutamate receptors

Glutamate receptors mediate the majority of excitatory neurotransmission in the mammalian CNS (Traynelis et al. 2010). They can be divided into two distinct classes based on their structures: metabotropic and ionotropic glutamate receptors (Traynelis et al. 2010). Metabotropic glutamate receptors (mGluRs) are G-protein coupled receptors (GPCRs) that

mediate slow modulatory signaling by initiating signaling cascades (Niswender and Conn 2010). Ionotropic glutamate receptors (iGluRs) are ligand-gated ion channels that mediate the majority of fast excitatory synaptic transmission (Dingledine et al. 1999a). Since the first glutamate receptor gene *Gria1* was cloned in 1989 (Michael Hollmann et al. 1989), more than 16 mammalian genes encoding ionotropic glutamate receptors have been identified (Traynelis et al. 2010). These genes encode four subtypes of ionotropic glutamate receptors: amino-3-hydroxy-5-methyl-4-isoxazole propionic acid (AMPA) receptors, N-methyl-D-Aspartate (NMDA) receptors, kainate receptors, and delta receptors(Traynelis et al. 2010). Compared with other three subtypes of ionotropic glutamate receptors, the delta receptors do not bind glutamate nor exhibit typical agonist-induced ion channel activity. Therefore, they are classified as ionotropic receptors based solely on sequence homology (Orth, Tapken, and Hollmann 2013). In this thesis, I will focus on the AMPA- and NMDA-type receptors.

AMPA receptors are widespread throughout the CNS and serve as the workhorse for fast excitatory synaptic transmission (Traynelis et al. 2010). AMPA receptors can assemble as homotetramers or heterotetramers with different combinations of four types of subunits. GluA1-GluA4, encoded by four individual AMPA receptor subunit genes in a single family: *Gria1, Gria2, Gria3,* and *Gria4*. Each of the AMPA receptor subunit contains four discrete domains: the extracellular amino-terminal domain (ATD), the extracellular ligand-binding domain (LBD), the transmembrane domain (TMD), and an intracellular carboxyl-terminal domain (CTD). The LBD and the TMD of different subunits are highly conserved, while the ATD and the CTD are divergent and subject to posttranslational modifications.

The four subunits of AMPA receptor are differentially expressed in different brain regions. GluA1, GluA2, and GluA3 are enriched in the hippocampus, the outer layer of the cortex, the basal ganglia, the olfactory regions, the lateral septum, and the amygdala of the CNS, whereas GluA4 is highly expressed in the cerebellum, thalamus, and brain stem (Yadav et al. 2017). All four subunit genes are alternatively spliced into mRNA isoforms called “flip” and

"flop" that are encoded by exons 14 and 15 (Sommer et al. 1991). These flip/flop variants of an AMPA receptor subunit have been reported to have different kinetic properties (Pei et al. 2009). For example, the flop variants of GluA2-A4 desensitize faster than the flip counterparts, while the flip/flop isoforms of GluA1 desensitize at the same rate (Pei et al. 2009). In addition to alternative splicing, GluA2 to GluA4 can undergo RNA editing at the R/G site in the S2 domain of the receptor (Lomeli et al. 1994), however, only the GluA2 subunit undergoes additional RNA editing at the Q607/R site in the re-entrant M2 membrane loop (Sommer et al. 1991). Receptors containing edited GluA2(R) is Ca^{2+} impermeable (M. Hollmann, Hartley, and Heinemann 1991) and display a linear current-voltage curve (Bowie and Mayer 1995).

NMDA receptors are assembled as heterotetramers, with seven different possible subunits (GluN1, etc.), encoded by seven genes: *Grin1, Grin2a, Grin2b, Grin2c, Grin2d, Grin3a,* and *Grin3b*, falling into three subfamilies. Like AMPA receptor subunits, all GluN subunits are made up by four distinct modular domains: the ATD, the LBD, the TMD and the CTD. Functional NMDA receptors typically associate GluN1 subunits with GluN2 subunits or a mixture of GluN2 and GluN3 subunits (Traynelis et al. 2010). *Grin1* has eight different splicing variants.

Biogenesis and Trafficking of AMPA receptors and NMDA receptors

Processing of AMPA receptors in the ER

Like other multimeric membrane proteins, AMPA receptor subunit polypeptides are inserted into the endoplasmic reticulum (ER), interacting with chaperone proteins for secondary folding and tertiary assembly (Hebert and Molinari 2007). Two well-characterized chaperones, Bip and calnexin, have been reported to be involve in the early processing of AMPA receptor in the ER (M. E. Rubio and Wenthold 1999). Bip and calnexin bind to GluA2 subunit to maintain the pool of immature GluA2 in the ER (M. E. Rubio and Wenthold 1999) and interact with immature forms of AMPA receptor during receptor assembly (M. E. Rubio and Wenthold 1999; Fukata et al. 2005). In addition to interaction with chaperone proteins, the GluA2 subunit itself

contains ER retention motifs that regulate ER export. It has been shown that the C-terminus of GluA2, including the PDZ motif, is required for ER exit (Greger, Khatri, and Ziff 2002a). Moreover, R607 of the RNA editing site plays an important role in ER retention (Greger, Khatri, and Ziff 2002a). Reversion of arginine residue to glutamine results in rapid release from the ER and elevated expression of GluA2 on the surface (Greger, Khatri, and Ziff 2002a).

AMPA receptor assembly is a multi-step process which involves interactions between different subunit domains. The dimerization of AMPA receptor initiates via the interaction of the ATD of one monomer with the ATD of another monomer (Ayalon and Stern-Bach 2001). Two dimers then interact to form an unstable proto-tetramer (Gan, Salussolia, and Wollmuth 2015) . Following this step, the M4 region of one subunit wraps around the M1-M3 regions of adjacent subunit resulting in proto-tetramer stabilization (Gan, Salussolia, and Wollmuth 2015). At the same time, the *cis* interactions of the LBDs of dimers rearrange to form a *trans* LBD in the proto-tetramer (Herguedas, Krieger, and Greger 2013; Gan, Salussolia, and Wollmuth 2015). However, the exact mechanisms that govern AMPA receptor subunit assembly still need to be further explored.

The newly assembled proteins will accumulate in the ER at ER exit sites (ERES) where proteins are loaded to COPII vesicles for forward transportation (Sato and Nakano 2007). Evidence has shown that the GluA2 subunit interacts with the COPII protein Sec23, suggesting AMPA receptor traffic via the COPII secretory pathway (Pick et al. 2017). Interactions with other proteins such as cornichons, transmembrane AMPA receptor regulatory proteins (TARPs), and protein interacting with c kinase (PICK) also regulate the efficiency of ER exit of AMPA receptors (Pick and Ziff 2018).

Trafficking of AMPA receptors from the ER to the synapse

After release from the ER, most AMPA receptors are processed in the somatic Golgi apparatus and transported in vesicles along cytoskeleton to synapses. However, because the

functional ER and Golgi outposts are present in dendrites and even in dendritic spines, AMPA receptors may be processed in those dendritic compartments prior to synaptic delivery.

Many proteins are involved in AMPA receptor trafficking. In general, PDZ-domain containing proteins are thought to anchor receptors at synapses (H.-C. Kornau, Seeburg, and Kennedy 1997). However, many studies have revealed that PDZ proteins may play an important role early in AMPAR forward trafficking (N. Sans et al. 2001). For example, the interaction between GluA1 and synapse-associated protein 97 (SAP97) seems to occur in the ER (Sans et al. 2001), and the SAP97-GluA1 interaction is necessary for correct synaptic targeting (Y. Hayashi et al. 2000). GluA2 subunit interactions with PICK1 may be necessary for the exit of GluA2 from the ER (Greger, Khatri, and Ziff 2002a). It is worth noting that different AMPAR subunits bind to different subsets of PDZ proteins (Shi et al. 2001). Therefore, AMPA receptors trafficking is subunit-specific (Shi et al. 2001). However, when AMPA receptors are expressed as GluA1/GluA2 heteromers, GluA1 trafficking signals dominate over GluA2 trafficking signals (Shepherd and Huganir 2007).

Once AMPA receptors enter the Golgi apparatus, they are subjected to various post-translational modifications (Jiang, Suppiramaniam, and Wooten 2006). AMPA receptors become fully glycosylated in the Golgi (Shepherd and Huganir 2007). In addition, lipid modification also occurs in the Golgi (Haucke and Di Paolo 2007). For example, palmitoylation occurs at a cysteine in the second TMD (TMD2) region and on a C-terminal cysteine (T. Hayashi, Rumbaugh, and Huganir 2005). The palmitoylation at these two sites regulates receptor trafficking and could impact synaptic plasticity (T. Hayashi, Rumbaugh, and Huganir 2005).

Vesicular/cytoskeletal trafficking is mediated by motor proteins such as kinesin and myosin (Shepherd and Huganir 2007). Microtubule transport is mediated by both kinesin KIF5 and KIF1 by interacting with the glutamate receptor-interacting protein 1 (GRIP1)/GluA2 complex (Setou et al. 2002; Shin et al. 2003a), while transportation along actin filament is carried out by myosin Va, Vb, and myosin VI (Lisé et al. 2006; Osterweil, Wells, and Mooseker

2005). The exact location of AMPA receptor exocytosis is still unclear. However, the prevailing view is that AMPA receptors are inserted into the plasma membrane close to, but not at, synapses, and then travel out into dendrites via lateral diffusion (Shepherd and Huganir 2007).

Activity-dependent AMPA receptors trafficking

Like other transmembrane proteins, AMPA receptors traffic in and out of the plasma membrane constitutively (Anggono and Huganir 2012). However, due to their important role in responding quickly to presynaptic inputs, the number of AMPA receptors on the surface is also regulated by synaptic activities (Anggono and Huganir 2012). In response to different synaptic activities, AMPA receptors can be rapidly inserted into or removed from the postsynaptic membrane, resulting in long-lasting changes in synaptic function (Huganir and Nicoll 2013).

To identify molecular mechanisms underlying activity-dependent AMPA receptors trafficking, the first question that needs to be addressed is how synapses transform different patterns of stimuli to biochemical signals. Although different mechanisms have been reported, numerous studies show that NMDA receptors are one of the key players in the initial steps of signal transduction (Lüscher and Malenka 2012). Induced by high-frequency stimulation (HFS) or theta-burst stimulation (TBS), NMDA receptors are activated by binding to glutamate but must be coupled with the postsynaptic depolarization (Malenka 1994). When the postsynaptic membrane is depolarized, NMDA receptor fully relieves the magnesium ion, which normally blocks the channel, resulting in a significant rise in the calcium level in dendritic spines (Malenka 1994). During low-frequency stimulation (LFS), NMDA receptors are activated modestly, leading to only a modest increase in postsynaptic calcium (Malenka 1994). The synaptic calcium level determines AMPA receptors insertion or removal (Malenka 1994).

When calcium levels increase significantly in the dendritic spine, protein kinases are often activated and play critical roles in regulating insertion of AMPA receptors to synapses (Malenka 1994). Calmodulin/calcium-dependent kinase II (CaMKII) is the primary downstream

target following calcium entry through NMDA receptors (J. Lisman, Yasuda, and Raghavachari 2012). CaMKII can phosphorylate the GluA1 subunit of AMPA receptor directly (McGlade-McCulloh et al. 1993) . However, the detailed molecular mechanisms by which the activation of CaMKII leads to the synaptic delivery of AMPA receptors remains to be determined. cAMP-dependent protein kinase A (PKA) and protein kinase C (PKC) also mediates AMPA receptors trafficking towards synapses. PKA phosphorylates the GluA4 subunit of AMPAR, leading to incorporation of the receptor into synapses (Esteban et al. 2003). PKC has been shown to phosphorylate S818 of the GluA1 subunit of AMPA receptor to regulate AMPA receptor insertion (Boehm et al. 2006). Interestingly, phosphorylation of different subunits of AMPA receptor could guide the receptor to opposite directions. Phosphorylation of the GluA2 subunit by PKC decreases interactions of AMPA receptors with GRIP and promotes interactions with PICK1 to facilitate AMPA receptor internalization (Anggono et al. 2013). In addition to AMPA receptor itself, protein kinases can act on AMPA receptor auxiliary proteins to impact AMPA receptor trafficking. For instance, both CaMKII and PKC can phosphorylate multiple sites on the C-terminal domain of TARPs (Tomita et al. 2005; Park et al. 2016). Phosphorylation of the TARP C-terminal domain inhibits its association with negatively-charged phospholipid, which in turn allows binding of the receptor complex to PSD95 and stabilization of AMPA receptors on the cell surface (Sumioka et al 2010). In contrast, a modest increase of postsynaptic calcium will preferentially activate protein phosphates such as calcineurin or protein phosphatase 1 (PP1), resulting in removal of AMPA receptors from the synapse (R. M. Mulkey et al. 1994).

In addition to kinases and phosphatases, proteins that interact with AMPA receptors also participate in the activity-dependent trafficking. For instance, the interaction of the GluA1 subunit with protein 4.1N regulates activity-dependent AMPA receptor insertion (Lin et al. 2009). Additional proteins that associate with AMPA receptor directly or indirectly are involved in removing AMPA receptors from the plasma membrane. Clathrin-mediated endocytosis is a well-accepted pathway that regulates activity-dependent AMPA receptors removal (Blanpied, Scott,

and Ehlers 2002). Endocytic adaptor protein complex AP2 plays an essential role in this process. AP2 binds GluA2 and GluA3 subunits directly to mediate AMPA receptor endocytosis (Kastning et al. 2007; S. H. Lee, Simonetta, and Sheng 2004). Although the precise cellular mechanism of AP2 binding to GluA2 has not been revealed, AP2 presumably functions to recruit and concentrate GluA2-containing AMPA receptors to endocytic sites (Hanley 2018). In addition to binding GluA2 directly, AP2 also interacts with calcium sensing protein hippocalcin, TARPs, and PICK, thereby recruiting AMPA receptors to endocytic sites (C. L. Palmer et al. 2005; Fiuza et al. 2017; Matsuda et al. 2013) .

Processing of NMDA receptors in the ER

Like the AMPA receptors, functional NMDA receptors are also assembled in the ER (Stephenson, Cousins, and Kenny 2008). To ensure functional receptor assembly, the GluN1 subunit is produced in the ER in large excess comparing to GluN2 and GluN3 subunits (Chazot and Stephenson 1997; Huh and Wenthold 1999). The unassembled subunits or misfolded receptors are retained in the ER via various mechanisms. For GluN1 subunits, the C-terminal domain, extracellular region, and the transmembrane domain are implicated in the regulation of ER processing of NMDA receptors (McIlhinney et al. 1998). Two motifs with 3-amino acid residues RxR and KKK in the C-terminal region were identified as ER retention motifs (Horak and Wenthold 2009). Phosphorylation by PKC at a specific serine in the C-terminal region can suppress RxR mediated ER retention (Scott et al. 2001). In the extracellular region, the glycine binding site of GluN1 has been reported to play a critical role for functional NMDA receptors release from the ER (Kenny et al. 2009). It has been reported that there is a structural determinant in the M3 domain of GluN1 that causes the unassembled subunit to be retained in the ER (Horak, Chang, and Wenthold 2008). For other GluN subunits, the regulation of ER processing needs to be elucidated in future studies.

NMDA receptor heterotetrameric assembly also requires multiple steps. Three models for the assembly of functional NMDA receptors have been proposed. One model suggests that the GluN1 and GluN2 form homodimers initially and then form the heterotetrameric complex (Hansen, Furukawa, and Traynelis 2010b). Another model proposes that GluN1-GluN2 forms heterodimers first and then assemble as a heterotetramer (Schüler et al. 2008a). The third model posits that the N-terminal domains of the GluN1 subunit initially form homodimers, and subsequent dimer dissociation is essential for formation of the functional GluN1/GluN2 heteromers (Farina et al. 2011a). However, the exact mechanisms underlying tetramer assembly are still unclear.

Trafficking of NMDA receptors from the ER to synapses

Similar to AMPA receptors, when NMDA receptors exit the ER, they are modified in the Golgi apparatus, sorted and packaged into vesicular carriers in the TGN and then distributed to their destination (Horak et al. 2014). It is worth noting that subunit composition of NMDA receptor varies at different brain regions and developmental stages, and can even differ at the subcellular localization level of the same synapse (Sanz-Clemente, Nicoll, and Roche 2013). Therefore, the mechanisms of NMDA receptor trafficking and targeting must be tightly regulated to meet the needs of neurons.

Many proteins are involved in NMDA receptors trafficking from the ER to cell surface. PDZ-domain containing proteins such as membrane-associated guanylate kinases (MAGUKs) were first identified as synaptic scaffolding proteins for anchoring NMDA receptors at synapses (Chen et al. 2015). However, recent studies have suggested that the interaction between NMDA receptors and MAGUKs occurs before they reach synapses and this interaction may play a role in regulating NMDA receptor trafficking (Standley et al. 2000). SAP102, one of the MAGUKs, binds to NMDA receptors in the ER and Golgi/TGN, forming a complex which then bind to the exocyst through interactions between an exocyst component, Sec8, and the PDZ domain of

SAP102 (Sans et al 2003). In addition to MAGUKs and the exocyst, other proteins such as mPin (mammalian homologue of *Drosophila melanogaster* protein partner of inscuteable) and the G protein subunit Gαi also make contributions to NMDA receptor transportation (Nathalie Sans et al. 2005) .

The long- distance transportation of NMDA receptors along dendrites or axons also depends on microtubules and motor proteins (Horak et al. 2014). KIF17 was the first kinesin found to be involved in the trafficking of GluN2B-containing NMDA receptors (Guillaud, Setou, and Hirokawa 2003). GluN2B binds to a complex consisting of mLin10, mLin7, and mLin2, which links the NMDA receptor to KIF17 (Setou M et al,2000, Guillaud L et al 2003). Another kinesin KIF1Bα may also participate in transporting NMDA receptors because it associates with NMDA receptor binding MAGUKs directly (Mok et al. 2002). However, the role of KIF1Bα in NMDA receptor trafficking is still unknown. NMDA receptors insert into cell surface via exocytosis either at the extrasynaptic region (Rao A et al 1998) or directly into synapses (Guillaud et al 2003). However, the exact locations are still unclear.

Endocytosis and recycling of NMDA receptors

Compared to AMPA receptors, NMDA receptors are stable. However, they can be cycled to and from synapses via regulated pathways (Petralia, Al-Hallaq, and Wenthold 2009). The regulated internalization of NMDA receptors requires various factors and depend largely on synaptic activity (Pérez-Otaño and Ehlers 2005). Activation of NMDA receptors (Nong Y et al, 2003) and mGluRs (Snyder EM, et al 2004) can induce NMDA receptor internalization.

NMDA receptors can be internalized via clathrin-mediated pathway. Many specific motifs of NMDA receptor subunits are involved in clathrin-mediated internalization. GluNR2B subunit contains a tyrosine-based endocytic C-terminus motif (YEKL) that binds to the u2 subunit of the AP-2 adaptor protein involved in clathrin-mediated endocytosis from the cell surface (Lavezzari et al. 2004). GluNR2A contains a dileucine motif in the C-terminus that may play a role in

receptor internalization (Lavezzari et al. 2004). In addition to the motifs near the distal C-termini, another tyrosine-containing motif near the last transmembrane domain are also involved in internalization of GluNR1 and GluNR2 subunits (Scott DB et al 2004). Besides the endocytic motifs of the NMDA receptor subunits, proteins associated with NMDA receptors also play an important role in clathrin-mediated endocytosis of NMDA receptors. Both GluNR2A and GluNR2B subunits can bind to PSD-95 via their PDZ-binding domain of the C-termini (H. C. Kornau et al. 1995) which may inhibit clathrin-mediated endocytosis of NMDA receptors (Petralia, Al-Hallaq, and Wenthold 2009). Other proteins such as candidate plasticity gene 2 (CPG2) and GAIP interacting protein C terminus (GIPC) have also been reported to contribute to NMDA receptor endocytosis (Cottrell J, et al 2004, Yi Z et al 2006).

Posttranslational modifications such as phosphorylation and ubiquitination also affect NMDA receptors endocytosis (Petralia, Al-Hallaq, and Wenthold 2009). Phosphorylation of the PDZ-binding domain of GluN2B will disrupt interactions between GluNR2B and PSD-95 and SAP102 (H. J. Chung et al. 2004), therefore increasing internalization of NMDA receptors from the surface (Sans N, et al 2005). However, phosphorylation at the different sites may inhibit the endocytosis of NMDA receptors. For example, Fyn kinase phosphorylates the tyrosine residue of GluNR2B which is in the AP-2 binding site, preventing AP-2 binding and thus promoting retention of GluNR2B-containing NMDA receptors at the surface (W. Lu et al. 2015). Ubiquitination is also important for direct regulation of NMDA receptors (Ehlers 2003), although the mechanism is not clear.

NMDA receptors can also be internalized via clathrin-independent pathways. Lipid rafts and associated proteins such as flotillin and caveolin interact with NMDA receptors under certain conditions (Swanwick et al. 2009), and they may have potential function in clathrin-independent endocytosis (Swanwick et al. 2009). Furthermore, NMDA receptors can be removed from the surface via clathrin-independent endocytosis after calpain-mediated cleavage of GluNR2 subunits induced by overactivity (Wu HY, et al 2005).

In addition to the various pathways that regulate NMDA receptors internalization, NMDA receptors are subject to selective endocytosis during different developmental stages (Lavezzari et al. 2004). The mechanisms that regulate different subunit-containing NMDA receptors may be very different. In general, GluNR2A enter late endosomes for degradation, while GluNR2B enters recycling endosomes for recycling to cell surface (Lavezzari G, et al 2004).

Subsynaptic localization of AMPA receptors and NMDA receptors

As I discussed in the previous section, AMPA receptors and NMDA receptors are the two major types of iGluRs that mediate fast excitatory synaptic transmission and synaptic plasticity (Dingledine et al. 1999a), while mGluRs act on much slower timescales to modulate synaptic transmission and cell excitability (Niswender and Conn 2010). Since these different types of glutamate receptors are co-expressed at individual synapses (Scheefhals and MacGillavry 2018), the relative localization of the receptors can significantly impact synaptic function. Many studies have suggested that glutamate receptors are not evenly distributed at synapses (Masugi-Tokita et al. 2007a; Z. Nusser et al. 1994a; Masugi-Tokita and Shigemoto 2007). Different types of glutamate receptors have their spatial preference (Kharazia and Weinberg 1997a). In this section, I will first discuss the subsynaptic localization of AMPA receptors and NMDA receptors, followed by analyzing the functional implications of the spatial segregation of these receptors. In the end, I will explore the potential mechanisms underlying the subsynaptic positioning of AMPA receptors and NMDA receptors.

Subsynaptic localization of AMPA receptors and NMDA receptors

At excitatory synapses, AMPA receptors mediate the vast majority of fast synaptic transmission (Traynelis et al. 2010), therefore, the number of AMPA receptors in the postsynaptic density (PSD) can greatly impact the efficiency of synaptic transmission and synaptic plasticity. A PSD of average size (300-400 nm in diameter) in an active synapse contains about 30-150 AMPA receptors (Zoltan Nusser et al. 1998; Tanaka et al. 2005;

Fukazawa and Shigemoto 2012). The number of AMPA receptors is linearly correlated with PSD size (Y. Takumi et al. 1999; Masugi-Tokita et al. 2007b; Z. Nusser et al. 1998). However, functional studies using advanced techniques such as glutamate uncaging, optogenetics, and stochastic optical reconstruction microscopy (STORM) have shown that the postsynaptic responses do not necessarily increase as more AMPA receptors are recruited to PSD (Patriarchi, Buonarati, and Hell 2018). These results indicate that the localization of AMPA receptors with respect to presynaptic release sites is also critical in determining synaptic efficacy. In fact, instead of even distribution within the PSD, AMPA receptors are concentrated in clusters of ~100 nm diameter (Nair et al. 2013a). These clusters are aligned with presynaptic glutamate release sites, forming trans-synaptic nanocolumns for effective activation and efficient synaptic transmission (A.-H. Tang et al. 2016; Biederer, Kaeser, and Blanpied 2017a). Moreover, many studies have shown that AMPA receptors preferentially localize toward the edge of the PSD (Bernard, Somogyi, and Bolam 1997; Kharazia and Weinberg 1997a; Chen et al. 2008a).

Like AMPA receptors, NMDA receptors also form clusters with 100-200 nm in diameter but tend to localize toward the center of the PSD (Kharazia and Weinberg 1997a; Chen et al. 2008a). Each PSD contains about 20-30 NMDA receptors. The number of NMDA receptors is fairly invariant between different size of synapses (Yutaka Takumi et al. 1999; Racca et al. 2000; Chen et al. 2015).

Functional implications of subsynaptic receptor distribution

When glutamate is released from presynaptic vesicles, glutamate concentration within the synaptic cleft rapidly rises to millimolar levels (Clements et al. 1992). However, the high concentration of glutamate is restricted to a small area (<200 nm) and only for a brief period of time (<100 μsec) (Bergles, Diamond, and Jahr 1999). Importantly, the affinity of AMPA receptors for glutamate is relatively low, and the EC50 of glutamate for activating AMPA

receptors is about 0.5 mM to 2 mM (Traynelis et al. 2010). Thus, AMPA receptors that reside far away from the release sites cannot be activated effectively. Because of these biophysical properties, numerous computational models have shown that the open probability of AMPA receptors directly from vesicle release sites is about 0.6, and the probability drops significantly if receptors are laterally relocated by 50 nm (Xie et al. 1997; Raghavachari and Lisman 2004a). In fact, a single release event may activate only a fraction of the total number of AMPA receptors at the synapse, which cover approximately 25% of an average PSD in a CA1 synapse (J. Lisman and Raghavachari 2006; J. E. Lisman, Raghavachari, and Tsien 2007).

Similar to AMPA receptors, the probability of NMDA receptor activation is also dependent on their localization. In contrast to AMPA receptors, NMDA receptors have a higher affinity for glutamate but low glutamate binding rate (Erreger, Geballe, et al. 2005). As a result, the opening probability of NMDA receptors is about 0.025 for whole-cell recording and 0.4 for outside-out patches during the transient glutamate peak (Rosenmund, Feltz, and Westbrook 1995). Moreover, the impact of localization of receptors on the open probability are also dependent on the subunit combination of NMDA receptor. For example, NR2B-containing receptors are highly affected by their location relative to the release sites, whereas NR2A-containing receptors are not (Santucci and Raghavachari 2008).

Potential mechanisms underlying the spatial segregation of glutamate receptors

As I discussed in the previous sections, the distribution of AMPA receptors and NMDA receptors in PSD is highly heterogenous. AMPA receptors, forming 1-3 nanoclusters, are enriched at the edge of the PSD, while NMDA receptors preferentially localized at the center of the PSD. What mechanisms position the different types of receptors after they entered PSD?

In general, the mechanisms underlying the spatial distribution of AMPA receptors within the PSD can be classified in two categories: mechanisms that rely on protein-protein interactions between AMPA receptors and PSD scaffolding proteins and mechanisms that

confine AMPA receptors without protein-protein interactions. AMPA receptors can interact with many scaffolding proteins via their PDZ ligand in the CTD (Tomita, Nicoll, and Bredt 2001). Therefore, intracellular scaffolding proteins may contribute to the formation and maintenance of AMPA receptor nanoclusters. One of the prominent candidates is PSD-95. As the name implies, PSD-95 is a scaffolding protein that is highly enriched in the PSD (Cheng et al. 2006). It interacts with AMPA receptor auxiliary proteins, such as TARP family proteins, to trap AMPA receptors at synaptic sites (Bats, Groc, and Choquet 2007; Schnell et al. 2002). EM tomography and super-resolution microscopy have shown that the distribution of PSD-95 is highly heterogenous, forming nanodomains, and they co-localize with AMPA receptor (MacGillavry et al. 2013a). This indicates that PSD-95 may play an essential role in retaining AMPA receptors in the nanodomains. Another candidate is SAP97. SAP97 is a member of the same MAGUK family as PSD-95. SAP97 interacts directly with GluA1 subunit of AMPA receptor via its first PDZ domain. EM studies revealed that SAP97 is concentrated near the edges of PSD (DeGiorgis et al. 2006; Valtschanoff et al. 2000). Moreover, different isoforms of SAP97 guide AMPA receptors to different locations in the PSD (Goodman et al. 2017). In addition to the interaction between intracellular domain of AMPA receptor and the postsynaptic scaffolding protein, the extracellular domain of AMPAR may also be involved in positioning AMPA receptors to its subsynaptic location. In fact, the extracellular domain of AMPA receptor is fairly large, taking up to 50% of the receptor (Herguedas, Krieger, and Greger 2013). The extracellular domain of AMPA receptor protrudes 13 nm to the synaptic cleft (Greger, Watson, and Cull-Candy 2017) and therefore is capable of interacting with synaptic cleft proteins to anchor the receptor. Several cell adhesion proteins have been found to interact with the extracellular domain of AMPA receptor. For example, N-cadherin interacts directly with an extracellular domain of the GluA2 subunit of AMPA receptor, which can influence AMPA receptors clustering (Saglietti et al. 2007).

Aside from the mechanisms involving protein-protein interactions, molecular confinement can also contribute to AMPA receptors positioning or clustering. As I discussed in previous sections, the PSD is a densely packed structures with numerous proteins (Farley, Swulius, and Waxham 2015). Therefore, the proteins within the PSD can act as series of barriers to confine AMPA receptors in clusters, even though they have no direct interaction with AMPA receptors (Santamaria et al. 2010). Several computational models have been developed to support molecular crowding mechanisms (Santamaria et al. 2010). However, future experiments are still required for fully understanding the mechanism.

Finally, in addition to proteins, membrane lipids may also play an important role in AMPA receptors positioning. It has been reported that excitatory synapses contain membrane rafts and glutamate receptors reside in synaptic membrane rafts (Delint-Ramirez et al. 2010; Swanwick et al. 2009). Recent studies have also reported that PIP3, a lipid-based second messenger, can recruit pleckstrin-homology domain containing proteins to the plasma membrane (X. Wang, Hills, and Huang 2015). This recruitment will tether membrane-associated signaling complexes to the subregions in the PSD, thereby facilitating the assembly of domains of molecular crowding or AMPA receptors clustering (T. P. Li et al. 2016).

In the previous sections, I have discussed the biogenesis, trafficking and the subcellular locations of glutamate receptors. With the development new techniques, emerging evidence suggests how the number of glutamate receptors are precisely regulated, how glutamate receptors are organized within synapses, and how the relative locations between release sites and the receptors affect neurotransmission and synaptic plasticity. This thesis focuses on two main topics: the locations of glutamate receptors relative to neurotransmitter release sites and a novel endocytic pathway at the postsynaptic terminals.

Chapter 2

Flash-and-Freeze: A Novel Technique to Capture Membrane Dynamics with Electron Microscopy

Abstract

Cells constantly change their membrane architecture and protein distribution, but it is extremely difficult to visualize these events at a temporal and spatial resolution on the order of ms and nm, respectively. We have developed a time-resolved electron microscopy technique, "flash-and-freeze," that induces cellular events with optogenetics and visualizes the resulting membrane dynamics by freezing cells at defined time points after stimulation. To demonstrate this technique, we expressed channelrhodopsin, a light-sensitive cation channel, in mouse hippocampal neurons. A flash of light stimulates neuronal activity and induces neurotransmitter release from synaptic terminals through the fusion of synaptic vesicles. The optogenetic stimulation of neurons is coupled with high-pressure freezing to follow morphological changes during synaptic transmission. Using a commercial instrument, we captured the fusion of synaptic vesicles and the recovery of the synaptic vesicle membrane. To visualize the sequence of events, large datasets were generated and analyzed blindly, since morphological changes were followed in different cells over time. Nevertheless, flash-and-freeze allows the visualization of membrane dynamics in electron micrographs with ms temporal resolution.

Introduction

Visualizing membrane and protein dynamics within a cell is a key step towards understanding the cell biology of particular processes. Dynamic trafficking events can be captured using light or fluorescence microscopy. However, the subcellular context is largely missing in such images because subcellular structures cannot be completely "painted" by dyes or fluorescent probes and resolved spatially and spectrally (D. Li et al. 2015; Betzig et al. 2006).

On the other hand, while electron microscopy can delineate subcellular architecture in exquisite detail, it cannot capture cellular dynamics, because specimens must be fixed prior to imaging. Thus, it is typically not sufficient to completely understand cellular dynamics using only one imaging modality. To overcome the limitations of light and electron microscopy, correlative microscopy techniques have been developed. Correlative Light and Electron Microscopy (CLEM) visualizes intracellular dynamics using light microscopy and underlying subcellular structures with electron microscopy. In CLEM, cells engaged in various processes, such as cytokinesis and endocytosis (Sjollema et al. 2012; Redemann and Müller-Reichert 2013; Kukulski et al. 2012; Kobayashi, Iwamoto, and Haraguchi 2016) are live-imaged and then processed for electron microscopy. Although CLEM captures certain aspects of intracellular dynamics, there are four factors that limit the utility of this approach. First, the temporal resolution is limited by how quickly the cells can be immobilized, which typically takes s - min due to the slow diffusion and reaction of fixatives (Start et al. 1992). Second, the subcellular architecture is observed post facto (Müller-Reichert et al. 2007); thus, the dynamic morphological changes cannot be captured using this approach. Third, the fluorescence and electron micrographs cannot be precisely aligned due to tissue shrinkage caused by dehydration during the sample preparation for electron microscopy (Bykov et al. 2016; Casanova et al. 2016). Fourth, events like cytokinesis and endocytosis do not take place at the same time in every cell (Kukulski et al. 2012; 2011) and thus, a particular cell that is engaged in the event must be identified from a large population of cells. This process is often laborious. Thus, a new method is necessary to induce particular events in every cell and to capture the resulting cellular dynamics by the rapid immobilization of cells at defined time points. Recently, several tools have been developed to induce particular cellular dynamics using light (optogenetics). Channelrhodopsin is a light sensitive, non-selective cation channel isolated from Chlamydomonas reinhardtii (Nagel et al. 2003; 2002). When channelrhodopsin is expressed in neuronal membranes, a brief flash of light induces an influx of sodium ions into neurons and

triggers an action potential (Boyden et al. 2005; Nagel et al. 2005). The action potential then propagates into the synaptic terminals, where synaptic vesicles fuse within milliseconds (Heuser and Reese 1981; Watanabe, Liu, et al. 2013a; Watanabe, Rost, et al. 2013c). Therefore, channelrhodopsin induces neuronal activity. To follow membrane dynamics at synaptic terminals, neurons must be immobilized at defined time points after stimulation with ms precision. To capture membrane dynamics after inducing neuronal activity, we coupled light stimulation with high-pressure freezing (Watanabe, Liu, et al. 2013a; Watanabe, Rost, et al. 2013c; Watanabe 2016). High-pressure freezing allows for the near-instantaneous immobilization of cells with reduced ice crystal formation (Steinbrecht and Zierold 1987). Ice crystals can rupture membranes and disrupt the subcellular architecture (Dubochet 2007). By varying the time intervals between stimulation and freezing, membrane trafficking within synaptic terminals was captured following the induction of an action potential. Here, we demonstrate experimental procedures using a commercialized high-pressure freezer that couples a ms temporal control of light stimulation with high-pressure freezing. Unlike other instruments that require an external device to control light stimulation and freezing, light stimulation is fully integrated in this system and can be applied with ms precision (Watanabe 2016). This process involves multiple steps. 1) Mouse hippocampal neurons are cultured on sapphire disks and infected with lentivirus carrying an expression vector for channelrhodopsin (Watanabe, Rost, et al. 2013c). 2) Neurons are stimulated and frozen at defined time points after stimulation. 3) The vitrified water is substituted with an organic solvent, while lipids and proteins are cross-linked by fixatives to preserve the intracellular architecture. 4) The samples are infiltrated and embedded in epoxy resin. 5) Ultrathin sections are collected using an ultramicrotome. 6) Thin sections are imaged on a transmission electron microscope. 7) Image acquisition and analysis are performed blindly with respect to time points or genotypes. Cellular dynamics can be determined through the reconstruction of time-resolved images (Watanabe,

Liu, et al. 2013a; Watanabe, Rost, et al. 2013c). Sample preparation (steps 2 - 5 above) requires a week, but the subsequent image analysis requires months to a year.

Protocol

All of the experiments were performed according to the rules and regulations of animal use by the National Institutes of Health. The protocol was approved by the Animal Care and Use Committee (IACUC) at Johns Hopkins School of Medicine.

1. Isolation and Culture of Mouse Hippocampal Neurons

1. Dissect cortices from a postnatal day 0 - day 2 (P0 - 2) mouse brain18. Isolate the astrocytes from the cortices. NOTE: The mouse brain was isolated after decapitation. Astrocytes serve as a feeder layer for hippocampal neurons.

2. Treat the cortices with 800 µL of 0.05% Trypsin-EDTA for 15 min at 37 °C to dissociate the astrocytes. 3. Culture the astrocytes in a T-75 flask with 13 mL of DMEM containing 10% fetal bovine serum (FBS) and 0.2% penicillin-streptomycin for one week at 37 °C and 5% CO2.

4. Place one acid-washed and sterilized 18 mm glass coverslip per well of a 12-well plate.

5. Briefly wash two 6 mm carbon-coated sapphire disks in 70% ethanol and place them on top of each glass coverslip.

6. Prepare Poly-D-Lysine (PDL) solution by mixing 3 mL of 17 nM acetic acid with 1 mL of rat tail collagen and 1 mL of PDL (1 mg/mL). Apply 200 µL of PDL solution to the sapphire disks and glass coverslips for 5 min at RT.

7. Remove the PDL solution and air dry. Prior to use, sterilize the plate as prepared in steps 1.4 - 1.6 for 30 min under ultraviolet light.

8. Seed the astrocytes from step 1.3 in 2 mL of DMEM at a density of 5x104 cells/well in the plate as prepared in steps 1.4 - 1.6. Grow them at 37 °C and 5% CO2 for one week.

9. Add 20 µL of fluoro-deoxyuridine (final concentration: 80 µM) to each well for at least a few h before culturing the neurons. NOTE: Fluoro-deoxyuridine stops astrocyte division.

10. Change the medium to 1.5 mL of neuronal basal medium containing 1% L-alanyl-L-glutamine, 2% serum-free supplement for neuronal cells, and 0.2% penicillin-streptomycin.

11. Prepare papain solution by adding 20 units of papain to 5 mL of enzyme solution (1.65 mM Cysteine, 1 mM CaCl2, and 0.5 mM EDTA in DMEM). Acidify the solution by passing CO2 gas for 20 min. Filter-sterilize with a 0.22 µm filter.

12. Harvest the brain from a P0 - 2 mouse18. Immediately transfer the brain to ice-cold Hanks'-balanced Salt Solution (HBSS). Dissect the hippocampi under a stereomicroscope, keeping the tissue submerged in HBSS.

13. Place the two hippocampi in 1 mL of the papain solution prepared in step 1.11. Incubate for 1 h on a thermomixer at 37 °C and 750 rpm.

14. Replace the papain with 1 mL of inactivating solution containing 2.5 mg of trypsin inhibitor and 0.5 mg of albumin per mL of DMEM. Incubate for 5 min at 37 °C. Aspirate off the inactivating solution.

15. Add 200 µL of neuronal basal medium to the isolated hippocampus. Triturate using a 200 µL pipette tip to dissociate the cells. Wait until the undissociated cells settle at the bottom. Carefully remove the medium with cells from the top.

16. Repeat step 1.15 3x. Pool all the dissociated cells in a new 1.5 mL centrifuge tube.

17. Count the number of cells using a hemocytometer. Plate neurons at a density of 6.5 x 10 4 cells/well on top of the astrocyte layer prepared in steps 1.1 - 1.10.

18. Infect the neurons with lentivirus expressing channelrhodopsin at DIV 3 (3 d in vitro).

19. Perform flash-and-freeze on DIV 14, as described in steps 2.1 - 2.5, below.

2. Flash-and-Freeze

1. Preparation of Fixative

1. In a chemical hood, add the following substances to a conical tube to prepare the fixative: 2.5 mL of glutaraldehyde (10% stock in acetone), 0.25 g of osmium tetroxide, 0.25 mL of water, and 22.25 mL of anhydrous acetone. NOTE: The final concentration of each component should be 1% in acetone. Glutaraldehyde is added to preserve the protein structures during freeze-substitution. CAUTION: The acute toxicity of osmium tetroxide is high. Exposure to vapors could damage the cornea of the eye. It should be handled only in a certified chemical hood.

2. Aliquot 1 mL of fixative into numbered cryogenic vials (2 mL). Keep the fixative frozen in liquid nitrogen until use.

NOTE: Osmium tetroxide and glutaraldehyde cross-react and precipitate; thus, once mixed, aliquot immediately, cap the tubes, and submerge the cryotubes in liquid nitrogen to freeze the fixative. Use a pencil to number the cryogenic vials, since acetone can wash off markers.

2. Preparation of Physiological Saline

1. Make physiological saline solution by mixing HEPES (10 mM, pH 7.5), NaCl (140 mM), KCl (2.4 mM), and glucose (10 mM). NOTE: These values are final concentrations. Cryo-protectants are not used for monolayer cultures. However, a proper cryo-protectant is required for specimens thicker than 5 µm. The use of 20% BSA is typically recommended.

Yeast paste and E. coli OP50 can also be used as cryo-protectants for fly larvae or C. elegans.

2. Add CaCl2 at 4 mM and MgCl2 at 1 mM final concentrations. NOTE: The concentrations of CaCl2 and MgCl2 vary depending on experiments. To ensure the capture of exocytic intermediates, 4 mM calcium is used for these particular experiments to increase the release probability of vesicles (Watanabe, Rost, et al. 2013c) .

3. Check the osmolarity using an osmometer. Ensure that it is 300 ± 5 mOsm.

4. Add AMPA receptor antagonist (NBQX) to a final concentration of 3 µM and GABA receptor antagonist (bicuculline) to a final concentration of 30 µM. NOTE: Neurotransmitter receptor antagonists are added to avoid recurrent network activity following neuronal stimulation (Watanabe, Rost, et al. 2013c).

5. Warm up the physiological saline to 37 °C for use.

3. Preparation of the Specialized High-pressure Freezer and an Automated Freeze Substitution Unit

1. Prior to high-pressure freezing, cool down an automated freeze substitution unit to -90 °C by filling the tank with liquid nitrogen.

2. Cool down acetone in a small cup to -90 °C by placing it inside the specimen chamber.

3. Fill the liquid nitrogen dewar and storage dewar of the high-pressure freezer with liquid nitrogen.

4. Set up the light stimulation protocol using the touch screen monitor.

    1. Name the program by clicking on "Edit" next to "Program name" on the light stimulation window. Another window will pop up.

    2. Set up a program by typing "15,000 ms" in "dark phase," "100 ms" in "period," "10 ms" in "pulse," and "1" in "number of periods" for a single stimulus of 10 ms. Freeze the cells 90 ms later (**Fig. 1C**).

NOTE: The "dark phase" allows the cells to recover from light exposure during sample loading. "Period" defines the stimulation frequency. For example, if the stimulus should be applied at 20 Hz, this column should be set at 50 ms. "Pulse" defines the duration of the light stimulus. Finally, the "number of periods" defines the total number of stimuli applied. For setting up a high frequency stimulation, please see **Fig. 1E**.

5. For a "no stimulation" control, type "15 s" in "dark phase," "0 ms" in "period," "1 ms" in "pulse," and "0" in "number of periods" in the light stimulation setup window, as described in step 2.3.4.

NOTE: By default, the "pulse" must be at least 1 ms.

6. On the main screen, make sure that the box for light stimulation is checked.

7. Set up the storage protocol by clicking "Specimen Storage" on the main screen. Click on "Edit." In the following window, use "+" or "-," to select "2" to store 2 disks in each channel (3 channels in total). Check "Storage LN2 enabled."

4. Sample Loading and Freezing in the High-pressure Freezer

NOTE: All the sample assembly and loading steps are done under a stereomicroscope with a 7.5-60X magnification range. A tweezer is used in steps 2.4.1 - 2.4.4 to manipulate the specimens. Experiments must be performed at physiological temperature.

1. Place one sapphire disk, cell-side facing up, in the well of the black, middle plate (**Fig. 1B**).

2. Place a 100 µm spacer ring over the sapphire disk (**Fig. 1B**).

3. Place a blank sapphire disk over the spacer ring (**Fig. 1B**) after dipping one side of the disk in the pre-warmed saline solution from step 2.2. Make sure that no air bubbles are trapped between the two sapphire disks.

4. Place another 100 µm spacer ring and a 400 µm spacer ring (**Fig. 1B**). Remove the extra liquid using filter paper.

5. Place the assembly from step 2.4.3 between the two transparent half-cylinders (**Fig. 1A**). Close the top red cover to initiate the freezing process.

NOTE: The preset protocol runs automatically once the cover is closed. The sample stays in the same orientation in the freezing chamber, and a flash of light is applied from the top of the sample assembly. The red cover pops back up automatically once the freezing process is completed.

6. Store the specimen in the storage dewar.

NOTE: After freezing, the specimen is automatically dropped into a storage dewar filled with liquid nitrogen and stored there until further processing. The storage dewar has three chambers, and each chamber can hold up to 3 samples at most. Typically, two specimens are frozen under the same stimulation conditions, and the high-pressure freezer is programmed to store both in the same chamber.

7. Repeat steps 2.4.1 - 2.4.6 for each specimen.

8. Proceed to step 2.5 once all the chambers are full.

NOTE: The device was set to store up to 6 specimens in the storage dewar at a time. Therefore, after every 6th sample, step 2.5 must be performed. Once unloaded, repeat steps 2.4.1 - 2.4.6.

5. Sample Collection and Transfer to an Automated Freeze-substitution Unit

1. Open the door to the storage dewar, which is located under the table of the high-pressure freezer. Remove the storage dewar and place it on the benchtop.

2. Using hands, remove the specimen chamber from the dewar and transfer it in the specialized sample tray filled with liquid nitrogen. Unlock the knob to release the specimen cup.

3. Remove the transparent half-cylinders from the specimen cup using a pair of tweezers after pre-cooling the tips of the tweezers with liquid nitrogen (~ -196 °C). Carefully transfer the middle, black plate to a small cup containing liquid nitrogen.

NOTE: The tips of the tweezers must be precooled to the temperature of liquid nitrogen. The sample must be kept under liquid nitrogen at all times to prevent ice crystal formation.

3. Freeze Substitution in the Automated Freeze-substitution Unit

1. Using precooled tweezers (tips at ~ -196 °C), quickly transfer the middle plate from step 2.5.3 to the precooled acetone (-90 °C).

2. Separate the sapphire disk from the middle plate by gently shaking or tapping. NOTE: Occasionally, it may be difficult to separate the sapphire disk from the middle plate. In such a situation, leave the middle plate in precooled acetone (-90 °C) for a few minutes. Gentle tapping with tweezers also helps to dissociate the sapphire from the middle plate.

3. Place a cryogenic vial containing fixatives (step 2.1) inside a specimen chamber of the substitution unit. Transfer the sapphire disk to the cryogenic vial and place a cap on the vial.

4. Set up the freeze substitution program as follows: (i) -90 °C for 5 - 30 h, (ii) -90 - -20 °C in 14 h (5 °C/h), (iii) -20 °C for 12 h, and (iv) -20 °C - 20 °C in 4 h (10 °C/h). NOTE: The duration of the first step at -90 °C could be varied. The total duration of freeze substitution is set in such a way that the program ends in the morning (~1.5 d post-experiment) around 8 am so that the subsequent steps can be performed during the daytime.

4. Infiltration and Plastic Embedding with Epoxy Resin

1. Once the program ends, use gloved hands to transfer the cryogenic vials containing the sapphire disks from the specimen chamber of the substitution unit to a chemical hood.

2. Using a pipette, add acetone (room temperature) to each cryogenic vial and wash each sapphire disk 4 - 6x for 1 - 2 h.

3. Optionally, incubate the specimens in 0.1% uranyl acetate for 1 h if extra contrast is needed. Wash 4 - 6x with acetone over 1 - 2 h. NOTE: CAUTION: There is risk associated with internal exposure following the inhalation of uranyl acetate, which causes irritation of the upper respiratory tract. High exposure can damage blood cells. Work with uranyl acetate should be done under exhaust ventilation. Protective clothing is recommended.

4. Prepare liquid epoxy resin medium by weighing 6.2 g of glycerol polyglycidyl ether, 4.4 g of bisphenol-A epoxy resin, and 12.2 g of dodecenyl succinic anhydride (DDSA). Mix thoroughly and add 800 µL of benzyl dimethylamine (BDMA) while mixing. De-gas for 10 min.

5. Prepare 30, 70, and 90% epoxy resin in acetone from the 100% epoxy resin prepared in step 4.4.

6. Add 30% epoxy resin to the cryogenic vials containing sapphire disks and incubate for 2 - 3 h at RT in an orbital shaker at 120 rpm.

7. Replace the 30% epoxy resin with 70% epoxy resin by pipetting and incubate for 3 - 4 h at RT in an orbital shaker.

8. Using tweezers, transfer each sapphire disk, cell-side-up, to the cap of an embedding capsule. Add 90% epoxy resin to the cap. Incubate O/ N at 4 °C.

9. The next day, make fresh epoxy resin medium, as in step 4.4.

10. Transfer each sapphire disk, cell-side facing up, to the cap of an embedding capsule. Fill the cap with freshly prepared 100% epoxy resin. Change to fresh 100% epoxy resin every 2 h, repeating three times.

11. Place the samples in a 60 °C oven for 48 h to polymerize.

5. Mounting Samples

1. Place the sample upside-down on the stereomicroscope so that the sapphire disk is located at the top of the resin block. Remove the thin layer of epoxy resin from the top by scratching it with a razor blade.

2. Using a razor blade, cut a shallow line along the edge of the sapphire disk; this line helps to separate the sapphire disk from the epoxy resin in step 5.3.

3. Separate the sapphire disk from the epoxy resin by dipping it into liquid nitrogen for approximately 10 s.

NOTE: The cells will stay in the epoxy resin.

4. After removing the sapphire disk, use a dissecting scope to find an area with cells (4-10X magnification). Cut around the region of interest (~2 x 2 mm) using a razor blade (double-edged). To keep the specimen in place, perform this step while the specimen is taped to the surface of the microscope.

5. Mount the small piece of plastic (~2 x 2 x 5 mm) containing the cells using glue containing ethyl cyanoacrylate on a cylindrical dummy block made of epoxy resin. Incubate the block at 60 °C for 1 h.

6. Sectioning

1. Use an ultramicrotome to section the sample.
    1. Trim the surface of the plastic-embedded specimen with a glass knife at a speed of 3 mm/s and a thickness of 200 nm/section. Cut 4 - 5 sections from the surface where the astrocytes are located.
    2. Switch to a diamond knife and section at a speed of 0.8 mm/s and a thickness of 40 nm/section. Cut 20 - 25 sections.
2. Collect ribbons of sections on single-slot copper grids covered with 0.7% polyvinyl acetate.

7. Imaging Using a Transmission Electron Microscope (TEM)

1. Prior to TEM imaging, stain the section with 2.5% uranyl acetate in methanol for 5 min.

2. Wash the grid 15x in 50% methanol. Then, wash in ultrapure water 15x, with each wash lasting 30 s.

3. Briefly air-dry the section and place the grid into a specimen holder of the TEM.

4. Image at 93,000X magnification.

5. Acquire images.

   NOTE: Imaging is typically done blind to the time points or genotypes, and typically ~200 images are collected/time point.

8. Image Analysis

1. Analyze the images using a software (e.g., ImageJ) with a custom macro (Watanabe, Davis, and Jorgensen, unpublished). NOTE: The x/y coordinates are recorded from vesicles, the plasma membrane, the active zone membrane, and all other membrane-bound organelles at synapses. The text files containing the information are exported to another software (e.g., Matlab). The data are further analyzed using custom programs.

Representative Results

Using the protocol described above, we performed "flash-and-freeze" experiments in mouse hippocampal neurons expressing channelrhodopsin. These neurons were frozen either 15 ms or 100 ms after light onset. We have previously shown that the exocytosis and endocytosis of synaptic vesicles occur in the synaptic terminals at the 15 ms and 100 ms time points, respectively (Watanabe, Rost, et al. 2013c). These events were successfully captured at the appropriate times (**Fig. 2**), suggesting that flash-and-freeze experiments can be successfully performed on the chosen specialized high-pressure freezer.

Discussion

The "flash-and-freeze" approach visualizes membrane dynamics by inducing a particular cellular event with optogenetics and by freezing cells at defined time points after stimulation (Watanabe 2016). In this demonstration, we used channelrhodopsin, a light-sensitive cation channel, to stimulate neurons and captured the fusion and recovery of synaptic vesicles at the synaptic terminals. In recent years, many optogenetic tools have been developed (Weitzman and Hahn 2014; Niu et al. 2016), all of which are compatible with flash-and-freeze. For example, organelle trafficking can be induced using light-induced heterodimerization of cryptochrome and CIB1 (van Bergeijk et al. 2015). Similarly, the lipid composition of the plasma membrane can be altered by the light-induced translocation of phosphoinositide phosphatases to the plasma membrane (Idevall-Hagren et al. 2012). Furthermore, small, light-sensitive compounds like azobenzene change conformation depending on the illumination wavelengths. This conformational change can be used to activate ligand-gated channels or to change lipid composition in the membrane (Kramer, Fortin, and Trauner 2009; Frank et al. 2016). Caged compounds can also be used to induce cellular activity. However, the LED used in the current setup may not produce sufficient energy for uncaging; thus, further optimizations of the system are likely necessary. Nevertheless, the applications of these light-activatable tools are flexible-

many cellular events can be induced by a flash of light. "Flash-and-freeze" can capture the resulting membrane dynamics. There are two main limitations to the "flash-and-freeze" method. First, it captures "snapshots" of a particular event from different cells. In other words, it is not possible to follow membrane dynamics in one cell over a period of time. Thus, for the reconstruction of any cellular event, one must acquire and analyze a large number of images from each sample and at each time point. Furthermore, in neurons, an even larger number of images is necessary, since the fusion of synaptic vesicles only takes places in 20 - 30% of the synapses in mouse hippocampal neurons (Watanabe, Rost, et al. 2013c; Rosenmund, Clements, and Westbrook 1993a). The analysis of such a large dataset requires tremendous amounts of time. In the future, image acquisition and analysis need to be automated to make the approach more efficient (Denk and Horstmann 2004a; Knott et al. 2008). The second limitation is imposed by the nature of the high-pressure freezing technique. When cells freeze, cellular water rearranges to form ice crystals if the freezing rate is below 100 K/s (Dubochet 2007). These ice crystals can penetrate membranes or concentrate solutes to alter local osmotic pressure, resulting in the rupture of membranes. To avoid ice crystals, high pressure (~2,000 atm) is applied to the specimens. Due to the supercooling effect, a freezing rate of 100 K/s is sufficient to prevent water from forming ice crystals at this pressure (Dubochet 2007). In theory, specimens as thick as 500 μm can be frozen without ice crystals, but approximately 200 μm is likely the practical limit, as cuboidal forms of ice tend to form in thick tissue, compromising morphology. When processing specimens thicker than 5 μm, the use of a proper cryo-protectant, such as BSA, is necessary. However, BSA will change the osmolarity of the solution and may affect the physiological response of cells. Therefore, extensive control experiments are required to validate the use of BSA in particular systems. Ice crystals can also form after high-pressure freezing if the specimens are accidently removed from the liquid nitrogen bath. Thus, it is critical to keep the specimens in the liquid nitrogen at all times and to use pre-cooled forceps to manipulate them. When planning experiments, the following three points should be

considered. First, the maximal intensity of light (the 460 nm line) is 5.5 - 8.0 mW/mm (Betzig et al. 2006). Whether this intensity is sufficient to induce activity must be verified with live-cell imaging on a fluorescence microscope prior to flash-and-freeze experiments. Second, experiments must be performed at physiological temperature. The stage of the high-pressure freezer is warmed up to 37 °C for the experiments with mouse hippocampal neurons (Watanabe et al. 2014a). Finally, the time points must be carefully chosen to capture the membrane dynamics. Initial studies indicated that endocytosis is complete after 100 ms of stimulation. Thus, three additional time points (15 , 30, & 50 ms) were also examined to follow the membrane dynamics (Watanabe, Liu, et al. 2013a; Watanabe, Rost, et al. 2013c). These time points were necessary to visualize membrane trafficking events during synaptic transmission. However, the requirement for the number of time points are different in each cellular event. Therefore, a few time points should be sampled before initiating large dataset collection.

Figures

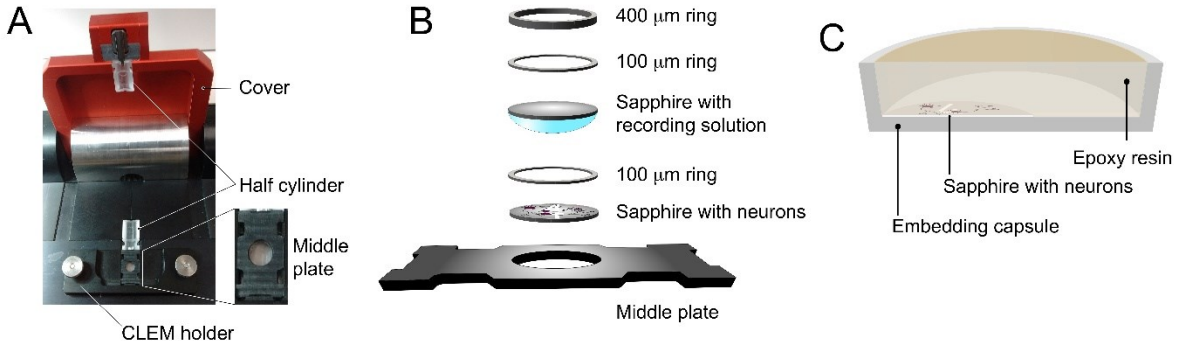

D A single stimulus, 90 ms rest

Line	Dark Phase [ms]	Period [ms]	Pulse [ms]	# Periods
1	15000	100	10	1
2	0	0	1	0

E 10 stimuli, 20 Hz, 5 ms rest

Line	Dark Phase [ms]	Period [ms]	Pulse [ms]	# Periods
1	15000	50	10	9
2	0	15	10	1

Figure 1 Sample loading and programming in the high-pressure freezer.

A) Sample loading table of a high-pressure freezer. The middle plate, shown in the inset for structural detail, is placed in a CLEM holder for sample loading. One of the half-cylinders is placed at the bottom part of the sample loading table, and the other is attached with a clip to the top cover. Once the sample is loaded, the middle plate is pushed forward to the bottom half-cylinder and the cover is closed to initiate the freezing. **B)** Specimen assembly. The sapphire disk containing neurons is placed in the well of the middle plate, with the cell-side facing up. A 100 µm ring is placed directly above the sapphire disk inside the well. Then, an empty sapphire disk dipped in physiological saline is placed with the solution-side down. Air bubbles must be avoided. Finally, a 100 µm ring and a 400 µm ring are snugly placed above. Any extra liquid is removed with filter paper. **C)** A cross-section of an embedding capsule with the sapphire disk submerged in epoxy resin. The sapphire disk is placed at the bottom of the capsule, with the cell-side facing up and covered with epoxy resin for infiltration and embedding. **D)** Programming the high-pressure freezer for a single, 10 ms stimulus. The specimens are frozen 90 ms after

the light pulse. **E)** Programming the high-pressure freezer for 10 stimuli at 20 Hz. The specimens are frozen 5 ms after the last light pulse.

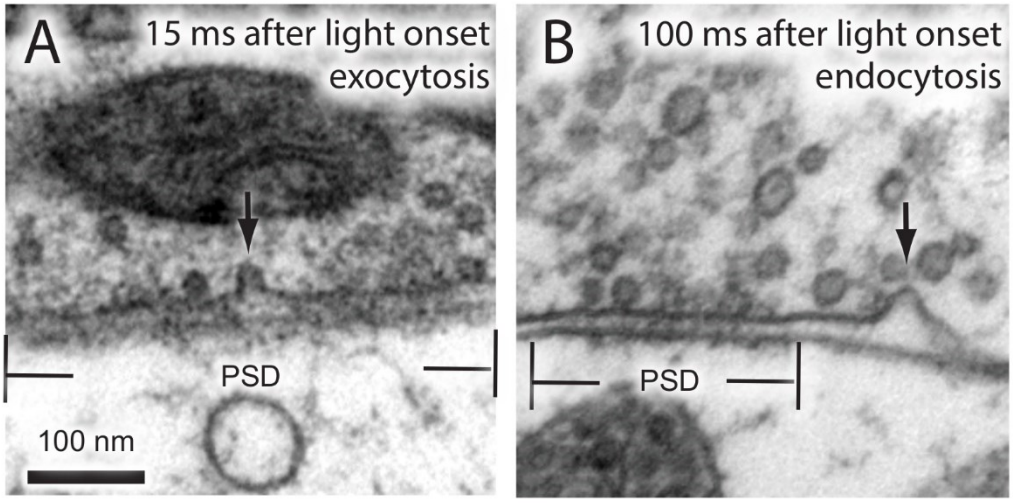

Figure 2 Visualization of exocytosis and endocytosis in mouse hippocampal neurons

Hippocampal neurons are stimulated once and frozen at the indicated times. Electron micrographs show the exocytosis of a synaptic vesicle **A)** and ultrafast endocytosis **B)**. PSD, post-synaptic Density.

Chapter 3

Asynchronous release sites align with NMDA receptors

Abstract

Neurotransmitter is released synchronously and asynchronously following an action potential. Our recent study indicates that the release sites of these two phases are segregated within an active zone, with asynchronous release sites enriched near the center in mouse hippocampal synapses. Here we demonstrate that synchronous and asynchronous release sites are aligned with AMPA receptor and NMDA receptor clusters, respectively. Computational simulations indicate that this spatial and temporal arrangement of release can lead to maximal membrane depolarization through AMPA receptors, alleviating the pore-blocking magnesium leading to greater activation of NMDA receptors. Together, these results suggest that release sites are likely organized to activate NMDA receptors efficiently.

Introduction

Neurotransmitter is release synchronously within a millisecond of an action potential and several milliseconds later (Kaeser and Regehr 2014). Bothe phases of release result from exocytosis of synaptic vesicles at a specialized membrane domain: the active zone (Heuser et al. 1979). Within the active zone lie one or more release sites individual units at which a single synaptic vesicle may fuse (Kaeser and Regehr 2017). Our recent work suggests that release sites for synchronous and asynchronous release occupy unique domains within an active zone: synchronous release sites are uniformly distributed, while asynchronous release sites are abundant near the center of an active zone (Kusick et al. 2020). However, the functional importance of this spatial organization is unknown.

For excitatory signaling in the central nervous system, glutamate released from presynaptic boutons activates receptors on the postsynaptic membrane. Two ionotropic

receptors are critical: α-amino-3-hydroxy-5-methyl-4-isoxazolepropionic acid (AMPA) receptors and N-methyl-D-aspartate (NMDA) receptors (John M. Bekkers and Stevens 1989; Dingledine et al. 1999b). These receptors are recruited to the receptive field by scaffolding proteins that make up electron-dense cytomatrix, or postsynaptic density (PSD) (Hunt, Schenker, and Kennedy 1996).

Given the low sensitivity of these receptors for glutamate binding (C. M. Tang, Dichter, and Morad 1989; Trussell and Fischbach 1989; Patneau and Mayer 1990; Erreger, Dravid, et al. 2005) activating them requires high concentration of glutamate. Thus, the spatial organization of synchronous and asynchronous release sites may be important for the activation of receptors by increasing the glutamate concentration near the receptors.

A large body of work suggests that the number of these receptors, rather than their location relative to release sites, is the main determinant of how signals are transmitted across synapses. At mammalian central synapses, the number of AMPA receptors is highly variable, ranging from zero to several hundred (Z. Nusser et al. 1994b; Popratiloff, Weinberg, and Rustioni 1996; Kharazia and Weinberg 1997b; Maria E Rubio and Wenthold 1997; Y. Takumi et al. 1999; Masugi-Tokita et al. 2007b). However, the number of AMPA receptors scales with the size of postsynaptic densities (Y. Takumi et al. 1999; Masugi-Tokita et al. 2007b; Tarusawa et al. 2009; Z. Nusser et al. 1998; Matsuzaki et al. 2001) and thus, the postsynaptic membrane is highly occupied by the receptors. Given ~2000 glutamate molecules released per fusion events (Burger et al. 1989), one would expect these receptors to be activated efficiently regardless in the PSD they are located relative to where glutamate is released. In fact, some computer simulation suggest that the receptor number is more important for the amplitude of synaptic signaling than the location of release (Tarusawa et al. 2009; Holmes 1995; Wahl, Pouzat, and Stratford 1996).

In contrast to this view, recent studies suggest that receptor activation is greatly influenced by receptors forming clusters that are positioned close to release sites (Biederer,

Kaeser, and Blanpied 2017b). Due to rapid diffusion (Uteshev and Pennefather 1996; Zheng et al. 2017; Bartol, Keller, et al. 2015), the concentration of glutamate necessary for maximal AMPA receptor activation is only achieved at the point of release. In fact, several computer simulations demonstrate that the open probability of AMPA receptors is reduced by 20-70% if located 100 nm away from the point of release (Tarusawa et al. 2009; Uteshev and Pennefather 1996; Xu-Friedman and Regehr 2004; Raghavachari and Lisman 2004b). Several electrophysiology experiments also suggest that glutamate release from single vesicles does not saturate postsynaptic receptors (Ishikawa, Sahara, and Takahashi 2002; Liu, Choi, and Tsien 1999; McAllister and Stevens 2000). In addition, localization studies suggest that AMPA receptors are clustered within the postsynaptic density (Nair et al. 2013b; MacGillavry et al. 2013b) and segregated from the NMDA receptor clusters (Goncalves et al. 2020). Release sites are aligned with clusters of AMPA receptors (A.-H. Tang et al. 2016) and their association through trans-synaptic adhesion proteins affects the magnitude of synaptic transmission (Haas et al. 2018). Thus, where glutamate is released relative to receptors may be important for their activation.

The timing of glutamate release is also a key component for receptor activation, particularly for NMDA receptors. NMDA receptors must bind two glutamate molecules to activate(Nahum-Levy et al. 2001; Vargas-Caballero and Robinson 2004). Depending on the concentration of glutamate, only a single binding site may be occupied, leading to desensitization rather than activation (Nahum-Levy et al. 2001; Vargas-Caballero and Robinson 2004). However, the single-bound state can last for tens of milliseconds, during which the second release can favor their activation (Nahum-Levy et al. 2001; Vargas-Caballero and Robinson 2004). In addition, at resting membrane potential the pore of NMDA receptors is blocked by magnesium ions, which must be removed by membrane depolarization (Mayer, Westbrook, and Guthrie 1984; Nowak et al. 1984; Seeburg et al. 1995). Classically, paired stimuli are applied for NMDA receptor activation (Malinow and Miller 1986; Kauer, Malenka, and

Nicoll 1988; Bi and Poo 1998). However, a single stimulus can potentially prime NMDA receptors for activation, with synchronous release depolarizing the postsynaptic membrane and asynchronous release providing extra glutamate. Thus, both the location and timing of glutamate release are likely important for determining how signals are transmitted at excitatory synapses.

To test whether asynchronous release sites have a spatial relationship with receptors, we developed an approach to localize fusion pits and receptors at the ultrastructural level. We demonstrate that synchronous and asynchronous release sites are aligned with cluster of AMPA and NMDA receptors, respectively. Computer simulation suggest that this organization can induce membrane depolarization through the AMPA receptors and activate NMDA receptors more efficiently. These data indicate that one potential role of this spatial organization of synchronous and asynchronous release sites is to prime NMDA receptors for activation.

Materials and methods

All animal procedures were performed according to the National Institute of Health guidelines and were approved by the Animal care and Use Committee at the Johns Hopkins University School of Medicine.

Animals

Wild type mice (C57/BL6J) were purchased from Charles Laboratory and Gria2$^{(+/-)}$ mouse line was kindly provided by Dr. Richard Huganir. Gria2$^{(+/-)}$ line was maintained as heterozygous and knock-out Gria2$^{(-/-)}$ pups at postnatal day 0 (P0) were used for neuronal culture.

Neuron culture

Both astrocytes and hippocampal neuron cultures were established from embryonic day 18 or P0 wild-type animals. Both sexes were indistinguishably used in this study. Astrocytes were harvested from cortices with trypsin treatment for 20 min at 37 °C with shaking, followed by

dissociation and seeding on T-75 flask. Astrocytes were grown in DMEM supplemented with 10% FBS and 0.1% penicillin-streptomycin at 37 °C and 5 % CO2 for 7-10 days. Two clean 6 mm sapphire disks (Technotrade Inc) were placed per well of 12-well tissue culture plate and coated with poly-D-lysine (1 mg/ml, Sigma) and collagen (ThermoFisher). Astrocytes serve as a feeder layer for neurons and were seeded (50,000/well) one week before hippocampal neuronal culture. On day 6, FUDR (80 uM) was added to inhibit cell division. On day 7, hippocampi were isolated and digested with papain (20 U/ml) for 30-60 min at 37 °C with shaking. An inactivation solution (2.5 mg of trypsin inhibitor and 0.5 mg of albumin per mL of DMEM) was then applied for 5 min at 37 °C. Hippocampi were triturated by pipetting 4 x 20 times, and cells were seeded on prepared astrocyte feeder layer with a density of 75,000/well and maintained in Neurobasal A media supplemented with B-27, Glutamax, and 0.2 % penicillin-streptomycin at 37 °C and 5 % CO_2. The cells were infected with lentivirus at days *in vitro* (DIV) 3-4 as needed and used for experiments on DIV 13-17.

Expression constructs

Lentiviral expression constructs were used to express transgenes in neurons. All vectors were based on the lentiviral shuttle vector FUGW (Lois et al. 2002). Gria2 cDNA was N-terminally tagged with HaloTag and cloned in frame downstream of synapsin-1 promoter with NLS-GFP-P2A (NGP) sequence (a gift from Christian Rosenmund lab). The NLS-GFP signals were used to evaluate viral infection and intensity of transgene expression from this polycistronic construct. Nucleotides corresponding to hexa-histidine residues were inserted in Gria2 sequence downstream of the signal sequence using Gibson cloning strategy and NEB builder kit (New England Biolab) to generate NGP-(His)6-GluA2. To generate NGP-SnapTag::GluA2, the hexa-histidine tag was replaced with a SnapTag by In-Fusion cloning (Takara Bio). pCI-SEP-NRI was a gift from Robert Malinow (Addgene plasmid # 23999; http://n2t.net/addgene:23999 ; RRID:Addgene_23999) (Kopec et al. 2006). Nucleotides

corresponding to hexa-histidine were inserted downstream of the signal sequence of NR1 using Gibson cloning strategy and NEB builder kit (New England Biolab) followed by sub-cloning into the lentiviral shuttle vector FUGW to obtain NGP-(His)6-NR1. To generate NGP-SnapTag-NR1, the hexa-histidine tag was replaced with a SnapTag by In-Fusion cloning (Takara Bio).

Lentivirus production and infection

Lentiviruses carrying the expression constructs were produced using the following procedures. The bottom surface of T-75 flasks was coated with poly-L-lysine (0.2 % in milliQ water). A day before the transfection, HEK293T cells were plated at $6.5x10^5$/ml (10 ml in T-75) in Neurobasal A (NBA) media containing 1 % glutamax, 2 % B27, and 0.2 % penicillin-streptomycin. The shuttle vector (FUGW) (Lois et al. 2002) containing expression constructs and helper plasmids (VSV-G and CMV-dR8.9) were mixed at 20, 5, and 7.5 µg, respectively, in 640 µl NaCl solution (150 mM) (Solution I). Another solution (solution II) was prepared as follows: 246.7 µl H_2O, 320 µl NaCl (300 mM), 73.3 µl polyethylenimine (0.6 µg/µl). Solution I and II were mixed by vortexing and incubated at room temperature for 10 minutes, followed by addition to the T-75 flask containing HEK293T cells. The cells were incubated at 37 ºC (5 % CO_2), and the viruses were harvested 3 days later. The media containing lentivirus was centrifuged at 4000 rpm to obtain 20-fold concentration using Amicon (Ultracel-100k). The infection efficiency was determined by infection in wild-type neurons that were separately prepared. For all the experiments, dissociated hippocampal neurons were infected on DIV 3-4 with lentiviruses carrying the expression constructs. The infection rate of 95 % was achieved in all cases.

Ni-NTA-gold labelling

For gold labelling, solution containing Ni-NTA-gold (Nanoprobes) was added to each well containing two sapphire disks so that the final concentration of 5 nM is achieved. Cells were incubated for 30 min in the CO_2 incubator set at 37 ºC. Each disk was washed thoroughly by

agitating in a small petri dish (30 mm) containing physiological saline solution (140 mM NaCl, 2.4 mM KCl, $CaCl_2$ 1.2 mM, and 3.8 mM $MgCl_2$, 10 mM HEPES, 10 mM glucose; pH adjusted to 7.3 with NaOH, 300 ± 5 mOsm). The washing procedure was repeated three times to minimize background labelling. Immediately after washing, cells were mounted for high-pressure freezing.

High-pressure freezing and freeze-substitution

Cells cultured on sapphire disks were frozen using a high-pressure freezer (EM ICE, Leica Microsystems). Following gold labelling, each disk with neurons was transferred into the physiological saline solution containing NBQX (3 µM, Tocris) and bicuculine (30 µM; Tocris), which were added to block recurrent synaptic activity during the zap-and-freeze experiments. The disk was mounted onto the photoelectric middle plate with neurons facing up. A 100 µm spacer ring was placed on top of the sapphire disk. Then, another blank sapphire disk was placed on top of the spacer ring to make a “sandwich”. Finally, a rubber ring was put on top of the “sandwich” to hold it in place. The entire assembled middle plate was then placed on a piece of filter paper to remove the excess liquid, loaded between two half cylinders, and transferred into the freezing chamber. An electrical field of 10 V/cm was applied for 1 ms to induce a single action potential, and cells were frozen 5 ms and 11 ms after the stimulus (Kusick et al. 2020). These time points are chosen based on our recent study suggesting that pits captured at these time points represent fusion intermediates during synchronous and asynchronous release, respectively (Kusick et al. 2020). The exact proportion of these events could not be determined, but based on EGTA experiments, asynchronous release may account for up to 20% of the currents in these synapses (Grauel et al. 2016; Hagler and Goda 2001). A 1-ms electrical pulse likely induces an action potential from all neurons on a disk uniformly, and approximately 35 % of synapses exhibit fusion pits (Kusick et al. 2020) – consistent with the synaptic release probability of these synapses (Hessler, Shirke, and Malinow 1993; Rosenmund, Clements, and Westbrook 1993b; Allen and Stevens 1994; Ermolyuk et al. 2013; Wenzel et al. 2012). For no

stimulation control, the photoelectric middle plate was programmed not to discharge. The frozen sample was automatically dropped into a storage dewar filled with liquid nitrogen.

After freezing, the middle plate with sapphire disks was transferred to a cup containing anhydrous acetone (-90 ºC), which was placed in an automated freeze substitution system (EM AFS2, Leica microsystems) using pre-chilled tweezers. The cryovials containing fixative (1% glutaraldehyde, 1% osmium tetroxide, and 1% water in anhydrous acetone) were stored in liquid nitrogen and moved to AFS2 before use. After disassembling the freezing apparatus, sapphire disks with neurons were transferred into cryovials in the AFS, which is set at -90 ºC, using pre-chilled tweezers. The freeze substitution program was as follows: -90 °C for 6-10 hours, -90 °C to -20 °C in 14 hours, -20 °C for 12 hours, and -20 °C to 20 °C in 4 hours.

Embedding, sectioning and transmission electron microscopy

Following freeze-substitution, fixatives were washed with anhydrous acetone for three times, 10 min each. After washing, samples were infiltrated through 30 %, 70 % and 90 % epon-araldite in anhydrous acetone every two hours. Then samples were transferred to caps of polyethylene BEEM capsules with 90 % epon araldite and incubate overnight at 4 °C. Next day, samples were incubated in the caps of polyethylene BEEM capsules with 100% epon araldite (epon 6.2 g; araldite 4.4 g; DDSA 12.2 g, and BDMA 0.8 ml) at room temperature. Samples were transferred to new caps with fresh 100 % epon araldite every 2 hours three times, after which samples were baked at 60 °C for 48 hours.

After resin was cured, sapphire disks were removed from resin. Cells were embedded in the resin block. Then, the block was cut into small pieces and place atop of a dummy block using super glue for sectioning. 40 nm sections were cut using an ultramicrotome (EM UC7, Leica microsystems) and collected on single-slot copper grids coated with 0.7 % pioloform. The sections were stained with 2.5 % uranyl acetate in 75 % methanol and then imaged at 80 kV at the 93,000x magnification on a Philips CM120 transmission electron microscope equipped with

an AMT XR80 camera. About 100 electron micrographs per sample were taken blindly. To avoid the sampling bias, synapses were found by bidirectional raster scanning along the section at 93,000x. Synapses were identified by a vesicle-filled presynaptic bouton and a postsynaptic density.

Spin-mill serial block face imaging

Samples were sent to ThermoFisher for spin-mill serial block face imaging. Spin-milling experiments were performed on a DaulBeam instrument (Thermo Fisher Scientific, Helios Hydra). A whole resin block (6 mm diameter) was glued onto a scanning electron microscope (SEM) stub using silver conductive epoxy without pre-trimming or sputter coating. The sample was positioned at the eucentric position of the system, and the stage was tilted to -34 degrees, such that the focused-ion beam (FIB) angle of incidence was 4 degrees from glancing relative to the sample surface.

The spin-milling process consists of the following sequence. First, oxygen FIB beam (12 keV, 65 nA) was applied in a 400 µm x 100 µm box pattern on desired sample area for 10 s (dwell time set at 200 ns) to expose a new surface of the sample. The stage was compucentrically rotated 60 degrees, and the sample milled again with another FIB exposure. This process was repeated 6 times to achieve a full 360-degree rotation of the sample. Ion flux was delivered to the sample from several different azimuthal directions to reduce textural artifacts generated during the ion milling. One full rotation of milling constituted a “z slice”. Second, the sample was tilted back to a stage tilt of zero degree to perform SEM imaging. Images were collected from multiple regions-of-interest. These two steps were automated with Autoscript software (Thermo Fisher Scientific) and repeated until the desired volume of images was collected – similar to the serial block face imaging technique (Denk and Horstmann 2004b). The milling slice thickness was controlled to achieve 20 nm. Ten areas of interests were acquired in parallel with a X, Y pixel size of 1 nm. A total of ~40 slices was collected from each

sample. The resulting 3-D datasets were aligned and visualized using the Amira software (Thermo Fisher Scientific).

Electron microscopy image analysis

All the images from a single experiment were shuffled for analysis as a single pool using a custom R (R Development Team) script. Images that could not be reliably segmented, either because the image was not of a bona fide synapse or morphology was too poor, were excluded from segmentation; this was done only after randomizing the images. No other data were excluded. The plasma membrane, active zone, postsynaptic density, docked synaptic vesicles, synaptic vesicles close to the active zone, pits (putative fusion events), and gold particles were annotated in ImageJ using a custom macro. The active zone was identified as the region of the presynaptic plasma membrane juxtaposed to the postsynaptic density. Docked vesicles were identified by their membrane appearing to be in contact with the plasma membrane at the active zone (0 nm from the plasma membrane), that is, there are no lighter pixels between the membranes. Pits were identified as smooth curvature (not mirrored by the postsynaptic membrane) in an otherwise straight membrane. These pits are considered exocytic (Kusick et al. 2020). Pits outside the active zone are considered endocytic or membrane ruffles, as this is the primary site for ultrafast endocytosis (Watanabe, Liu, et al. 2013b). Under these criteria, we could miss or over-annotate vesicles and pits. To minimize the bias and maintain consistency, all image segmentation, still in the form of randomized files, was thoroughly checked by a second member of the lab. However, no corrections were made for synaptic vesicles since vesicles are much more abundant, and the same criteria were used to annotate them in all conditions. A similar amount of overestimate is expected in this case. Features were then quantitated using custom MATLAB (MathWorks) scripts.

Location of pits, docked vesicles, and gold particles within the active zone/postsynaptic density from single sections were calculated from the distance from the center of the pit to the

center and the edge of the active zone in 2D. Distance from the center was normalized by dividing the distance to the edge by the half-width of the active zone. For 3D data, the distance to the center of the active zone was calculated from serial sections. First, the location in 2D was calculated as above. Then, the 3D distance was calculated to the center of the active zone in the middle section of the series using the Pythagorean theorem with the assumption that each section is the same thickness and the center of the active zone aligns in each image. Locations in 3D data were further corrected to be the density of vesicles/pits at each distance from the center of the active zone or postsynaptic density. To calculate density of vesicles, pits, and gold particles from the center to the edge in 3D reconstructions, the radial position of each vesicle/pit/gold particle was converted to the fractional area of a circle bounded by that radius. In the case of a unit circle (distance from center to edge is by definition 1 when data normalized to the size of the postsynaptic density), this is simply the square of the original normalized distance to the center. Example micrographs shown were adjusted in brightness and contrast to different degrees (depending on the varying brightness and contrast of the raw images), rotated, and cropped in Adobe Photoshop.

Cluster analysis

Sequential annotated electron microscopy slices of gold-labelled NMDA and AMPA receptors were used to generate a 3-D spatial map of receptors for each synapse (MATLAB 2019b, Mathworks). For each synapse, K-means clustering (Lloyd's algorithm) was performed for 1 to N number clusters, where N is the total number of gold-labelled receptors. The optimal number of clusters was obtained by calculating the knee-point of the within-cluster sum of square differences (SSD) as a function of number of clusters. A final generated synapse with the optimized number of clusters was then rendered over each synapse for both AMPA and NMDA receptors. These spatial maps allow visualization and measurement of the locations of each receptor with respect to the center of the synapse. To determine whether the clustering of

these receptors was due to chance, for each mapped synapse and respective number of particles, we generated 50 maps with randomized particle positions using custom scripts. The above K-means clustering paradigm was then run on all 50 maps and the mean SSD was recorded for each synapse. 2D scatter plots of SSD and synaptic sizes for the experimental and randomized condition for AMPA and NMDA receptors were generated, where low SSD indicates more tightly packed clusters. Linear regression analysis (Prism 8.2.0, GraphPad) was run for each set of conditions to determine whether the experimentally-clustered receptors were significantly different than randomized clusters.

Computer simulations

Computer modeling was performed using the MCell/CellBlender simulation environment (mcell.org) version 3.5.0-9 for Linux. The realistic model of glutamatergic synaptic environment was constructed from 3-D electron microscopy of hippocampal area CA1 neuropil as previously described (Bartol, Keller, et al. 2015; Bartol, Bromer, et al. 2015; Kinney et al. 2013). The kinetic scheme and kinetic rate constants for AMPAR (GluAR) activation and desensitization by glutamate were obtained from previously published reports ,see ref (Jonas, Major, and Sakmann 1993) for details of the kinetic scheme and ref (Haas et al. 2018) for the rate constants. The NMDAR kinetics were obtained from Vargas-Caballero and Robinson (Vargas-Caballero and Robinson 2004). Since the time course of the diffusion and presence of glutamate in the synaptic cleft is especially important in the model presented here, our model also included realistic extracellular space a kinetic model of glutamate transporters distributed on astrocytic glial processes in the surrounding neuropil as previously described (Bartol, Keller, et al. 2015).

The initial distribution of AMPA and NMDA receptors as well as the location of the presynaptic neurotransmitter release site was established by running a dynamic simulation to allow self-organization of the distributions. To accomplish this, two surface properties were defined: the synapse and the postsynaptic density (identified on electron microscopy data).

According to the literature 200 PSD-95 molecules, 60 AMPA receptors, and 30 NMDA receptors were available on the spine head. These molecules were allowed to freely diffuse at the synapse. Inside the postsynaptic density, PSD-95 was reversibly palmitoylated (pPSD-95) at a defined rate (kon=35, koff=0.7).

A clusterization point called “L” was placed at the center of the postsynaptic density. pPSD-95 aggregates in contact with L (kon = 7, koff = 1) to form a domain. Mobile NMDA receptors interacted with this domain and were trapped into an NMDA receptor cluster (kon = 10, koff = 1). A mobile “G” molecule was released inside the postsynaptic density and was immobilized at random location when it randomly interacted with a pPSD-95. After immobilization, the molecule of “G” recruited the insertion of a pre-synaptic neurotransmitter release site into the pre-synaptic membrane at the point closest to the location of G. At the same time, “G” clustered pPSD-95 (kon = 100, koff = 1) which, in turn, clustered AMPA receptor (kon = 10, koff = 1).

The approach to a final steady-state organization of AMPA receptor, and NMDA receptor at the synapse was simulated with a time step of 1 ms for 10,000 iterations (10 s), until reaching a steady. It is important to note that the means employed here to achieve receptor organization is only intended to give the desired final organization in our model and is not intended to model the physiological mechanisms by which this occurs in real synapses. After reaching the desired organization, the simulations were switched to a time step of 1 μs for 250,000 iterations to model the AMPA receptor and NMDA receptor and when the glutamate was released at the pre-synaptic level, in front of the “G” aligned with AMPA receptor or in front of “L” aligned with the NMDA receptor.

After binding neurotransmitter, the flux of ionic current through activated NMDAR is voltage-dependent due to channel blockade by Mg^{2+} at hyperpolarized membrane potential (Nowak et al. 1984). We simulated this voltage-dependent blockade by a method described previously (Bartol, Keller, et al. 2015). Briefly, the neural simulation program NEURON was used to simulate excitatory postsynaptic potentials of the desired timing and amplitude in the

spine head located on the dendritic branch of a modeled pyramidal neuron. The time-varying voltages recorded at the spine during these stimuli were used to drive voltage-dependent transition rates in the model of NMDA receptor activation kinetics. The membrane potential waveform simulated following a single vesicle release is consistent with the previous estimate of voltage change in spines (L. M. Palmer and Stuart 2009; Harnett et al. 2012). The voltage changes alter the kinetic constants for relief of the Mg^{2+} block of the NMDA receptors and determine the ion current flux through open NMDA receptors. Each individual NMDA receptor channel opens and fluxes current in the simulation only when glutamate is bound to the receptor at the time that the Mg^{2+} block is relieved. MCell uses stochastic Monte Carlo methods and simulation results reflect the realistic behavior of stochastic channel fluctuations. For all computational experiments, 48 trials were performed, allowing estimation of the mean and standard deviation of the time course of channel activation.

Statistical analysis

All data showing distribution of receptors, vesicles, and pits are pooled from multiple experiments. The number data shown are per experiment. All data were initially examined on a per-experiment basis (with all freezing done on the same day and all segmentation done in a single randomized batch); none of the pooled data show any result that was not found in each replicate individually. We did not predetermine sample sizes using power analysis, but based them ($N = 2\text{-}3$, $n > 200$) on our prior experience with flash-and-freeze data (Watanabe, Liu, et al. 2013b; Watanabe, Rost, et al. 2013a; Watanabe et al. 2014b). An alpha of 0.05 was used for statistical hypothesis testing. All data were tested for normality by D'Agostino-Pearson omnibus test to determine whether parametric or nonparametric methods should be used. Comparisons between two groups were performed using a two-tailed Welch two-sample t-test or Wilcoxon rank-sum test. Comparisons between multiple groups followed by full pairwise comparisons were performed using one-way analysis of variance (ANOVA) followed by Tukey's HSD test or

Kruskal-Wallis test followed by Dunn's multiple comparisons test. For testing whether locations of pits or receptors were biased toward the center or edge of the synapse, a two-tailed one-sample t-test or Wilcoxon rank-sum test with a theoretical median of 0.5 was used (each of these p-values, as well as that of the comparisons between pit locations in different samples, were accordingly corrected for multiplicity using Bonferroni's method). All statistical analyses were performed and all graphs created in Graphpad Prism.

Results

Validation of small-metal affinity staining of His-tag proteins

To reveal the spatial and temporal relationship between release sites and receptors, we need an approach to visualize receptors relative to fusions events observed by electron microscopy. To this end, we developed a method to label these receptors with gold particles using a high-affinity interaction between nickel and polyhistidine (His-tag, hereafter; **Fig. 3a**) (Hainfeld et al. 1999). GluA2 (AMPA receptor subunit) tagged on its extracellular domain with His-tag or HaloTag (Los et al. 2008) was expressed in the cultured wild-type mouse hippocampal neurons using lentivirus. HaloTag::GluA2 served as a negative control to test the specificity of Ni-NTA-gold labelling. We incubated these neurons with Ni-NTA-gold (5 nM) for 30 min and subjected them to high-pressure freezing. Frozen samples were then prepared for electron microscopy, and 40-nm thick sections collected. About 100 electron micrographs were acquired per experiment from each condition and quantified blinded to treatment (**Fig. 6a** for example micrographs), and each experiment was repeated three times. In the wild-type neurons expressing His-tag::GluA2, approximately 70% of synaptic profiles contained gold particles in the synaptic cleft; the median number of gold particles was 2.6 per synaptic profile (**Fig. 6c,d**; note that synaptic profiles are random 40-nm segments of synapses). The amount of staining is consistent with antibody-based approaches (Z. Nusser et al. 1994b; Popratiloff, Weinberg, and Rustioni 1996; Kharazia and Weinberg 1997b; Maria E Rubio and Wenthold 1997). In contrast, almost no gold particles were observed in controls expressing HaloTag::GluA2 (~4% synaptic profiles, 0.03 gold/synapse, **Fig. 6a,c-d**, **Table 1** for details), suggesting that the labelling is specific.

We next repeated the same experiments in GluA2 knock-out neurons (*Gria2*$^{-/-}$) to test if the overexpression of the GluA2 in wild type would significantly change the number of receptors at the postsynaptic density. No differences were observed between wild-type and knock-out

neurons (**Fig. 6b-f**). These results suggest that this affinity-based labelling can report the distribution of receptors at the ultrastructural level. We named this approach small-metal affinity staining of His-tag, or SMASH.

AMPA and NMDA receptors are segregated within the PSD

With the labelling approach validated, we next measured the locations of AMPA and NMDA receptors within the postsynaptic density. We expressed either His-tag::GluA2 or His-tag::NR1 in wild-type neurons. In single profiles, AMPA receptors were biased towards the edge of the postsynaptic density ($p < 0.001$), whereas NMDA receptors were uniformly distributed (**Fig. 3b-d**; $p > 0.8$), suggesting they may occupy different domains within the postsynaptic density (**Fig. 3b-d**; $p < 0.001$). However, single synaptic profiles are random representations of synapses; each image represents a 40-nm segment of a synapse, sliced at a random location. These slices are not necessarily going through the center of an active zone/postsynaptic density. Nonetheless, the data from synaptic profiles can be used to estimate the distributions when sufficient data are collected (**Fig. 7a**). To more accurately localize receptors, we reconstructed synapses using spin-mill serial block face imaging (**Fig. 3e**, **Fig. 7**, N = 2; see **Methods** for details). Unlike traditional serial block face imaging approaches, spin milling using an oxygen plasma ion beam enables imaging of large areas (400 µm x 400 µm) with isotropic resolution of ~5 nm (Sergey et al. 2018). At least 17 synapses were reconstructed from each sample, and experiments repeated from two independent samples. Similar to single profiles, AMPA and NMDA receptors were differentially distributed in the reconstructed postsynaptic densities (**Fig. 3f**, $p < 0.001$). As in single profiles (**Fig. 3d**), AMPA receptors were biased towards the edge (**Fig. 3f**, $p < 0.001$, **Fig. 7b** for more example). Interestingly, NMDA receptors were enriched around the center of the postsynaptic density (**Fig. 3e, f**, $p < 0.001$, **Fig. 7d** for more example). The distributions of these receptors are consistent with previous experiments using single-molecule localization microscopy (Nair et al. 2013b; Goncalves et al. 2020) and

electron microscopy (Kharazia and Weinberg 1997b; Chen et al. 2008b). These data suggest that AMPA receptors and NMDA receptors are differentially localized within the postsynaptic density.

AMPA and NMDA receptors are clustered in the PSD

Both AMPA and NMDA receptors qualitatively seemed clustered (Nair et al. 2013b) in the reconstructed synapses. To test this quantitatively, we performed K-means cluster analysis on the reconstructed synapses (**Fig. 3g, h**). The same analysis was then repeated 50 times with particle locations randomized within the postsynaptic density for each synapse. The sums of square differences were compared between the actual locations and randomized locations (see **Methods** for detail). The areas of postsynaptic densities were similar between samples (**Fig. 3i**), and thus the data are not normalized. The median numbers of the AMPA receptor and NMDA receptor clusters were 2 and 1 per synapse, respectively, based on the K-means analysis (**Fig. 3j**). The median numbers of AMPA and NMDA receptors were 8 and 6 per cluster (**Fig. 3k,** ranges: 4-23 AMPA receptors and 4-18 NMDA receptors), or 16 and 10 per synapse (**Fig. 3l**, full ranges: 0-58 AMPA receptors and 0-55 NMDA receptors). These numbers correspond to 200 and 135 per μm^2, respectively (full ranges: 0-1021 AMPA receptors and 0-1079 NMDA receptors) and comparable to previous estimates from the freeze-fracture immuno-gold labelling of adult rat cerebellum (Masugi-Tokita et al. 2007b) and immuno-electron microscopy of rat hippocampus (Z. Nusser et al. 1998). Since ~20 AMPA receptors are likely available in each nano-domain (ranges: 7.3-42.2) (Nair et al. 2013b), our labeling efficiency is likely ~50 %. Nonetheless, these results are consistent with the single molecule localization study (Goncalves et al. 2020)and suggest that AMPA receptors tend to form ~2 clusters (**Fig. 3i**) and surround the NMDA receptor cluster, located near the center of the postsynaptic density.

Asynchronous release sites are aligned with NMDA receptors

Recent studies suggest that release sites are trans-synaptically aligned with AMPA receptors (A.-H. Tang et al. 2016). Our data indicate that NMDA receptors occupy different domains within the postsynaptic density (**Fig. 3d, f**). Thus, it is not clear if NMDA receptors also align with release sites. Interestingly, their distribution near the center of the postsynaptic density mirrors the recently described distribution of asynchronous release sites in the active zone (Kusick et al. 2020). To test whether asynchronous release sites and NMDA receptors are aligned, we performed zap-and-freeze experiments after SMASH labelling. Neurons expressing SnapTag::GluA2 or SnapTag::NR1 were used as controls for background gold staining (**Fig. 8a-f**). Specifically, we stimulated neurons expressing fusion proteins once and froze them after 5 and 11 ms. Our recent study suggested that fusion intermediates captured at 5 ms represent remnants of synchronously fusing vesicles, while those at 11 ms represent asynchronously fusing vesicles, since the treatment with EGTA-AM only eliminated the latter events (Kusick et al. 2020). The numbers and distributions of docked vesicles and exocytic pits were all consistent with our previous studies (docked: 1.9 ± 0.05 per synaptic profile; pits: 0.28 ± 0.03 per synaptic profile **Fig. 4c, Fig. 8g,h**) (Kusick et al. 2020; Watanabe, Liu, et al. 2013b; Watanabe, Rost, et al. 2013a) . Of note, asynchronous fusion intermediates at 11 ms were strongly biased towards the center (**Fig. 4a-b, d**, median = 0.1, $p < 0.001$, **Fig. 8a-d** for more example micrographs). Thus, the distribution of fusion events during asynchronous release is similar to that of NMDA receptors.

To test the spatial relationship between fusion events and receptors, we measured the distance between receptors and docked vesicles or exocytic pits. The median distances from docked vesicles to AMPA and NMDA receptors were 95 nm and 73 nm, respectively, at rest (**Fig. 4e** inset), and remained largely unchanged following stimulation (**Fig 4e** inset: AMPA receptors, 102 nm at 5 ms; and 92 nm at 11 ms; **Fig. 4e** inset: NMDA receptors, 63 nm at 5 ms, 88 nm at 11 ms). This relationship between docked vesicles and receptors is expected given the

uniform distribution of docked vesicles in the active zone before and after stimulation (**Fig. 4c**) (Kusick et al. 2020).

In contrast, the distribution of exocytic pits relative to receptors was not uniform. During the synchronous phase of release (5 ms time points in our assay), pits were distributed throughout the active zone (**Fig. 4d**). However, when measured relative to each type of receptors, exocytic pits were found closer to AMPA receptors (median = 67 nm) than NMDA receptors (median = 139 nm; **Fig. 4f**). Interestingly, exocytic pits during asynchronous phase of release (11 ms) were distant from AMPA receptors (**Fig. 4f**, median = 120 nm) but closer to NMDA receptors (**Fig. 4f**, median = 56 nm). These results suggest that neurotransmitter is likely released synchronously near AMPA receptors and asynchronously around NMDA receptors.

The location, but not the sequence, of release is important for NMDA receptor activation

The spatial organization of release sites and receptors and temporal sequence of their usage could allow preferential activation of NMDA receptors. First, synchronous release activates AMPA receptors, depolarizing the postsynaptic membrane and alleviating Mg^{2+} block of NMDA receptors (Nowak et al. 1984; Mayer, Westbrook, and Guthrie 1984). Asynchronous release then increases the glutamate concentration in the synaptic cleft to favor the activation of NMDA receptors, potentially of those in the single-bound state. To test this possibility, we need to assess how NMDA receptors respond to asynchronous release in the absence of a Mg^{2+} block and compare it to the response following AMPA receptor-mediated membrane depolarization in the presence of Mg^{2+} block. In addition, the locations of synchronous and asynchronous release must be swapped to assess the importance of the spatial organization. To address these points, we performed computational simulations using the MCell platform that we have recently developed (Bartol, Keller, et al. 2015; Haas et al. 2018). This model simulates receptor activation in dendritic spines by incorporating realistic synapse morphology as well as the measured kinetics of molecules (Bartol, Keller, et al. 2015; Haas et al. 2018). We further

incorporated the observed distributions of receptors and their numbers revealed by super-resolution imaging (Goncalves et al. 2020) (**Fig. 3**): clusters containing ~20 AMPA receptors and ~15 NMDA receptors were placed around the periphery and the center of the postsynaptic density, respectively. The centroid to centroid distance between the clusters was set at 100 nm (Haas et al. 2018). We simulated the activation of AMPA and NMDA receptors with a sequence of two release events, with one occurring near the AMPA receptor cluster and another occurring near the NMDA receptor cluster. The timing of these two release events was varied from 0 ms to 50 ms apart (0 ms means simultaneous release at these two locations).

Using this model, we first determined how AMPA and NMDA receptors behave in response to asynchronous release in the absence of Mg^{2+}. Asynchronous release increased the responses of AMPA receptors by 50 % and NMDA receptors by 84 %, when compared to the responses from a single release (**Fig. 9a-f**). For AMPA receptors, the desensitization of the receptors (Jonas, Major, and Sakmann 1993; Colquhoun, Jonas, and Sakmann 1992) hampered their response to asynchronous release during the first 15 ms (**Fig. 9a-c**). In contrast, the responses of NMDA receptors were higher as the timing of the release was delayed, reaching a 122% increase at 50 ms (**Fig. 9d-f**). This increase is likely due to the binding of glutamate to those single-bound receptors since this state can be maintained for tens of milliseconds and is favoured for activation by the second release. These results suggest that asynchronous release favours the activation of NMDA receptors in the absence of a Mg^{2+} block.

Interestingly, the proportion of NMDA and AMPA receptors activated by these two release events was similar to the proportion activated when a single vesicle release occurs near NMDA receptors, but not around AMPA receptors or at random locations (**Fig. 9g**). These results suggest that the location of release also influences the activation of NMDA receptors.

We next tested the effect of the AMPA receptor-mediated membrane depolarization on NMDA receptor activation in the presence of Mg^{2+}. Two release events were induced simultaneously while the membrane potential was depolarized by 30 or 45 mV, mimicking the

changes in membrane potential after a single release event near AMPA receptors or after simultaneous release at both AMPA and NMDA receptors, respectively (**Fig. 5a**). The constant voltage at resting potential was used as a control. 45 mV depolarization doubled NMDA receptor activation compared to no membrane potential change (**Fig. 5a, b**). This response is substantially higher than the responses from a single release near the AMPA receptors (~4x increase) or NMDA receptors (~3x increase; **Fig. 5a, b**). These results suggest that NMDA receptors can be efficiently activated by two release events (multivesicular release) (Tong and Jahr 1994; Rudolph et al. 2015), which are prevalent in these neurons (Kusick et al. 2020).

To test whether the timing of asynchronous release is important for NMDA receptor activation, we varied the timing of the second release by 5, 8, 10, and 20 ms (**Fig. 5c**). The kinetics of depolarization and repolarization following AMPA receptor activation are integrated into the platform (Bartol, Keller, et al. 2015; Haas et al. 2018; Mainen et al. 1995) the depolarization peaks between 3 to 5 ms after the release, increasing by ~25 mV, and declines to 2/3 of the maximum after 8 ms and almost to the resting potential by 10 ms (**Fig. 9h**). The response from NMDA receptors peaked when asynchronous release occurred at 5 ms and decreased progressively as the asynchronous release was further delayed (**Fig. 5d**). These results are in sharp contrast to the activation of NMDA receptors in the absence of Mg^{2+}, indicating that the kinetics of membrane depolarization and repolarization, and thereby Mg^{2+} unbinding and binding, determine the activity of NMDA receptors.

To test the importance of the location and order of release, we either flipped the order of release (first on NMDA receptors, and then on AMPA receptors) or applied both release at the same locations (**Fig. 5e**). The two release events were paired 5 ms apart to test the maximal response. Flipping the order did not change the response of NMDA receptors (**Fig. 5f**). However, when both release events were applied near NMDA receptors consecutively, the response was 19% lower (**Fig. 5f**), presumably because the membranes cannot be maximally depolarized. In fact, when we simulated with a higher level of depolarization, matching the

degree of depolarization expected from releasing near AMPA receptors, the response of NMDA receptors was much stronger (~32% increase, **Fig. 5f** and **Fig. 9i-j**), suggesting activation of AMPA receptors is essential for NMDA receptor activity. In fact, two consecutive release events near AMPA receptors leads to a better activation of NMDA receptors (**Fig. 5f**), but this increase occurs at the expense of an increased number of desensitized AMPA receptors and thereby faster synaptic depression. Together, these results suggest that the trans-synaptic alignment of release sites and receptors likely ensures the maximal depolarization through AMPA receptors and thereby efficient activation of NMDA receptors, while avoiding saturation of AMPA receptors from a single stimulus.

Discussion

Here we demonstrated the trans-synaptic alignment of synchronous and asynchronous release sites with AMPA receptor and NMDA receptor clusters, respectively. These findings have implications for how signals are transmitted at synapses and how release sites and receptors are organized.

The presence of receptor clusters and their trans-synaptic alignment with release sits suggests that where glutamate is released relative to receptors is likely important for their activation. This is in sharp contrast with the original view that large number of receptors are present in the postsynaptic receptive field (Jonas, Major, and Sakmann 1993) with no particular pattern of localization, and that glutamate released from single vesicles anywhere in the active zone can efficiently activate both AMPA and NMDA receptors (John M. Bekkers and Stevens 1989; J M Bekkers, Richerson, and Stevens 1990). However, several lines of recent data seem to support the idea that release in the proximity of receptors is a major determinant of synaptic strength. First, release evoked by an action potential does not saturate the receptor activation (Liu, Choi, and Tsien 1999). Second, activation of AMPA receptors is sharply dependent on their distances from the point of release (Tarusawa et al. 2009; Uteshev and Pennefather 1996;

Raghavachari and Lisman 2004b; Xu-Friedman and Regehr 2004). Third, AMPA receptors need to be in the clusters to enhance the amplitude of signals. Simply increasing the number of AMPA receptors in postsynaptic densities using optogenetics does not change the quantal amplitude nor strength of response from existing synapses, suggesting that the organization of receptors is likely more important (Sinnen et al. 2017). Forth, the alignment is modulable and can potentially alter the signal strength (A.-H. Tang et al. 2016; Hruska et al. 2018). Our data are consistent with these studies and further support the idea that the precise location of release influences efficiency of receptor activation at excitatory synapses.

In addition, this is the first demonstration that the NMDA receptor activation is also influenced by such trans-synaptic nano-architectures. NMDA receptors have a higher affinity for glutamate and thus their locations within a postsynaptic density are thought to be less critical. Previous simulations demonstrated that whether they are in the cluster or randomly localized, NMDA receptors can be activated equally well from a single vesicle release (Goncalves et al. 2020). Our data here also suggest that locations of release are less important for NMDA receptor activation as long as AMPA receptors are activated. In fact, NMDA receptors are activated to a greater degree when both synchronous and asynchronous release occurs near AMPA receptors. However, this release pattern would increase the number of desensitized AMPA receptors, leading to faster depression at these synapses. Thus, one release event near AMPA receptors and another release event near NMDA receptors likely maximize the membrane depolarization and NMDA receptor activation, while ensuring that a sufficient number of naïve AMPA receptors are available to respond to the next stimulus.

Whether glutamate is released spontaneously from single vesicles or actively following an action potential, similar proportions of AMPA and NMDA receptors are thought to be activated (John M. Bekkers and Stevens 1989). Our data indicates that an action potential may induce glutamate release from two vesicles: synchronous near AMPA receptors and asynchronously near NMDA receptors. Although we do not know often a synapse release

glutamate both synchronously and asynchronously after a single action potential, evoked release likely leads to greater activation of NMDA receptors, given that multivesicular release is also quite prominent in these synapses (Kusick et al. 2020). Therefore, to achieve a similar proportion of activation by single vesicles, glutamate need to be released at a particular location during spontaneous release. Our computer simulations suggest that a single vesicle release near the NMDA receptors may be able to activate both AMPA and NMDA receptors with a similar proportion to the evoked release, suggesting that spontaneous release may occur near NMDA receptors. However, spontaneous release has been proposed to use a distinct pool of synaptic vesicles (Sara et al. 2005; C. Chung et al. 2010; Fredj and Burrone 2009), which may not be readily available at active zones. In addition, a distinct set of postsynaptic receptors may be activated by spontaneous release (Atasoy et al. 2008; Sara et al. 2011). In fact, the NMDA receptor activated during spontaneous release does not seem to depend on the dendritic depolarization or AMPA receptor activity (Espinosa and Kavalali 2009). Thus, spontaneous release may elicit the postsynaptic currents by a completely different mechanism. However, these ideas are still contentious and require further testing (Kavalali 2015).

Here, we propose that trans-synaptic organization of NMDA receptors may allow them to be activated during asynchronous release. However, it is possible that this organization may serve different functions. To test this point, the actual function output from NMDA receptors must be measured experimentally while manipulating their organization. A recent study suggests that neuroligin-1 may align release sites with AMPA receptors (Haas et al. 2018). It is unknown how asynchronous release sites are aligned with NMDA receptors. Many synaptic adhesion molecules exist, and they all interact with the presynaptic release machinery as well as postsynaptic receptors and their scaffolding proteins (Biederer, Kaeser, and Blanpied 2017b; Haas et al. 2018; Jang, Lee, and Kim 2017; Williams, de Wit, and Ghosh 2010). Thus, it is tempting to speculate that the arrangement of these molecules give rise to this unique trans-synaptic organization of release sites and receptors at excitatory synapses.

Figures

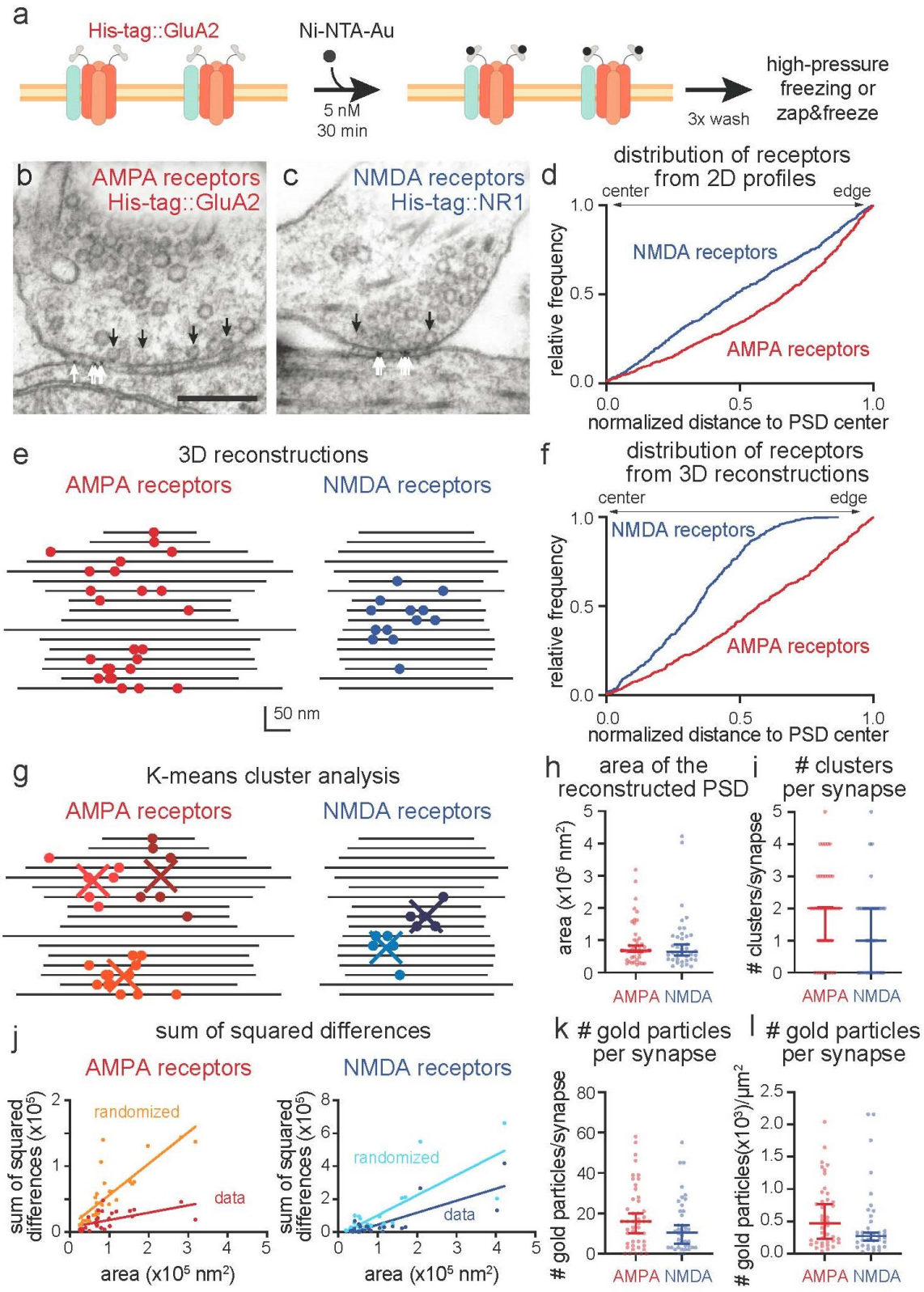
a
His-tag::GluA2
Ni-NTA-Au
5 nM
30 min
3x wash
high-pressure freezing or zap&freeze
b
AMPA receptors
His-tag::GluA2
c
NMDA receptors
His-tag::NR1
d
distribution of receptors from 2D profiles
center
edge
NMDA receptors
AMPA receptors
relative frequency
normalized distance to PSD center
e
3D reconstructions
AMPA receptors
NMDA receptors
50 nm
f
distribution of receptors from 3D reconstructions
center
edge
NMDA receptors
AMPA receptors
relative frequency
normalized distance to PSD center
g
K-means cluster analysis
AMPA receptors
NMDA receptors
h
area of the reconstructed PSD
area (x10⁵ nm²)
AMPA NMDA
i
clusters per synapse
clusters/synapse
AMPA NMDA
j
sum of squared differences
AMPA receptors
NMDA receptors
randomized
data
sum of squared differences (x10⁵)
area (x10⁵ nm²)
k
gold particles per synapse
gold particles/synapse
AMPA NMDA
l
gold particles per synapse
gold particles(x10³)/µm²
AMPA NMDA

Figure 3 AMPA receptors and NMDA receptors cluster at the periphery and the center of the postsynaptic density, respectively.

a, Schematic of the small metal affinity staining of His-tag (SMASH) strategy for live-cell labelling of overexpressed His-tagged surface GluA2 (AMPA receptors) with nickel-NTA-gold (5 nm). b-c, Example transmission electron micrographs of synapses after SMASH labelling and high-pressure freezing, showing gold particles in the synaptic cleft of wild-type neurons expressing His-tag::GluA2 (b) and His-tag::NR1 (c). Black arrows: docked synaptic vesicles. White arrows: gold particles. d, Cumulative relative frequency distribution of lateral distances from gold particles to the center of the postsynaptic density (PSD) from 2-D profiles. Distances are normalized to the length of the PSD: a gold particle at 0 would be exactly at the center and at 1 exactly at the edge. AMPA receptors are biased towards the edge (median = 0.7, p 0.8, n=746 particles, N = 4 cultures). e, Examples of synapses from spin-mill serial block face scanning electron microscopy; each line indicates the extent of the cleft in a single 20 nm-thick 2-D profile, each circle indicates the location of a gold particle. f, Cumulative relative frequency distribution of lateral distances from gold particles to the center of the postsynaptic density (PSD) from 3-D profiles. Distances are normalized to the size of the PSD and corrected as fractional area assuming a circular PSD: a gold particle at 0 would be exactly at the center, at 1 exactly at the edge, and at 0.25 equidistant between center and edge. AMPA receptors are slightly biased towards the edge (median = 0.6, p 0.6, Mann-Whitney test. i, Number of clusters per synapse determined by k-means clustering. Each dot: a single reconstructed synapse. Error bars: median and 95% confidence interval, p = 0.06, Mann-Whitney test. j, Sum of squared differences, calculated from each particle to the centroid of the cluster. Data: the actual distances of gold particles to their cluster center. Randomized: the distances of gold particles to their putative cluster center after randomizing the locations of gold particles at each synapse. Each dot: a synapse. Simple linear regression test: AMPA receptors, data, R2 =0.32, randomized = 0.67, $p < 0.001$; NMDA receptors, data, R2 =0.63, randomized = 0.62, p = 0.04.

kl, Number of gold particles per synapse (k) and per μm2 (l). Bias of particle locations toward the center or edge of the postsynaptic density in d and f was tested by comparing each group to a theoretical median of 0.5 using one-sample two-tailed Wilcoxon signed-rank tests.

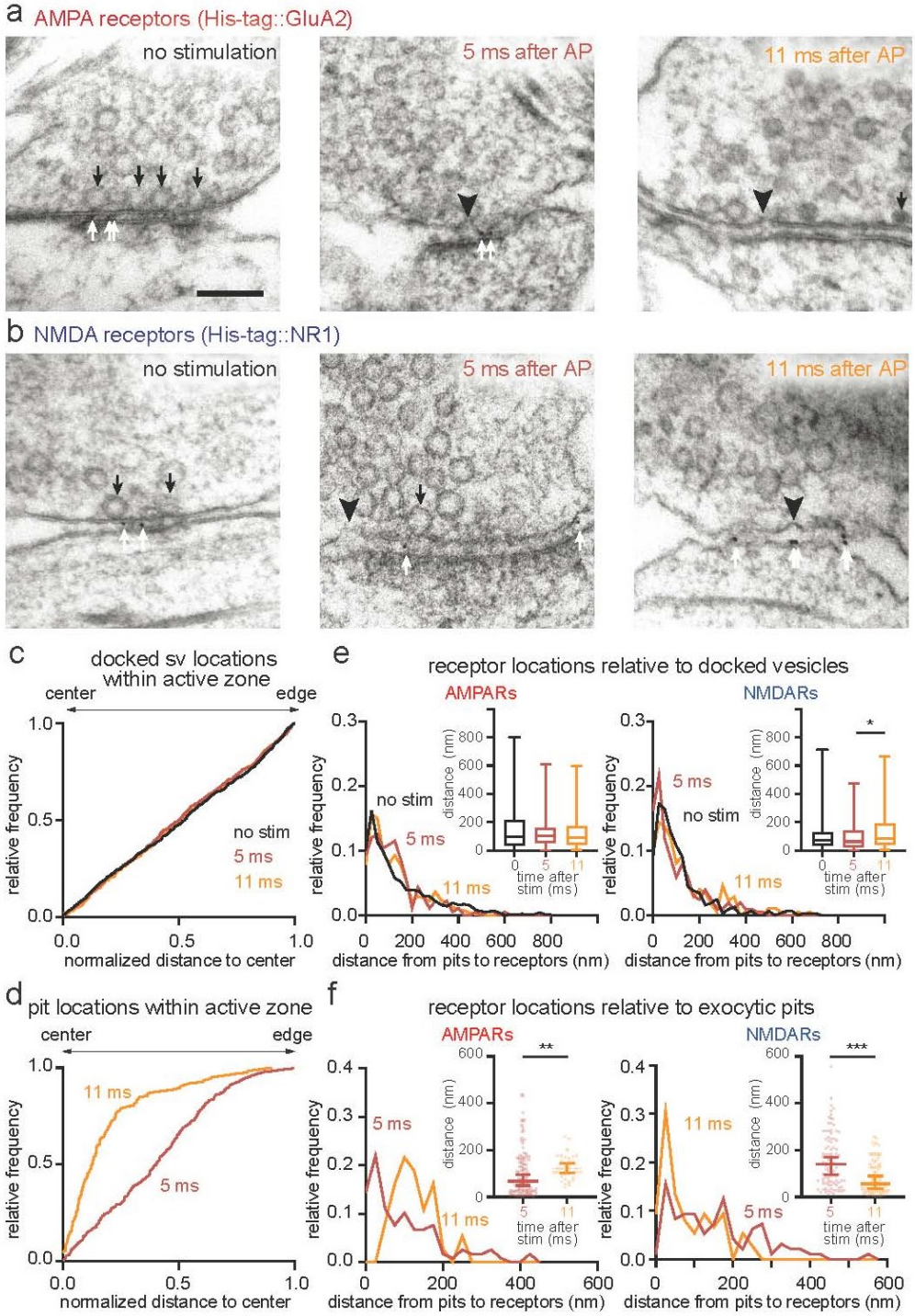
a AMPA receptors (His-tag::GluA2)
no stimulation
5 ms after AP
11 ms after AP
b NMDA receptors (His-tag::NR1)
no stimulation
5 ms after AP
11 ms after AP
c
docked sv locations within active zone
center
edge
relative frequency
normalized distance to center
no stim
5 ms
11 ms
e
receptor locations relative to docked vesicles
AMPARs
NMDARs
distance from pits to receptors (nm)
distance (nm)
time after stim (ms)
*
d
pit locations within active zone
f
receptor locations relative to exocytic pits
**
***

Figure 4 Synchronous and asynchronous release are aligned to AMPA receptors and NMDA receptors, respectively.

a-b, Example transmission electron micrographs of synapses after SMASH labelling and highpressure freezing at the indicated time points post stimulus (1-ms pulse), showing pits (black

arrowheads), docked vesicles (black arrows) and gold particles (white arrows) at synapses of wild-type neurons expressing His-tag::GluA2 (a) and His-tag::NR1 (b). c-d, Cumulative relative frequency distribution of lateral distances between docked vesicles (c) or exocytic pits (d) and the active zone center at 5 or 11 ms after stimulation, as measured within 2-D profiles by transmission electron microscopy. Exocytic pits were biased towards the center both at 5 ms (median = 0.4, $p < 0.001$, n = 286 pits, N = 7 samples) and 11 ms (median = 0.13, $p < 0.001$, n = 124 pits, N = 7 samples), but pits at 11 ms were more strongly biased towards the center ($p < 0.001$, Kolmogorov-Smirnov D test). Bias of vesicles and pits locations toward the center or edge of the active zone in c and d was tested by comparing each group to a theoretical median of 0.5 using one-sample two-tailed Wilcoxon signed-rank tests. e-f, Relative frequency distribution of lateral distances between docked vesicles (e) or exocytic pits (f) and gold particles within the cleft at 5 ms (red) and 11 ms (orange) after stimulation. Insets: the same data plotted as box and whiskers for docked vesicles (e) and scattered dots (f) to show the median distances. Error bars: median and 95% confidence interval for the scattered dot plots. Kolmogorov-Smirnov D tests were performed in each case, with additional post hoc Dunn's multiple comparisons tests for docked vesicle data. * $p < 0.05$, ** $p < 0.01$, *** $p < 0.001$. See Supplementary Data Table 1 for full pairwise comparisons and summary statistics.

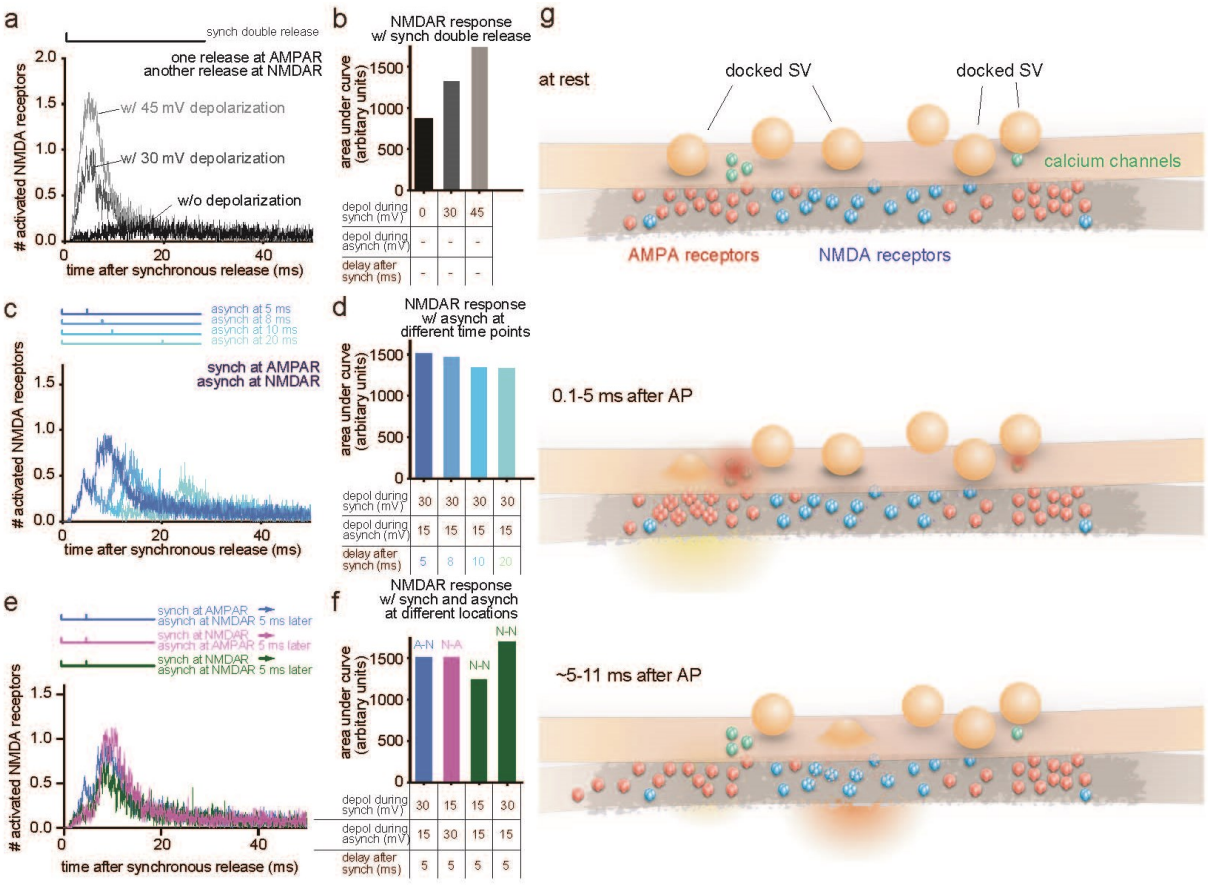

Figure 5 Computer simulations predict better activation of NMDA receptors with asynchronous release.

a, Time course of simulated NMDA receptor activation, resulting from two release events at the indicated locations while varying the degree of depolarization of the postsynaptic membrane. The number averaged from 48 simulations are plotted. The vertical lines in the diagrams shown above the plot indicate when synchronous and asynchronous release occur. Synchronous release always occurs at time 0. Double release means two release events happen simultaneously. Synch = synchronous. Asynch = asynchronous. b, The area under curve calculated from each dataset in (a) and plotted as a bar graph. The locations of release are described in a, and the degree of depolarization (depol) and the delay between synchronous and asynchronous release used in simulated are listed at the bottom. c, Same as a, but varying the interval between two release events. d, Same as b, but plotted from each dataset in (c). e,

Same as in a, but varying the order of the release. f, Same as in b, but plotted from each dataset in (e) and plotted as a bar graph. AN: synchronous release at AMPA receptors and asynchronous release at NMDA receptors. N-A: synchronous release at NMDA receptors and asynchronous release at AMPA receptors. N-N: both synchronous and asynchronous release at NMDA receptors. g, Schematic of proposed synaptic organization and events. Docked vesicles are found throughout the active zone. AMPA receptors are found towards the edge, while NMDA receptors are biased towards the center. Synchronous fusion begins within hundreds of microseconds near the AMPA receptor cluster. Released glutamate activates AMPA receptors, which in turn depolarizes the membrane and alleviates the Mg2+ block of NMDA receptors. Between 5 and 11 ms, residual calcium triggers asynchronous fusion, preferentially toward the center of the active zone and across from the NMDA receptor cluster, favoring the NMDA receptors. Although shown here as taking place in the same active zone, the degree to which synchronous and asynchronous release may occur at the same active zone after a single action potential is unknown. This trans-synaptic organization allows the maximal depolarization of the postsynaptic membrane and efficient activation of NMDA receptors.

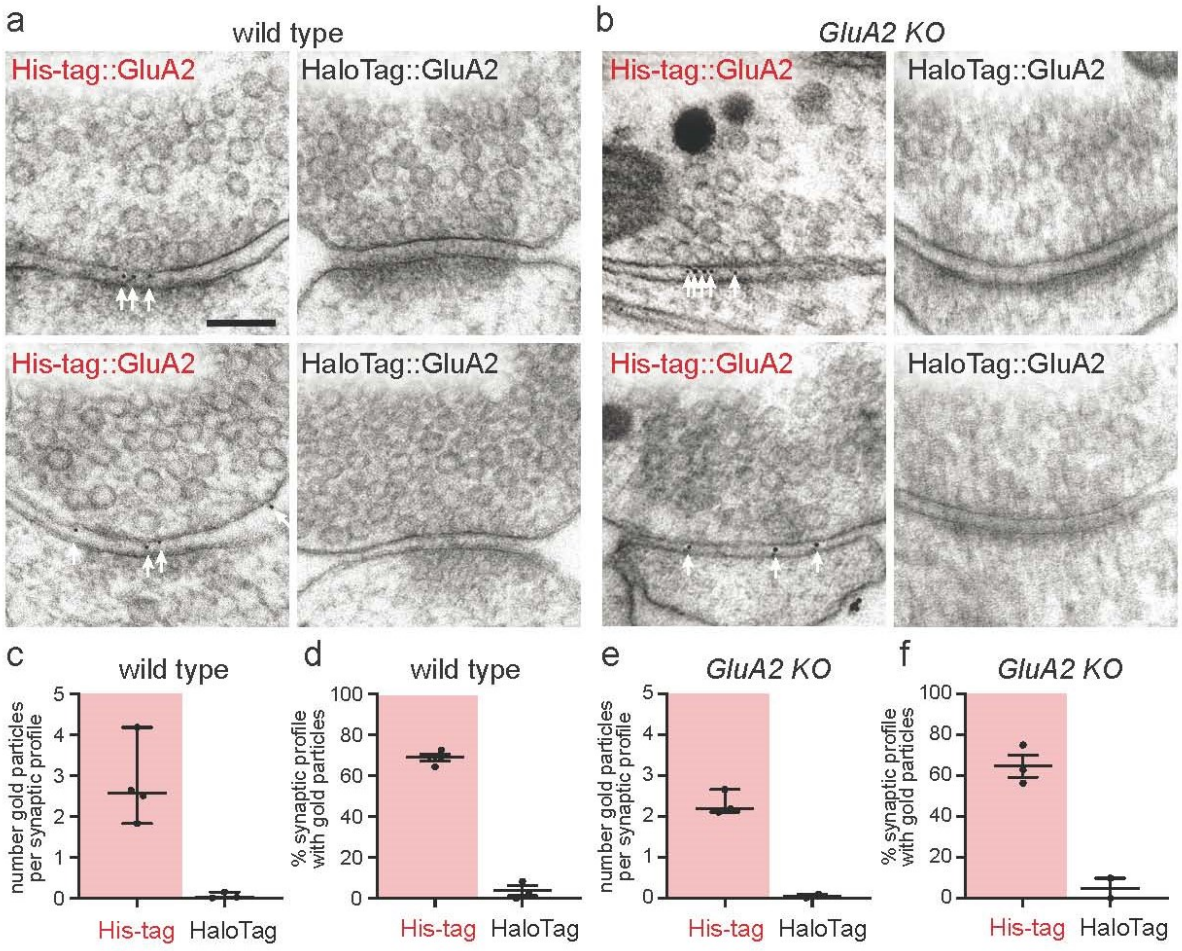

Figure 6 The receptor labelling approach and its validation.

a-b, Example transmission electron micrographs of synapses after SMASH labelling and high pressure freezing, showing gold particles in the synaptic cleft of wild-type (a) and GluA2 knockout (b, Gria2-/-) neurons expressing His-tag::GluA2. Control samples with neurons expressing HaloTag::GluA2. Scale bar: 100 nm. White arrows indicate gold particles. c, Number of gold particles per synaptic cleft in the wild-type neurons. Each dot: an average number from a single experiment, analyzing ~100 micrographs. Error bars: median and 95 % confidence interval, p=0.01, Welch's T-test. d, Percentage of synaptic profiles containing gold particles in synaptic cleft in the wild-type neurons. Each dot: a percentage from a single experiment, analyzing ~100 micrographs. Error bars: mean and SEM, p<0.001, Welch's T-test. e, Same as in c, except showing the number from the GluA2 knockout (KO) neurons. Error bars: median

and 95% confidence interval, $p<0.01$, Welch's T-test. f, Same as in d, except showing the number from the GluA2 knockout (KO) neurons. Error bars: mean and SEM, $p<0.01$, Welch's T-test.

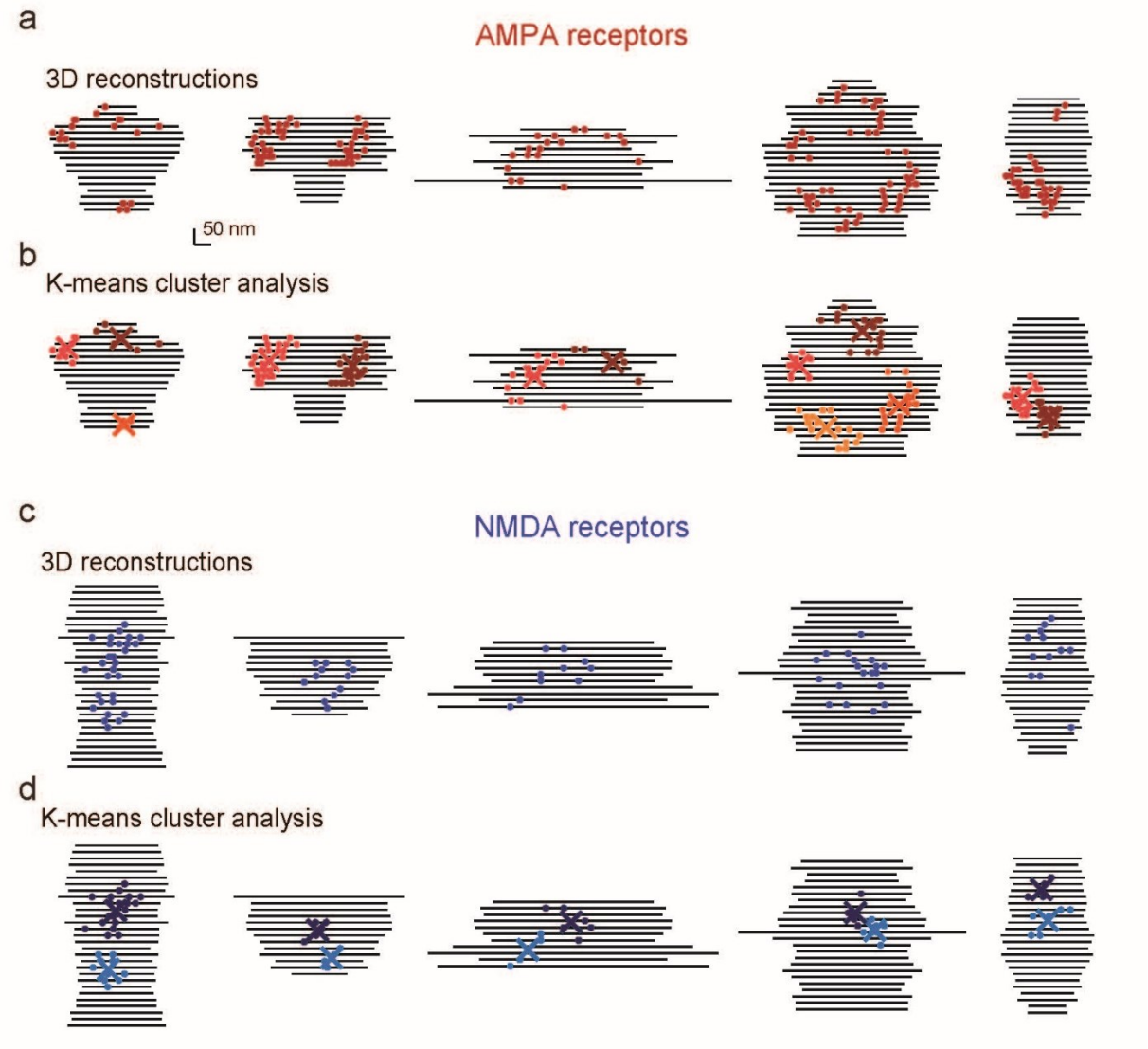

Figure 7 Additional 3-D representations of AMPA receptors and NMDA receptors.

a, Examples of synapses of neurons expressing His-tag::GluA2 from spin-mill serial block face scanning electron microscopy; each line indicates the extent of the cleft in a single 20 nm-thick 2-D profile, each circle indicates the location of a gold particle. b, Same as a, except showing the centers of clusters determined by k-means clustering. c, Examples of synapses of neurons expressing His-tag::NR1 from 3-D serial imaging; each line indicates the extent of the cleft in a single 20 nm-thick 2-D profile, each circle indicates the location of a gold particle. d, Same as c, except showing the centers of clusters determined by k-means clustering.

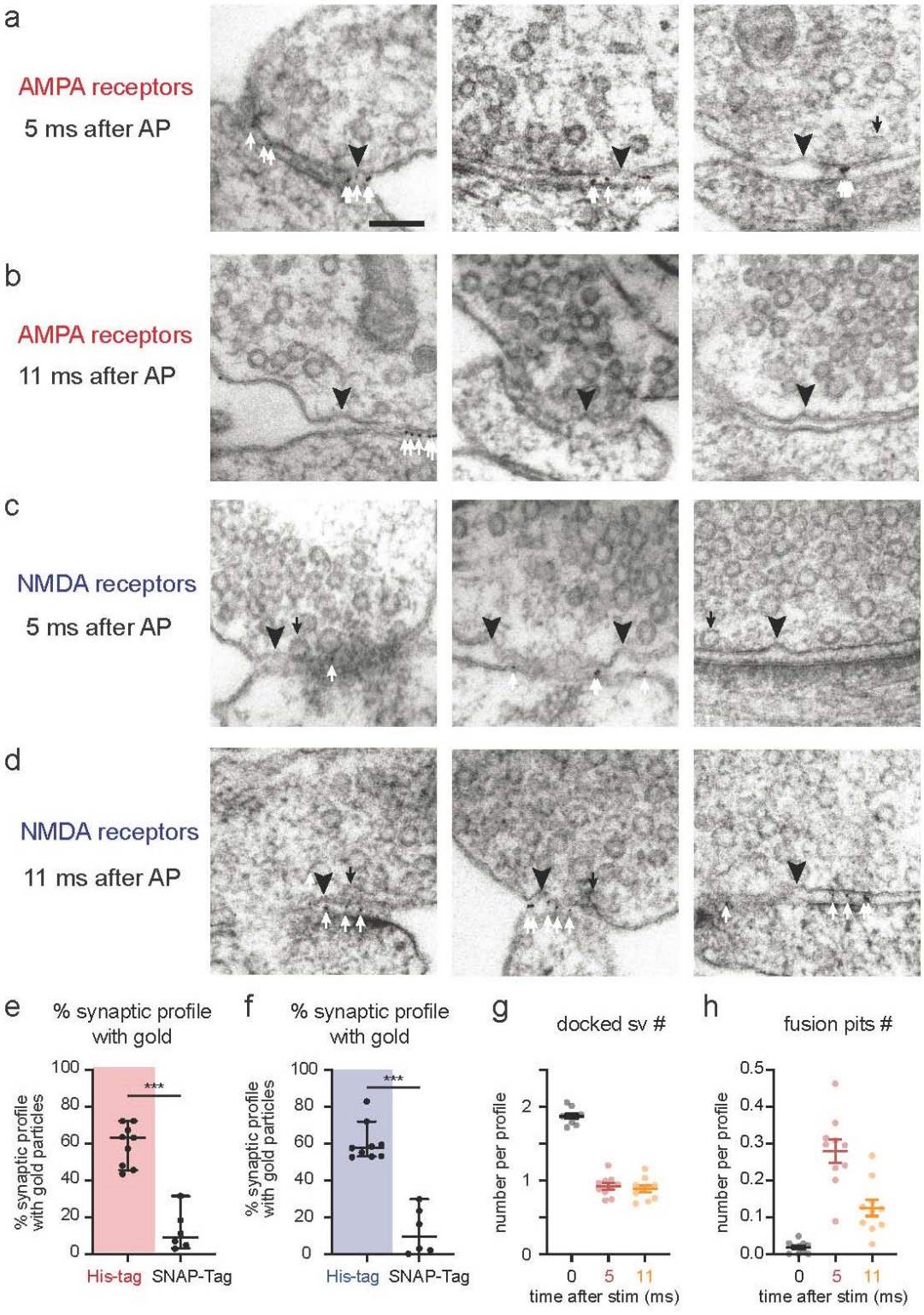
a
AMPA receptors
5 ms after AP
b
AMPA receptors
11 ms after AP
c
NMDA receptors
5 ms after AP
d
NMDA receptors
11 ms after AP
e
% synaptic profile with gold
% synaptic profile with gold particles
100
80
60
40
20
0
***
His-tag
SNAP-Tag
f
% synaptic profile with gold
% synaptic profile with gold particles
100
80
60
40
20
0
***
His-tag
SNAP-Tag
g
docked sv #
number per profile
2
1
0
0
5
11
time after stim (ms)
h
fusion pits #
number per profile
0.5
0.4
0.3
0.2
0.1
0.0
0
5
11
time after stim (ms)

Figure 8 Synchronous and asynchronous release are aligned to AMPA receptors and NMDA receptors, respectively.

a-d, Additional example transmission electron micrographs of synapses after SMASH labelling and high-pressure freezing at 5 ms (a, c) and 11 ms (b, d) post stimulus (1-ms pulse), showing pits (black arrowheads), docked vesicles (black arrows) and gold particles (white arrows) at synapses of wild-type neurons expressing His-tag::GluA2 (a-b) and His-tag::NR1 (c-d). e-f, Percentage of synaptic profiles containing gold particles in synaptic cleft in the wild-type neurons expressing His-tag::GluA2 or SNAP-Tag::GluA2 (e) and His-tag::NR1 or SNAPTag::NR1 (f). Each dot: a percentage from a single experiment, analyzing ~100 micrographs.

Error bars: mean and SEM, $p<0.001$, Welch's T-test. g-h, Number of docked vesicles (g) and pits (h) in the active zone per synaptic profile from the neurons either unstimulated (black) or stimulated once (a 1-ms pulse) 5 ms (red) or 11 ms (orange) before freezing. Each dot: a mean from a single experiment, analyzing ~100 micrographs. Error bars: mean and SEM, $p<0.001$ in all cases except for the numbers of docked vesicles between 5 and 11 ms ($p>0.6$), 2-way ANOVA with post hoc Turkey's multiple comparisons test. His-tag::NR1 (c-d). e-f, Percentage of synaptic profiles containing gold particles in synaptic cleft in the wild-type neurons expressing His-tag::GluA2 or SNAP-Tag::GluA2 (e) and His-tag::NR1 or SNAPTag::NR1 (f). Each dot: a percentage from a single experiment, analyzing ~100 micrographs. Error bars: mean and SEM, p0.6), 2-way ANOVA with post hoc Turkey's multiple comparisons test

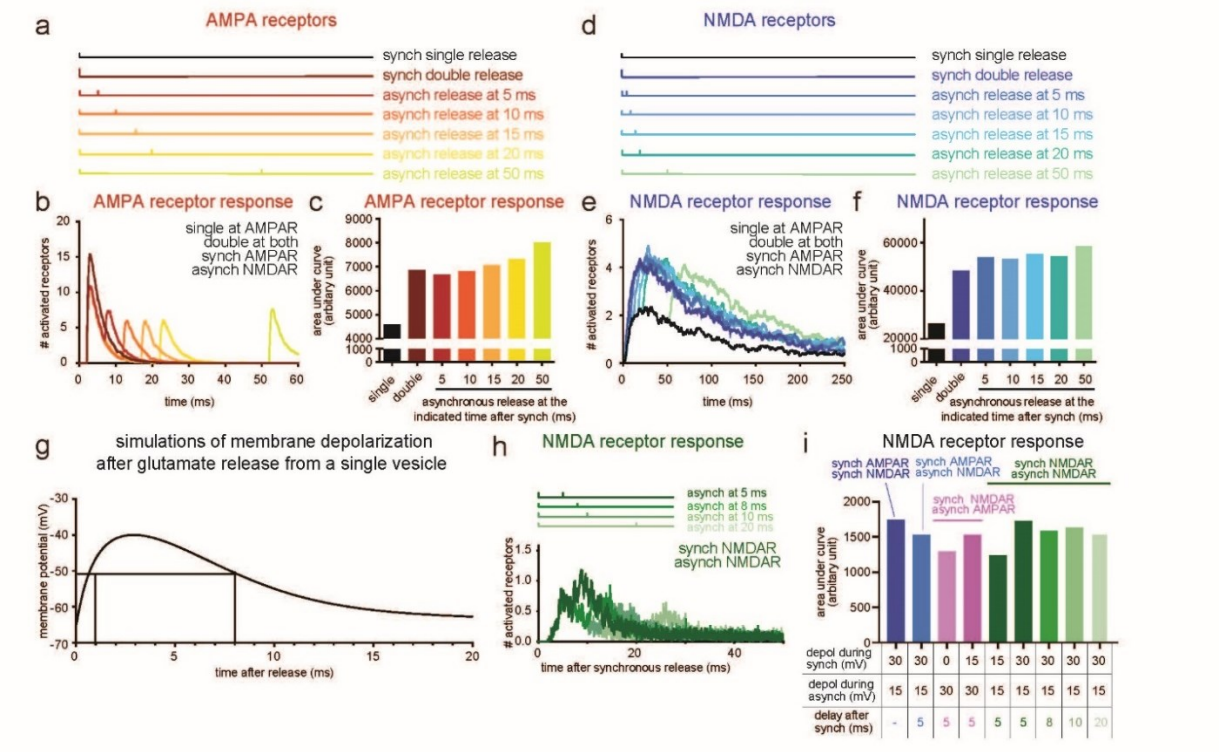

Figure 9 Computer simulations predict better activation of NMDA receptors with asynchronous release.

a-b, Time course of simulated AMPA receptor activation in the absence of Mg2+ (b), resulting from release events at the timing and locations as indicated in (a) and (b), respectively. The vertical lines in (a) indicate when synchronous and asynchronous release was applied. The number averaged from 48 simulations are plotted in (b). The synchronous release was applied at time 0. Double release means two release events were applied simultaneously. Synch = synchronous. Asynch = asynchronous. c, the area under curve calculated from each dataset in (b) and plotted as a bar graph. d-e, same as in a-b, but for NMDA receptors. f, same as in c but for NMDA receptors. g, Time course of simulated membrane depolarization due to the activation of AMPA receptors. The depolarization peaks between 3 to 5 ms after the glutamate release, declines to 2/3 of the maximum after 8 ms, and is almost back to the baseline by 10 ms. h, Time course of simulated NMDA receptor activation in the presence of Mg2+, resulting from both synchronous and asynchronous release occurring near the NMDA receptors. The membrane depolarization due to synchronous release was simulated at 30 mV. i, The area under curve

calculated from each dataset in (h) and plotted as a bar graph. The locations of synchronous and asynchronous release are as indicated. The degree of depolarization (depol) and the delay between synchronous and asynchronous release used in simulated are listed at the bottom.

Tables

Table 1 Sum of squared differences

simple linear regression for AMPA receptor data		
Best-fit values		
Slope	0.1111	0.4758
Y-intercept	7199	8648
X-intercept	-64780	-18174
1/slope	8.998	2.102
Std. Error		
Slope	0.03124	0.06146
Y-intercept	3546	7049
95% Confidence Intervals		
Slope	0.04704 to 0.1752	0.3503 to 0.6014
Y-intercept	-76.37 to 14474	-5747 to 23043
X-intercept	-284850 to 470.8	-62854 to 10002
Goodness of Fit		
R squared	0.3192	0.6664
Sy.x	11518	23726
Is slope significantly non-zero?		
F	12.66	59.94
DFn, DFd	1, 27	1, 30
P value	0.0014	<0.0001
Deviation from zero?	Significant	Significant
Equation	Y = 0.1111*X + 7199	Y = 0.4758*X + 8648
Data		
Number of X values	40	42
Maximum number of Y replicates	1	1
Total number of values	29	32
Number of missing values	11	10
Are the slopes equal?	F = 26.33. DFn = 1, DFd = 57	
	P<0.0001	

simple linear regression for NMDA receptor data		
Best-fit values		
Slope	0.7289	1.224
Y-intercept	-28509	-21430
X-intercept	39112	17511
1/slope	1.372	0.8171
Std. Error		
Slope	0.1199	0.1943
Y-intercept	18046	28172
95% Confidence Intervals		
Slope	0.4802 to 0.9776	0.8228 to 1.625
Y-intercept	-65934 to 8916	-79573 to 36714
X-intercept	-16498 to 75908	-40257 to 54282
Goodness of Fit		
R squared	0.6267	0.6231
Sy.x	60011	99280
Is slope significantly non-zero?		
F	36.94	39.67
DFn, DFd	1, 22	1, 24
P value	<0.0001	<0.0001
Deviation from zero?	Significant	Significant
Equation	Y = 0.7289*X - 28509	Y = 1.224*X - 21430
Data		
Number of X values	39	39
Maximum number of Y replicates	1	1
Total number of values	24	26
Number of missing values	15	13
Are the slopes equal?	F = 4.560. DFn = 1, DFd = 46	
	P=0.0381	

Table 2 Number of gold particles per cluster

	His-tag::GluA2	His-tag::NR
N (samples)	2	2
Number of values	76	62
Minimum	4	4
25% Percentile	6	5
Median	8	6
75% Percentile	12	8.25
Maximum	23	18
Range	19	14
95% CI of median		
Actual confidence level	97.1%	97.0%
Lower confidence limit	7	5
Upper confidence limit	10	7
Mean	9.68	7.35
Std. Deviation	5.09	3.65
Std. Error of Mean	0.584	0.464
Lower 95% CI of mean	8.52	6.43
Upper 95% CI of mean	10.8	8.28
Coefficient of variation	52.6%	49.7%
Skewness	1.07	1.65
Kurtosis	0.333	2.29
Mann Whitney test		
P value	0.0024	
Exact or approximate P value?	Exact	
P value summary	**	
Significantly different (P < 0.05)?	Yes	
One- or two-tailed P value?	Two-tailed	
Sum of ranks in column A,B	5982 , 3610	
Mann-Whitney U	1657	
Difference between medians		
Median of column A	8.00, n=76	
Median of column B	6.00, n=62	
Difference: Actual	-2	
Difference: Hodges-Lehmann	-2	

Table 3 Number of gold particles per synapse

	His-tag::GluA2	His-tag::NR1
N (samples)	2	2
Number of values	47	40
Minimum	0	0
25% Percentile	5	3
Median	16	10.5
75% Percentile	27	21
Maximum	58	55
Range	58	55
95% CI of median		
Actual confidence level	96.00%	96.15%
Lower confidence limit	10	5
Upper confidence limit	20	14
Mean	17.87	13.78
Std. Deviation	15.45	13.48
Std. Error of Mean	2.254	2.132
Lower 95% CI of mean	13.34	9.463
Upper 95% CI of mean	22.41	18.09
Coefficient of variation	86.44%	97.89%
Skewness	0.9399	1.41
Kurtosis	0.1706	1.591
Mann Whitney test		
P value	0.1997	
Exact or approximate P value?	Exact	
P value summary	ns	
Significantly different (P < 0.05)?	No	
One- or two-tailed P value?	Two-tailed	
Sum of ranks in column A,B	2219 , 1609	
Mann-Whitney U	789	
Difference between medians		
Median of column A	16.00, n=47	
Median of column B	10.50, n=40	
Difference: Actual	-5.5	
Difference: Hodges-Lehmann	-3	

Table 4 Cumulative relative frequency distribution of lateral distances from docked vesicles to the center of the active zone from 2-D profiles

ANOVA summary					
F	0.27				
P value	0.7634				
P value summary	ns				
Significant diff. among means (P < 0.05)	No				
R squared	0.000191				
Brown-Forsythe test					
F (DFn, DFd)	1.03 (2, 2820)				
P value	0.3587				
P value summary	ns				
Are SDs significantly different (P < 0.05)	No				
Bartlett's test					
Bartlett's statistic (corrected)	1.15				
P value	0.5623				
P value summary	ns				
Are SDs significantly different (P < 0.05)	No				
ANOVA table	SS	DF	MS	F (DFn, DFd	P value
Treatment (between columns)	0.0476	2	0.0238	F (2, 2820) =	P=0.7634
Residual (within columns)	248	2820	0.0881		
Total	249	2822			
Data summary					
Number of treatments (columns)	3				
Number of values (total)	2823				
Tukey's multiple comparisons test	Mean Diff.	95.00% C	Significant?	Summary	Adjusted P Value
no stim vs. 5 ms	0.0101	-0.0221 to	No	ns	0.7439
no stim vs. 11 ms	0.00392	-0.0275 to	No	ns	0.954
5 ms vs. 11 ms	-0.00613	-0.0391 to	No	ns	0.9003

Table 5 Cumulative relative frequency distribution of lateral distances from exocytic pits to the center of the active zone from 2-D profiles

	5 ms	11 ms
N (samples)	6	6
Number of values	286	124
Minimum	0.004588	0
25% Percentile	0.195	0.05911
Median	0.404	0.1275
75% Percentile	0.5788	0.2292
Maximum	0.9956	0.9031
Range	0.991	0.9031
95% CI of median		
Actual confidence level	96.17%	96.16%
Lower confidence limit	0.3669	0.09333
Upper confidence limit	0.4398	0.1475
Mean	0.3984	0.1904
Std. Deviation	0.2392	0.2018
Std. Error of Mean	0.01415	0.01812
Lower 95% CI of mean	0.3706	0.1545
Upper 95% CI of mean	0.4263	0.2262
Coefficient of variation	60.04%	106.0%
Skewness	0.199	1.771
Kurtosis	-0.7496	2.682
one sample Wilcoxon test (against a theoretical median)		
Theoretical median	0.5	0.5
Actual median	0.404	0.128
Number of values	286	124
Wilcoxon Signed Rank Test		
Sum of signed ranks (W)	-18161	-7176
Sum of positive ranks	11440	287
Sum of negative ranks	-29601	-7463
P value (two tailed)	<0.0001	<0.0001
Exact or estimate?	Approximate	Exact
P value summary	****	****
Significant (alpha=0.05)?	Yes	Yes
How big is the discrepancy?		
Discrepancy	-0.096	-0.372
95% confidence interval	-0.133 to -0.0602	-0.407 to -0.353
Actual confidence level	96.2	96.2

Kolmogorov-Smirnov test		
P value	<0.0001	
Exact or approximate P value?	Approximate	
P value summary	****	
Significantly different (P < 0.05)?	Yes	
Kolmogorov-Smirnov D	0.4931	

Table 6 Receptor locations relative to docked vesicles

AMPA receptors	no stim	5 ms	11 ms	
N (samples)	3	3	3	
Number of values	995	183	551	
Minimum	0	0.74	0.94	
25% Percentile	34.42	49.33	40.65	
Median	94.91	101.6	92.41	
75% Percentile	215.9	159.8	171.6	
Maximum	799.7	609.6	595.3	
Range	799.7	608.8	594.3	
95% CI of median				
Actual confidence level	95.07%	96.18%	95.01%	
Lower confidence limit	86.13	77.75	81.92	
Upper confidence limit	103.9	117.4	104.4	
Mean	147.4	124.8	123.8	
Std. Deviation	148.4	111.3	106.8	
Std. Error of Mean	4.704	8.228	4.548	
Lower 95% CI of mean	138.1	108.6	114.9	
Upper 95% CI of mean	156.6	141.1	132.7	
Coefficient of variation	100.7%	89.17%	86.23%	
Skewness	1.485	1.65	1.16	
Kurtosis	2.134	3.357	0.8445	
Kruskal-Wallis test				
P value	0.6254			
Exact or approximate P value?	Approximate			
P value summary	ns			
Do the medians vary signif. (P < 0.05)?	No			
Number of groups	3			
Kruskal-Wallis statistic	0.9388			
Dunn's multiple comparisons test	Mean rank diff.	Significant?	Summary	Adjusted P Value
no stim vs. 5ms	19.17	No	ns	>0.9999
no stim vs. 11ms	24.7	No	ns	>0.9999
5ms vs. 11ms	5.532	No	ns	>0.9999

NMDA receptors	no stim	5 ms	11 ms	
N (samples)	3	3	3	
Number of values	317	203	174	
Minimum	0.74	0	2.102	
25% Percentile	34.97	23.13	37.8	
Median	73.42	62.62	87.49	
75% Percentile	130.7	142.3	188.7	
Maximum	712.2	470.8	663.3	
Range	711.4	470.8	661.2	
95% CI of median				
Actual confidence level	95.70%	95.09%	95.96%	
Lower confidence limit	65.09	45.73	73.54	
Upper confidence limit	86.97	81.69	111.1	
Mean	110.4	103.9	133.5	
Std. Deviation	120	109.5	134.2	
Std. Error of Mean	6.74	7.687	10.18	
Lower 95% CI of mean	97.19	88.74	113.4	
Upper 95% CI of mean	123.7	119	153.5	
Coefficient of variation	108.7%	105.4%	100.6%	
Skewness	2.467	1.423	1.634	
Kurtosis	7.265	1.383	2.579	
Kruskal-Wallis test				
P value	0.034			
Exact or approximate P value?	Approximate			
P value summary	*			
Do the medians vary signif. (P < 0.05)?	Yes			
Number of groups	3			
Kruskal-Wallis statistic	6.764			
Dunn's multiple comparisons test	Mean rank diff.	Significant?	Summary	Adjusted P Value
no stim vs. 5ms	23.86	No	ns	0.5564
no stim vs. 11ms	-29.99	No	ns	0.3387
5ms vs. 11ms	-53.85	Yes	*	0.028

Table 7 Receptor locations relative to pits

AMPA receptors	5 ms	11 ms
N (samples)	3	3
Number of values	118	37
Minimum	1.88	40.41
25% Percentile	24.31	92.06
Median	67.14	120.1
75% Percentile	148.8	160.1
Maximum	436.2	258.7
Range	434.3	218.3
95% CI of median		
Actual confidence level	96.62%	95.30%
Lower confidence limit	48.61	104
Upper confidence limit	95.87	143.6
Mean	98.85	124.9
Std. Deviation	97.03	50.78
Std. Error of Mean	8.932	8.348
Lower 95% CI of mean	81.16	108
Upper 95% CI of mean	116.5	141.8
Coefficient of variation	98.16%	40.66%
Skewness	1.417	0.7065
Kurtosis	1.773	0.5238
Kolmogorov-Smirnov test		
P value	0.0002	
Exact or approximate P value?	Approximate	
P value summary	***	
Significantly different (P < 0.05)?	Yes	
Kolmogorov-Smirnov D	0.4052	
Mann Whitney test		
P value	0.0014	
Exact or approximate P value?	Exact	
P value summary	**	
Significantly different (P < 0.05)?	Yes	
One- or two-tailed P value?	Two-tailed	
Sum of ranks in column A,B	8453 , 3637	
Mann-Whitney U	1432	

NMDA receptors	5 ms	11 ms
N (samples)	3	3
Number of values	96	75
Minimum	8.521	2.82
25% Percentile	62.11	26.65
Median	138.6	56.25
75% Percentile	238.9	134.6
Maximum	558.2	258.8
Range	549.7	256
95% CI of median		
Actual confidence level	96.85%	96.30%
Lower confidence limit	94.39	36.25
Upper confidence limit	171.5	89.57
Mean	155.4	83.75
Std. Deviation	112.2	71.39
Std. Error of Mean	11.45	8.243
Lower 95% CI of mean	132.7	67.32
Upper 95% CI of mean	178.2	100.2
Coefficient of variation	72.19%	85.25%
Skewness	0.8974	0.835
Kurtosis	0.6163	-0.4438
Kolmogorov-Smirnov test		
P value	0.0006	
Exact or approximate P value?	Approximate	
P value summary	***	
Significantly different (P < 0.05)?	Yes	
Kolmogorov-Smirnov D	0.312	
Mann Whitney test		
P value	<0.0001	
Exact or approximate P value?	Exact	
P value summary	****	
Significantly different (P < 0.05)?	Yes	
One- or two-tailed P value?	Two-tailed	
Sum of ranks in column A,B	9727 , 4979	
Mann-Whitney U	2129	

Table 8 NMDA response to synchronous and asynchronous release events in the presence of Mg2+, while varying the time of the asynchronous release

timing of asynchronous release	5 ms	8 ms	10 ms	20 ms
N (number of simulations)	48	48	48	48
area under curve (arbitary unit)	1527	1488	1357	1351

Table 9 NMDA response to synchronous and asynchronous release events in the presence of Mg2+, while varying the location of release (asynchronous release at 5 ms)

locations of synchronous release	AMPAR	NMDAR	NMDAR 15 mV	NMDAR 30 mV
locations of asynchronous release	NMDAR	AMPAR	NMDAR	NMDAR
N (number of simulations)	48	48	48	48
area under curve (arbitary unit)	1527	1527	1241	1725

Table 10 Percentage of synaptic profile with gold particles

wild type	His-tag::GluA2	HaloTag::GluA2
N (samples)	4	3
Number of values	4	3
Number of images	385	214
Minimum	64.4	0
25% Percentile	65.7	0
Median	69.5	2.7
75% Percentile	71.8	8.3
Maximum	72.5	8.3
Range	8.1	8.3
95% CI of median		
Actual confidence level	87.5%	75.0%
Lower confidence limit	64.4	0
Upper confidence limit	72.5	8.3
Mean	69	3.67
Std. Deviation	3.36	4.23
Std. Error of Mean	1.68	2.44
Lower 95% CI of mean	63.6	-6.85
Upper 95% CI of mean	74.3	14.2
Coefficient of variation	4.88%	115%
Skewness	-0.905	0.974
Kurtosis	1.95	
Unpaired t test with Welch's correction		
P value	<0.0001	
P value summary	****	
Significantly different (P < 0.05)?	Yes	
One- or two-tailed P value?	Two-tailed	
Welch-corrected t, df	t=22.01, df=3.777	
How big is the difference?		
Mean of column A	68.98	
Mean of column B	3.667	
Difference between means (B - A) ± SEM	-65.31 ± 2.967	
95% confidence interval	-73.74 to -56.88	
R squared (eta squared)	0.9923	
F test to compare variances		
F, DFn, Dfd	1.585, 2, 3	
P value	0.6781	
P value summary	ns	
Significantly different (P < 0.05)?	No	

Table 11 Number of gold particles per synaptic profile

knockout	His-tag::GluA2	HaloTag::GluA2
N (samples)	3	2
Number of values	3	2
Number of images	353	165
Minimum	2.11	0.00962
25% Percentile	2.11	0.00962
Median	2.19	0.054
75% Percentile	2.66	0.0984
Maximum	2.66	0.0984
Range	0.55	0.0888
95% CI of median		
Actual confidence level	75.0%	50.0%
Lower confidence limit	2.11	0.00962
Upper confidence limit	2.66	0.0984
Mean	2.32	0.054
Std. Deviation	0.297	0.0628
Std. Error of Mean	0.172	0.0444
Lower 95% CI of mean	1.58	-0.51
Upper 95% CI of mean	3.06	0.618
Coefficient of variation	12.8%	116%
Skewness	1.59	
Kurtosis		
Unpaired t test with Welch's correction		
P value	0.0038	
P value summary	**	
Significantly different (P < 0.05)?	Yes	
One- or two-tailed P value?	Two-tailed	
Welch-corrected t, df	t=12.79, df=2.257	
How big is the difference?		
Mean of column A	2.32	
Mean of column B	0.05401	
Difference between means (B - A) ± SEM	-2.266 ± 0.1772	
95% confidence interval	-2.951 to -1.581	
R squared (eta squared)	0.9864	

Table 12 Percentage of synaptic profile with gold particles

knockout	His-tag::GluA2	HaloTag::GluA2
N (samples)	3	2
Number of values	3	2
Number of images	353	165
Minimum	56.4	0
25% Percentile	56.4	0
Median	62.9	4.9
75% Percentile	75	9.8
Maximum	75	9.8
Range	18.6	9.8
95% CI of median		
Actual confidence level	75.0%	50.0%
Lower confidence limit	56.4	0
Upper confidence limit	75	9.8
Mean	64.8	4.9
Std. Deviation	9.44	6.93
Std. Error of Mean	5.45	4.9
Lower 95% CI of mean	41.3	-57.4
Upper 95% CI of mean	88.2	67.2
Coefficient of variation	14.6%	141%
Skewness	0.855	
Kurtosis		
Unpaired t test with Welch's correction		
P value	0.0047	
P value summary	**	
Significantly different (P < 0.05)?	Yes	
One- or two-tailed P value?	Two-tailed	
Welch-corrected t, df	t=8.169, df=2.835	
How big is the difference?		
Mean of column A	64.77	
Mean of column B	4.9	
Difference between means (B - A) ± SEM	-59.87 ± 7.329	
95% confidence interval	-83.98 to -35.76	
R squared (eta squared)	0.9592	

Table 13 Cumulative relative frequency distribution of lateral distances from receptors to the center of the active zone from 2-D profiles

	ampa first 25	nmda first 25	ampa first 100	nmda first 100	ampar total	nmdar total
Number of values	25	25	100	100	808	551
Minimum	0.093	0.03	0.0423	0.0174	0	0
25% Percentile	0.296	0.239	0.267	0.204	0.277	0.149
Median	0.639	0.649	0.526	0.416	0.569	0.33
75% Percentile	0.789	0.878	0.848	0.664	0.819	0.508
Maximum	0.959	0.982	0.989	0.982	1	0.991
Range	0.866	0.952	0.947	0.964	1	0.991
95% CI of median						
Actual confidence level	95.7%	95.7%	96.5%	96.5%	95.5%	95.0%
Lower confidence limit	0.334	0.346	0.397	0.356	0.541	0.296
Upper confidence limit	0.738	0.856	0.683	0.503	0.608	0.355
Mean	0.559	0.555	0.536	0.443	0.547	0.348
Std. Deviation	0.286	0.332	0.311	0.276	0.297	0.24
Std. Error of Mean	0.0573	0.0665	0.0311	0.0276	0.0105	0.0102
Lower 95% CI of mean	0.441	0.418	0.474	0.389	0.526	0.328
Upper 95% CI of mean	0.677	0.692	0.598	0.498	0.567	0.368
Coefficient of variation	51.2%	59.8%	58.1%	62.3%	54.4%	69.1%
Skewness	-0.188	-0.241	-0.0385	0.293	-0.196	0.574
Kurtosis	-1.32	-1.38	-1.44	-0.955	-1.27	-0.355
one sample Wilcoxon test (against a theoretical median)						
Theoretical median	0.5	0.5	0.5	0.5	0.5	0.5
Actual median	0.639	0.649	0.526	0.416	0.569	0.33
Number of values	25	25	100	100	808	551
Wilcoxon Signed Rank Test						
Sum of signed ranks (W)	79	63	754	-1182	58476	-94302
Sum of positive ranks	202	194	2902	1934	192656	28887
Sum of negative ranks	-123	-131	-2148	-3116	-134180	-123189
P value (two tailed)	0.2996	0.4068	0.1961	0.0419	<0.0001	<0.0001
Exact or estimate?	Exact	Exact	Exact	Exact	Approximate	Approximate
P value summary	ns	ns	ns	*	****	****
Significant (alpha=0.05)?	No	No	No	Yes	Yes	Yes
How big is the discrepancy?						
Discrepancy	0.139	0.149	0.0264	-0.0837	0.0689	-0.17
95% confidence interval	-0.166 to 0.23	-0.154 to 0.35	-0.103 to 0.183	-0.144 to 0.002	0.0407 to 0.108	-0.204 to -0.145
Actual confidence level	95.7	95.7	96.5	96.5	95.5	95

Table 14 Percentage of synaptic profile with gold particles

	His-tag::GluA2	SnapTag::GluA2
Number of cultures	3	2
Number of values	9	6
Number of images	934	834
Minimum	0.434	0.0286
25% Percentile	0.468	0.0429
Median	0.63	0.089
75% Percentile	0.697	0.216
Maximum	0.722	0.315
Range	0.288	0.286
95% CI of median		
Actual confidence level	96.1%	96.9%
Lower confidence limit	0.455	0.0286
Upper confidence limit	0.721	0.315
Mean	0.591	0.125
Std. Deviation	0.112	0.108
Std. Error of Mean	0.0373	0.044
Lower 95% CI of mean	0.505	0.0122
Upper 95% CI of mean	0.677	0.238
Coefficient of variation	18.9%	86.0%
Skewness	-0.31	1.3
Kurtosis	-1.6	1.18
Unpaired t test with Welch's correction		
P value	<0.0001	
P value summary	****	
Significantly different (P < 0.05)?	Yes	
One- or two-tailed P value?	Two-tailed	
Welch-corrected t, df	t=8.08, df=11.2	
How big is the difference?		
Mean of column A	0.591	
Mean of column B	0.125	
Difference between means (B - A) ± SEM	-0.466 ± 0.0577	
95% confidence interval	-0.593 to -0.339	
R squared (eta squared)	0.854	
F test to compare variances		
F, DFn, Dfd	1.08, 8, 5	
P value	0.9803	
P value summary	ns	
Significantly different (P < 0.05)?	No	

Table 15 Percentage of synaptic profile with gold particles

	His-tag::NR1	SnapTag::NR1
Number of cultures	3	2
Number of values	9	3
Number of images	836	584
Minimum	0.524	0
25% Percentile	0.529	0.0144
Median	0.574	0.0955
75% Percentile	0.656	0.25
Maximum	0.828	0.297
Range	0.303	0.297
95% CI of median		
Actual confidence level	96.1%	96.9%
Lower confidence limit	0.529	0
Upper confidence limit	0.718	0.297
Mean	0.603	0.124
Std. Deviation	0.103	0.126
Std. Error of Mean	0.0343	0.0513
Lower 95% CI of mean	0.524	-0.00825
Upper 95% CI of mean	0.682	0.255
Coefficient of variation	17.1%	102%
Skewness	1.67	0.42
Kurtosis	2.12	-2.06
Unpaired t test with Welch's correction		
P value	<0.0001	
P value summary	****	
Significantly different (P < 0.05)?	Yes	
One- or two-tailed P value?	Two-tailed	
Welch-corrected t, df	t=7.77, df=9.32	
How big is the difference?		
Mean of column A	0.603	
Mean of column B	0.124	
Difference between means (B - A) ± SEM	-0.480 ± 0.0617	
95% confidence interval	-0.619 to -0.341	
R squared (eta squared)	0.866	
F test to compare variances		
F, DFn, Dfd	1.49, 5, 8	
P value	0.5879	
P value summary	ns	
Significantly different (P < 0.05)?	No	

Table 16 Number of docked vesicles per synaptic profile

Number of cultures	3	3	3		
Number of values	10	10	10		
Number of images	740	835	791		
Minimum	1.72	0.726	0.685		
25% Percentile	1.77	0.816	0.745		
Median	1.87	0.919	0.902		
75% Percentile	1.92	0.995	0.958		
Maximum	2.06	1.2	1.16		
Range	0.34	0.474	0.47		
95% CI of median					
Actual confidence level	97.9%	97.9%	97.9%		
Lower confidence limit	1.75	0.74	0.714		
Upper confidence limit	2.01	1.01	1.03		
Mean	1.87	0.919	0.883		
Std. Deviation	0.106	0.138	0.145		
Std. Error of Mean	0.0336	0.0437	0.0458		
Lower 95% CI of mean	1.79	0.82	0.78		
Upper 95% CI of mean	1.94	1.02	0.987		
Coefficient of variation	5.69%	15.0%	16.4%		
Skewness	0.463	0.538	0.392		
Kurtosis	-0.101	0.934	-0.112		
Two-way ANOVA	Ordinary				
Alpha	0.05				
Source of Variation	% of total va	P value	P value summary	Significant?	
Interaction	1.172	0.0004	***	Yes	
Row Factor	0.5597	0.0107	*	Yes	
Column Factor	20.02	<0.0001	****	Yes	
ANOVA table	SS (Type III)	DF	MS	F (DFn, DFd)	P value
Interaction	31.31	18	1.739	F (18, 2921) = 2.505	P=0.0004
Row Factor	14.94	9	1.66	F (9, 2921) = 2.392	P=0.0107
Column Factor	534.5	2	267.2	F (2, 2921) = 384.9	P<0.0001
Residual	2028	2921	0.6942		
Tukey's multiple comparisons test	Predicted (L	95.00% CI of c	Significant?	Summary	Adjusted P Value
no stim vs. 5 ms	0.9488	0.8569 to 1.04	Yes	****	<0.0001
no stim vs. 11 ms	0.9841	0.8910 to 1.07	Yes	****	<0.0001
5 ms vs. 11 ms	0.0353	-0.05155 to 0.	No	ns	0.6066

Table 17 Number of pits per synaptic profile

Number of cultures	3	3	3		
Number of values	10	10	10		
Number of images	740	835	791		
Number of values	10	10	10		
Minimum	0	0.0885	0.02655		
25% Percentile	0	0.2248	0.07657		
Median	0.01984	0.2961	0.1195		
75% Percentile	0.02844	0.3247	0.1606		
Maximum	0.04808	0.4623	0.2667		
Range	0.04808	0.3738	0.2402		
95% CI of median					
Actual confidence level	97.85%	97.85%	97.85%		
Lower confidence limit	0	0.2	0.06863		
Upper confidence limit	0.02885	0.3558	0.2135		
Mean	0.01782	0.2794	0.1249		
Std. Deviation	0.01563	0.09906	0.07061		
Std. Error of Mean	0.004944	0.03133	0.02233		
Lower 95% CI of mean	0.006632	0.2085	0.07439		
Upper 95% CI of mean	0.029	0.3502	0.1754		
Coefficient of variation	87.75%	35.46%	56.54%		
Skewness	0.4709	-0.1392	0.8931		
Kurtosis	-0.05549	1.395	0.7211		
Two-way ANOVA	Ordinary				
Alpha	0.05				
Source of Variation	% of total variation	P value	P value summary	Significant?	
Interaction	1.781	<0.0001	****	Yes	
Row Factor	1.316	<0.0001	****	Yes	
Column Factor	7.814	<0.0001	****	Yes	
ANOVA table	SS (Type II)	DF	MS	F (DFn, DFd)	P value
Interaction	7.298	18	0.4055	F (18, 2921) = 3.272	P<0.0001
Row Factor	5.392	9	0.5991	F (9, 2921) = 4.835	P<0.0001
Column Factor	32.02	2	16.01	F (2, 2921) = 129.2	P<0.0001
Residual	362	2921	0.1239		
Tukey's multiple comparisons test	Predicted (LS) mean diff.	95.00% CI of diff.	Significant?	Summary	Adjusted P Value
no stim vs. 5 ms	-0.2616	-0.3004 to -0.2227	Yes	****	<0.0001
no stim vs. 11 ms	-0.1071	-0.1464 to -0.06774	Yes	****	<0.0001
5 ms vs. 11 ms	0.1545	0.1178 to 0.1912	Yes	****	<0.0001

Table 18 AMPAR response to synchronous and asynchronous release events in the absence of Mg2+, while varying the timing of asynchronous release

locations of synchronous release	random	NMDAR	AMPAR	AMPAR+NMDAR	AMPAR	AMPAR	AMPAR	AMPAR	AMPAR
locations of asynchronous release	-	-	-	-	NMDAR	NMDAR	NMDAR	NMDAR	NMDAR
timing of asynchronous release (ms)	-	-	-	-	5	10	15	20	50
N (number of simulations)	48	48	48	48	48	48	48	48	48
area under curve (arbitary unit)	3431	3267	4581.271	6857.813	6667.521	6807.447	7070.021	7325	8006.625

Table 19 NMDAR response to synchronous and asynchronous release events in the absence of Mg2+, while varying the timing of the asynchronous release

locations of synchronous release	random	NMDAR	AMPAR	AMPAR+NMDAR	AMPAR	AMPAR	AMPAR	AMPAR	AMPAR
locations of asynchronous release	-	-	-	-	NMDAR	NMDAR	NMDAR	NMDAR	NMDAR
timing of asynchronous release (ms)	-	-	-	-	5	10	15	20	50
N (number of simulations)	48	48	48	48	48	48	48	48	48
area under curve (arbitary unit)	6970	24470	26367.02	48406.75	53986.9	53172.98	55250.13	54429.69	58565.92

Table 20 NMDAR response to synchronous and asynchronous release events in the absence of Mg2+, while varying the location of release, the timing of the synchronous release and the membrane potentials

locations of synchronous release	AMPAR+NMDAR	AMPAR	NMDAR	NMDAR	NMDAR	NMDAR	NMDAR	NMDAR	NMDAR
depolarization during synchronous (mV)	45	30	0	15	15	30	30	30	30
locations of asynchronous release	-	NMDAR	AMPAR	AMPAR	NMDAR	NMDAR	NMDAR	NMDAR	NMDAR
depolarization during asynchronous (mV)	-	15	30	30	15	15	15	15	15
timing of asynchronous release (ms)	-	5	5	5	5	5	8	10	20
N (number of simulations)	48	48	48	48	48	48	48	48	48
area under curve (arbitary unit)	1725	1527	1293.468	1527	1241	1725	1586	1631	1544

Table 21 AMPAR and NMDAR response to single or double release events in the absence of Mg2+, while varying the locations of release

locations of synchronous release	AMPAR	NMDAR	random	AMPAR
locations of asynchronous release	-	-	-	NMDAR
NMDAR response	26367	24470	12800	53986
AMPAR respponse	4581	3267	3431	6667
NMDA/AMPA ratio	5.76	7.49	3.73	8.09
N (number of simulations)	48	48	48	48

Chapter 4

Ultrafast endocytosis at postsynaptic terminals

Abstract

Currently, clathrin-mediated endocytosis is thought to be the major model of endocytosis at the postsynaptic terminals. It occurs at perisynaptic or extrasynaptic regions termed endocytic zone. Here, we identified a novel form of endocytosis-ultrafast endocytosis using the time-resolved electron microscopy technique, “flash-and-freeze”. which takes places directly within the PSD within 100 ms. Moreover, our preliminary pharmacological results suggest that ultrafast endocytosis is clathrin-independent and actin is required for the formation of the ultrafast endocytosis.

Introduction

Endocytosis is a basic cellular process that allows cells to internalize extracellular molecules, remove plasma membrane, and regulate the abundance of specific transmembrane proteins (Mukherjee, Ghosh, and Maxfield 1997). In neurons, endocytosis also plays an important role in maintaining the efficiency of neurotransmission. After synaptic vesicle fusion, neurons must remove synaptic proteins and any extra membrane to sustain neurotransmitter release and prevent expansion of the plasma membrane (Saheki and De Camilli 2012). Thus, at the presynaptic compartment, one major function of endocytosis is to recycle synaptic vesicles (Heuser and Reese 1973). On the postsynaptic side, the number of neurotransmitter receptors has to be precisely controlled to tune the signal strength during neurotransmission(Lüscher et al. 1999) . Therefore, endocytosis at the post-synapse plays an essential role in regulating the number of the receptors.

Currently, CME at the postsynaptic terminals is thought to be the predominant mechanism of endocytosis (Man et al. 2000). One of the important functions of postsynaptic

CME at excitatory synapses is to remove AMPA-type glutamate receptors from the plasma membrane in an activity-dependent manner (Carroll et al. 1999; Y. T. Wang and Linden 2000; Man et al. 2000). In the process, AMPA receptors dissociate from the PSD when certain signaling cascades are triggered and then laterally diffuse to endocytic zones (EZs) adjacent to the PSD (J. Lu et al. 2007; Blanpied, Scott, and Ehlers 2002; Rácz et al. 2004). At EZs, clathrin coats assemble into a lattice on the intracellular surface of the membrane by binding the adaptors and the cargo. Eventually, the coated vesicles with AMPARs are pinched off (Brodsky 2012).

In the present study, we have identified a novel endocytic pathway at the postsynaptic terminals using the “flash-and-freeze” technique. In contrast to CME observed at the post-synapse, this novel mechanism of endocytosis takes place directly at PSD in a millisecond time scale; we therefore named it ultrafast endocytosis. Moreover, our preliminary results from pharmacological experiments indicate that ultrafast endocytosis at the PSD is actin-dependent but clathrin-independent. However, the induction mechanisms and physiological function of ultrafast endocytosis still need to be further studied.

Materials and methods

Neuron culture

Both astrocytes and hippocampal neuron cultures were established from embryonic day 18 or P0 wild-type animals. Both sexes were indistinguishably used in this study. Astrocytes were harvested from cortices with trypsin treatment for 20 min at 37 °C with shaking, followed by dissociation and seeding on T-75 flask. Astrocytes were grown in DMEM supplemented with 10% FBS and 0.1% penicillin-streptomycin at 37 °C and 5 % CO_2 for 7-10 days. Two clean 6 mm sapphire disks (Technotrade Inc) were placed per well of 12-well tissue culture plate and coated with poly-D-lysine (1 mg/ml, Sigma) and collagen (ThermoFisher). Astrocytes served as a feeder layer for neurons and were seeded (50,000/well) one week before hippocampal

neuronal culture. On day 6, FUDR (80 uM) was added to inhibit cell division. On day 7, hippocampi were isolated and digested with papain (20 U/ml) for 30-60 min at 37 °C with shaking. An inactivation solution (2.5 mg of trypsin inhibitor and 0.5 mg of albumin per mL of DMEM) was then applied for 5 min at 37 °C. Hippocampi were triturated by pipetting 4 x 20 times, and cells were seeded on prepared astrocyte feeder layer with a density of 75,000/well and maintained in Neurobasal A media supplemented with B-27, Glutamax, and 0.2 % penicillin-streptomycin at 37 °C and 5 % CO_2. The cells were infected with lentivirus at days *in vitro* (DIV) 3-4 as needed and used for experiments on DIV 13-17.

Expression constructs

Lentiviral expression constructs were used to express transgenes in neurons. All vectors were based on the lentiviral shuttlevector FUGW (Lois et al. 2002). A mouse CHC-1 specific shRNA target sequence (5'- GTTGGTGACCGTTGTTATG-3′) and scrambled shRNA control sequence (5′-TTCGCACCCTACTTCGTGG-3) were cloned into a lentiviral shuttle vector under the control of a U6 promoter. Channelrhodopsin-2-E123T/T159C-eYFP was cloned under control of the synapsin promoter (a gift from the Christian Rosenmund lab). eYFP signals were used to evaluate viral infection and intensity of transgene expression from this polycistronic construct.

Lentivirus production and infection

Lentiviruses carrying the expression constructs were produced using the following procedures. The bottom surface of T-75 flasks was coated with poly-L-lysine (0.2 % in milliQ water). A day before the transfection, HEK293T cells were plated at $6.5x10^5$/ml (10 ml in T-75) in Neurobasal A (NBA) media containing 1 % glutamax, 2 % B27, and 0.2 % penicillin-streptomycin. The shuttle vector (FUGW) containing expression constructs and helper plasmids (VSV-G and CMV-dR8.9) were mixed at 20, 5, and 7.5 µg, respectively, in 640 µl NaCl solution

(150 mM) (Solution I). Another solution (solution II) was prepared as follows: 246.7 µl H_2O, 320 µl NaCl (300 mM), 73.3 µl polyethylenimine (0.6 µg/µl). Solution I and II were mixed by vortexing and incubated at room temperature for 10 minutes, followed by addition to the T-75 flask containing HEK293T cells. The cells were incubated at 37 ºC (5 % CO_2), and the viruses were harvested 3 days later. The media containing lentivirus was centrifuged at 4000 rpm to obtain 20-fold concentration using Amicon (Ultracel-100k). The infection efficiency was determined by infection in wild-type neurons that were separately prepared. For all the experiments, dissociated hippocampal neurons were infected on DIV 3-4 with lentiviruses carrying the expression constructs. The infection rate of 95 % was achieved in all cases.

Pharmacology

Pitstop2, Latranculin A, and Jasplakinolide was added to the cell culture medium from stock in DMSO to a final concentration of 30 µM,10 µM, and 100 nM. Following incubation for 30 mins, cells were transferred to the extracellular solution containing 140 mM NaCl, 2.4 mM KCl,10 mM HEPES, 10 mM glucose, 4 mM $CaCl_2$, and 1 mM $MgCl_2$ with final concentration of 30 µM Bicuculine and 3 µM NBQX. (pH adjusted to 7.3 with NaOH, 300 mOsm). Cells were then subjected to flash-and-freeze.

Flash-and-freeze and freeze

Cells cultured on sapphire disks were frozen using a high-pressure freezer (EM ICE, Leica Microsystems). Each disk with neurons was transferred into the physiological saline solution containing NBQX (3 µM, Tocris) and bicuculine (30 µM; Tocris), which were added to block recurrent synaptic activity during the flash-and-freeze experiments. The disk was mounted onto the middle plate with neurons facing up. A 100 µm spacer ring was placed on top of the sapphire disk. Then, another blank sapphire disk was placed on top of the spacer ring to make a “sandwich”. Finally, a 400 µm ring was put on top of the “sandwich” to hold it in place. The entire assembled middle plate was then placed on a piece of filter paper to remove the excess liquid,

loaded between two half cylinders, and transferred into the freezing chamber. A blue light was applied for 10 ms after a 15 s dark phase to induce a single action potential, and cells were frozen 50 ms,100 ms, 300 ms, 1 s, 3 s, or 10 s after the stimulus These time points were chosen based on our previous study of ultrafast endocytosis at presynaptic terminals of mouse hippocampal neurons. For no stimulation control, a blue light was applied for 1 ms. The frozen sample was automatically dropped into a storage dewar filled with liquid nitrogen.

After freezing, the middle plate with sapphire disks was transferred using pre-chilled tweezers to a cup containing anhydrous acetone (-90 ºC), which was placed in an automated freeze substitution system (EM AFS2, Leica microsystems). The cryovials containing fixative (1% glutaraldehyde, 1% osmium tetroxide, and 1% water in anhydrous acetone) were stored in liquid nitrogen and moved to AFS2 before use. After disassembling the freezing apparatus, sapphire disks with neurons were transferred into cryovials in the AFS, which is set at -90 ºC, using pre-chilled tweezers. The freeze substitution program was as follows: -90 °C for 6-10 hours, -90 °C to -20 °C in 14 hours, -20 °C for 12 hours, and -20 °C to 20 °C in 4 hours.

Embedding, sectioning and transmission electron microscopy

Following freeze-substitution, fixatives were washed with anhydrous acetone three times for 10 min each. After washing, samples were infiltrated through 30 %, 70 %, and 90 % epon-araldite in anhydrous acetone every two hours. Then samples were transferred to caps of polyethylene BEEM capsules with 90 % epon araldite and incubate overnight at 4 °C. Samples were incubated in the caps of polyethylene BEEM capsules with 100% epon araldite (epon 6.2 g; araldite 4.4 g; DDSA 12.2 g, and BDMA 0.8 ml) at room temperature the next day. Samples were transferred three times to new caps with fresh 100 % epon araldite every 2 hours, after which samples were baked at 60 °C for 48 hours.

After resin was cured, sapphire disks were removed from resin. Cells were embedded in the resin block. Then, the block was cut into small pieces and placed atop of a dummy block using super glue for sectioning. 40 nm sections were cut using an ultramicrotome (EM UC7,

Leica microsystems) and collected on single-slot copper grids coated with 0.7 % pioloform. The sections were stained with 2.5 % uranyl acetate in 75 % methanol and then imaged at 80 kV at 93,000x magnification on a Philips CM120 transmission electron microscope equipped with an AMT XR80 camera. About 100 electron micrographs per sample were taken blindly. To avoid the sampling bias, synapses were found by bidirectional raster scanning along the section at 93,000x. Synapses were identified by a vesicle-filled presynaptic bouton and a postsynaptic density.

Results

Ultrafast endocytosis occurs at the PSD

In the study of presynaptic ultrafast endocytosis, we occasionally observed membrane invagination in at the postsynaptic terminals. To test whether these are endocytic structures, we expressed channelrhodopsin in these neurons, stimulated them with a 10-ms light pulse, and subjected them to high pressure freezing at defined time points after stimulation ranging from 5 ms to 10 s (**Fig. 10**). The prevalence of pits peaked at 100 ms after stimulation (**Fig. 10A&E**). As pits decline in number, large vesicles of the same diameter (**Fig. 10G**) were observed within 50 nm of the postsynaptic density (300 ms-1s: **Fig. 10B&E**, red line). These vesicles diffuse into the postsynaptic terminals (**Fig. 10E**) at later time points (1s-10s) indicating precursor-product relationship between pits and large vesicles.

To further determine whether these truly represent endocytic events, we performed ferritin uptake assay using flash-and-freeze. Cationized ferritin particles can serve as fluid phase markers for endocytic trafficking (Watanabe, Rost, et al. 2013b) . Ferritin particles were found mostly in endocytic pits at 100 ms and exclusively in large vesicles inside the postsynaptic terminals (**Fig. 10C, D&F**). These data indicate that membrane invagination observed within postsynaptic density represent endocytic intermediates. Based on the time scale and morphology, this endocytic pathway is similar to ultrafast endocytosis observed in presynaptic terminals that recovers synaptic vesicle membrane. Moreover, the obvious clathrin coats were not observed around the pits; therefore, we speculated that ultrafast endocytosis at PSD is clathrin-independent.

Ultrafast endocytosis is clathrin-independent and actin-dependent

To test whether clathrin is involved in this endocytic pathway, we infected neurons with lentivirus expressing either short hairpin RNA (shRNA) against clathrin heavy chain or scrambled shRNA as a control. Clathrin knockdown had no significant effect on ultrafast

endocytosis at postsynaptic terminals. At 3 s after stimulation, ferritin-containing endosome were found in both control and clathrin knockdown cells (**Fig. 11A&B**). The number of ferritin-containing endosome did not change in the control and clathrin knockdown cells (**Fig. 11E**). We also applied pitstop2 to inhibit clathrin-mediated endocytosis. Pitstop2 is a drug that inhibits the interaction of amphiphysin and the amino terminal domain of clathrin, leading to inhibition of clathrin-mediated endocytosis (von Kleist et al. 2011). The ferritin containing endosome were found in both control and pitstop2 treatment (**Fig. 11C&D**), and the number of ferritin containing endosome were similar (**Fig. 11F**). However, the endosome in pitstop2 treatment seemed larger than control endosomes, suggesting clathrin might act on endosome to regenerate vesicles. Our previous study showed that actin polymerization is required for ultrafast endocytosis at presynaptic terminals. To investigate the role of actin polymerization in ultrafast endocytosis at the postsynaptic terminals, we applied latrunculin A and jasplankinolide to cultured hippocampal neurons to disrupt the dynamics of actin polymerization (Holzinger and Blaas 2016). Ultrafast endocytosis at postsynaptic terminals was normal in DMSO treated neurons (**Fig. 11G**). However, no endocytic structures were observed in both latrunculin-A and jasplankinolide treatment (**Fig. 11G**), suggesting the dynamics of actin polymerization is required for ultrafast endocytosis at the PSD.

Discussion

Using the “flash-and-freeze” technique, we have identified a novel endocytic pathway, ultrafast endocytosis, at the postsynaptic terminals. Contrary to clathrin-mediated endocytosis occurring at the dedicated endocytic zone adjacent to PSD (Blanpied, Scott, and Ehlers 2002), ultrafast endocytosis takes place directly within the postsynaptic density in a clathrin-independent manner. Currently, the major approach used to study endocytosis is light microscopy (Salavessa and Sauvonnet 2021; Weigert 2014). However, light microscopy may not achieve resolution high enough to pinpoint the specific locations where endocytosis occurs. Furthermore, due to the technical limitations, most studies are focused on the long-term regulation of endocytosis, in the range of minutes (H. K. Lee et al. 1998; Rosel M. Mulkey and Malenka 1992). We have a little knowledge about the initiation of endocytosis especially in the first few hundred milliseconds. Although it is preliminary, our results in this study provides a new insight into the initiation and location of endocytosis at postsynaptic terminals.

In addition, our results also provide new information about spike-timing dependent plasticity. Spike-timing dependent plasticity is a type of synaptic modification that is dependent on the order of pre and postsynaptic spiking (Caporale and Dan 2008). In our flash-and-freeze experiments, the optogenetic stimulation resembles the post-and-pre order of spike-timing stimulation (Caporale and Dan 2008). Based on our previous study, the plasma membrane is depolarized immediately after the light onset, but additional 5 ms is necessary for membranes to depolarize sufficiently to generate an action potential (Watanabe, Rost, et al. 2013b). In this case, the postsynaptic terminal depolarization occurs before the presynaptic glutamate release, mimicking the post-to-pre order of spike timing stimulation. Because this post-to-pre pairing leads to the reduction in AMPA receptor currents and thereby synaptic depression, I speculate that clathrin-independent ultrafast endocytosis may be related to an endocytic pathway to remove AMPA receptors after spike-timing dependent depression.

Currently, the induction mechanism and physiological role of this endocytic pathway is unknown. The calcium influx through NMDA receptors is involved in activity-dependent endocytosis of AMPA receptors. Therefore, it is quite possible that activation of NMDA receptors and thereby calcium signaling is required for the induction of ultrafast endocytosis. To test this hypothesis, we need to block NMDA receptors by inhibitors, such as AP5, MK801 and 7-Chlorokynurenate. In addition, calcium chelator EGTA can be used to assess the requirement for calcium signaling. Furthermore, to test whether AMPA receptors are removed from the postsynaptic terminals, we need to examine whether ultrafast endocytosis engulf AMPA receptors in the future.

Figures

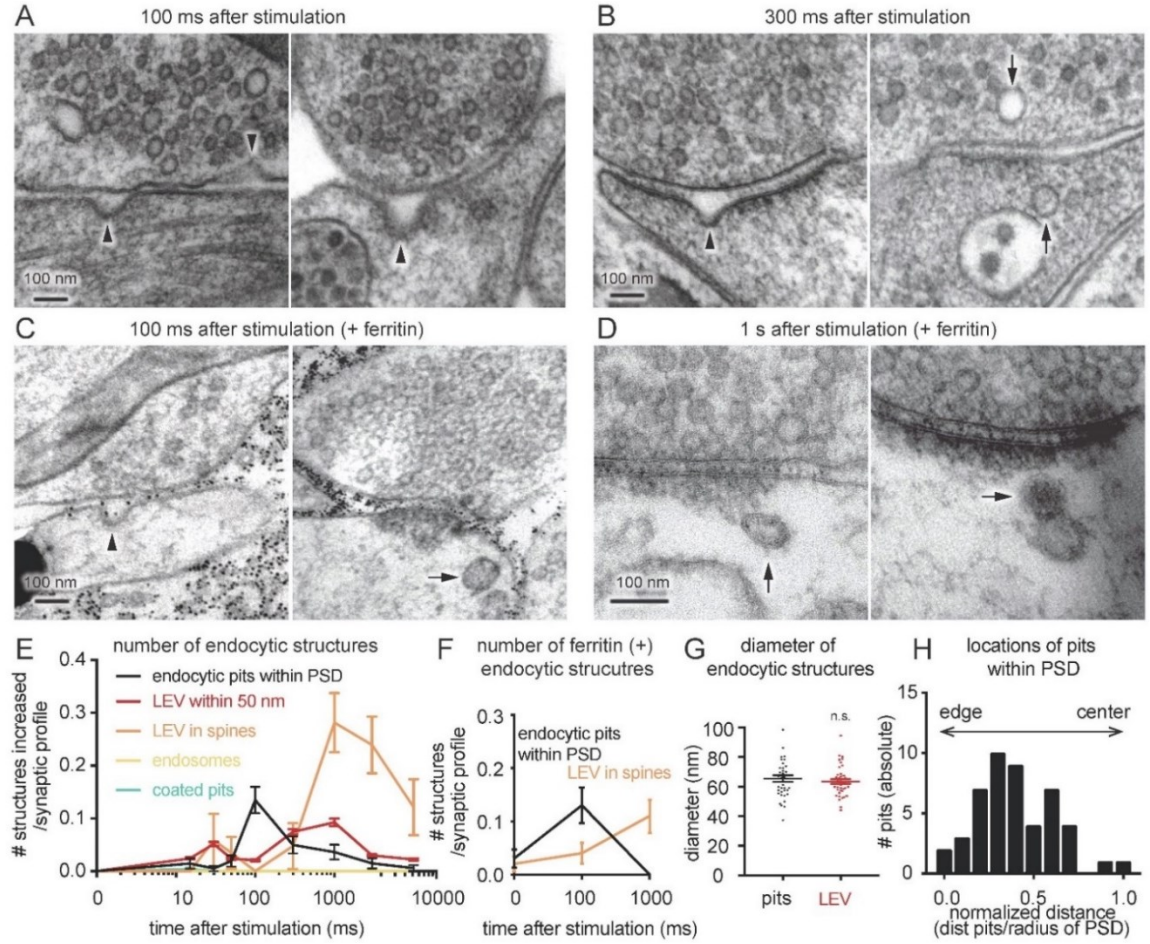

Figure 10 Ultrafast endocytosis occurs at postsynaptic density.

Mouse primary cultured hippocampal neurons were stimulated by light and frozen at defined time points. Black arrowheads point to invaginations and black arrows point to endocytic vesicles in Figure A-D. **A, B.** representative micrographs showing invaginations (**A** black arrowheads) and large endocytic vesicles (**B** black arrows) were observed at postsynaptic terminals. **C, D.** representative micrographs showing ferritin-containing invaginations (**C** black arrowheads) and ferritin-containing vesicles (**D** black arrows) were observed at postsynaptic terminals. **E**. Graph showing the number of endocytic structures per synaptic profile after a single stimulus. After stimulation, endocytic pits within the PSD were observed in 10% of the synapses (black line). The prevalence of large endocytic vesicles (LEV) within 50 nm of the

postsynaptic terminals (red line) and in spine (orange line) are increased at later time points. The number of clathrin coated pits (green line) and endosomes (yellow line) remain similar after stimulation. Endosomes were defined as vesicles larger than 100 nm. **F**. Graph showing the number of ferritin-containing endocytic structures per synaptic profile. Endocytic pits were observed at 100 ms in 10% of the synapses (black line) followed by an increase in the number of large endocytic vesicles (orange line). **G.** Average diameter of endocytic pits and large endocytic vesicles. **H.** Location of pits within the PSD (0 indicates the edge of the PSD, 1 indicates the center of the PSD).

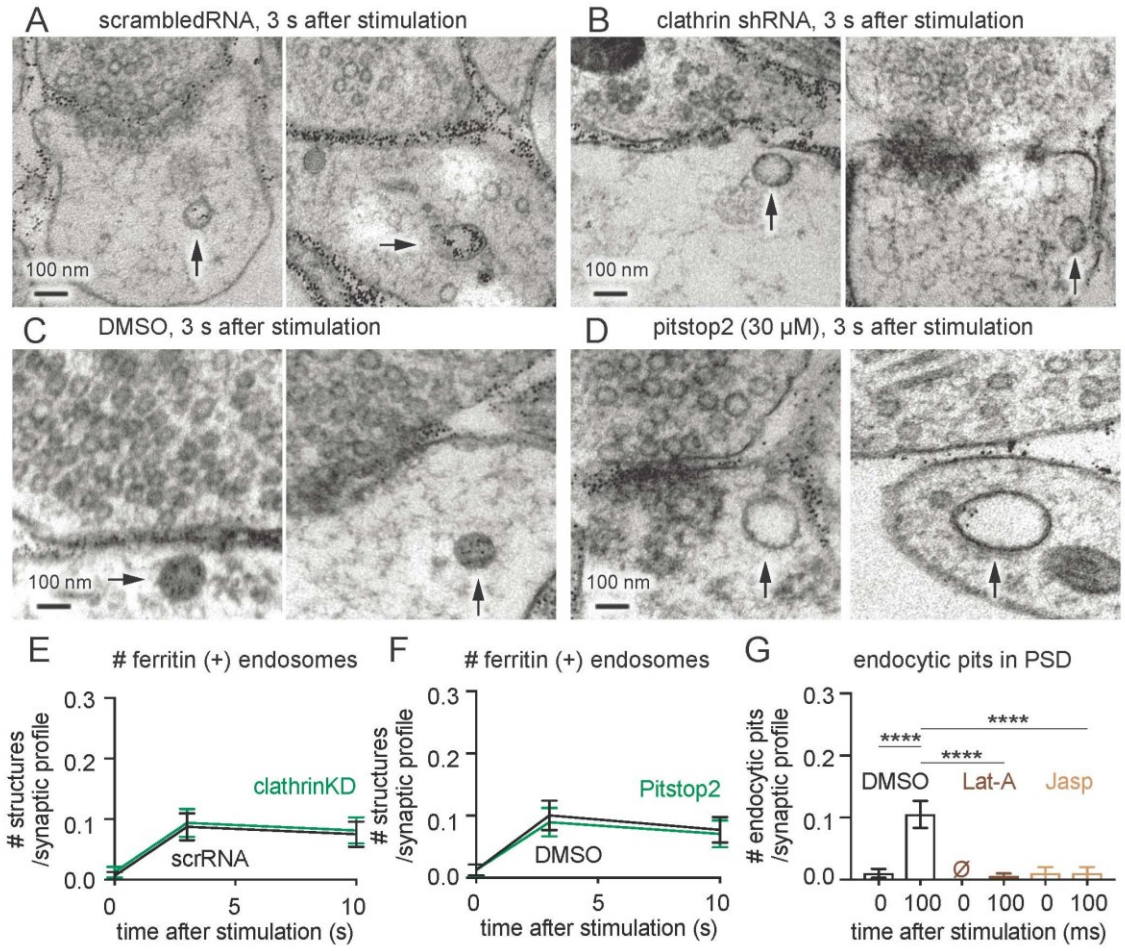

Figure 11 Ultrafast endocytosis is clathrin-independent.

Mouse primary cultured hippocampal neurons were treated with shRNA and drugs and stimulated by light and frozen at defined time points. **A,B**, representative micrographs showing scrambled shRNA- **(A)** and clathrin shRNA- **(B)** treated cells 3 s after light stimulation. **C,D,** representative micrographs showing 0.1% DMSO- **(C)** and 30 µM pitstop2- **(D)** treated cells 3 s after light stimulation. Ferritin-containing endosome are observed in the postsynaptic terminals (black arrow). **E.** Number of ferretin-containing endosome per synaptic profile in scrambled shRNA (black line) and clathrin-KD-treated cells (green line). **F.** Number of ferritin-containing endosome in control (black line) and pitstop2-treated cells (green line). **G.** Number of endocytic pits of no stimulated control and 100 ms after treatment with 0.1% DMSO, 10 µM latrunculin-A, or 100 nM jasplakinolide.

Bibliography

Allen, C., and C. F. Stevens. 1994. “An Evaluation of Causes for Unreliability of Synaptic Transmission.” *Proceedings of the National Academy of Sciences* 91 (22): 10380–83. https://doi.org/10.1073/pnas.91.22.10380.

Anggono, Victor, and Richard L. Huganir. 2012. “Regulation of AMPA Receptor Trafficking and Synaptic Plasticity.” *Current Opinion in Neurobiology* 22 (3): 461–69. https://doi.org/10.1016/j.conb.2011.12.006.

Anggono, Victor, Yeliz Koç-Schmitz, Jocelyn Widagdo, Jan Kormann, Annie Quan, Chih-Ming Chen, Phillip J. Robinson, et al. 2013. “PICK1 Interacts with PACSIN to Regulate AMPA Receptor Internalization and Cerebellar Long-Term Depression.” *Proceedings of the National Academy of Sciences* 110 (34): 13976–81. https://doi.org/10.1073/pnas.1312467110.

Atasoy, Deniz, Mert Ertunc, Krista L. Moulder, Justin Blackwell, ChiHye Chung, Jianzhong Su, and Ege T. Kavalali. 2008. “Spontaneous and Evoked Glutamate Release Activates Two Populations of NMDA Receptors with Limited Overlap.” *Journal of Neuroscience* 28 (40): 10151–66. https://doi.org/10.1523/JNEUROSCI.2432-08.2008.

Bartol, Thomas M, Jr, Cailey Bromer, Justin Kinney, Michael A Chirillo, Jennifer N Bourne, Kristen M Harris, and Terrence J Sejnowski. 2015. “Nanoconnectomic Upper Bound on the Variability of Synaptic Plasticity.” Edited by Sacha B Nelson. *ELife* 4 (November): e10778. https://doi.org/10.7554/eLife.10778.

Bartol, Thomas M., Daniel X. Keller, Justin P. Kinney, Chandrajit L. Bajaj, Kristen M. Harris, Terrence J. Sejnowski, and Mary B. Kennedy. 2015. “Computational Reconstitution of Spine Calcium Transients from Individual Proteins.” *Frontiers in Synaptic Neuroscience* 7 (October). https://doi.org/10.3389/fnsyn.2015.00017.

Bats, Cecile, Laurent Groc, and Daniel Choquet. 2007. “The Interaction between Stargazin and PSD-95 Regulates AMPA Receptor Surface Trafficking.” *Neuron* 53 (5): 719–34. https://doi.org/10.1016/j.neuron.2007.01.030.

Bekkers, J M, G B Richerson, and C F Stevens. 1990. “Origin of Variability in Quantal Size in Cultured Hippocampal Neurons and Hippocampal Slices.” *Proceedings of the National Academy of Sciences of the United States of America* 87 (14): 5359–62.

Bekkers, John M., and Charles F. Stevens. 1989. “NMDA and Non-NMDA Receptors Are Co-Localized at Individual Excitatory Synapses in Cultured Rat Hippocampus.” *Nature* 341 (6239): 230–33. https://doi.org/10.1038/341230a0.

Bergeijk, Petra van, Max Adrian, Casper C. Hoogenraad, and Lukas C. Kapitein. 2015. “Optogenetic Control of Organelle Transport and Positioning.” *Nature* 518 (7537): 111–14. https://doi.org/10.1038/nature14128.

Bergles, D. E., J. S. Diamond, and C. E. Jahr. 1999. “Clearance of Glutamate inside the Synapse and Beyond.” *Current Opinion in Neurobiology* 9 (3): 293–98. https://doi.org/10.1016/s0959-4388(99)80043-9.

Bernard, Véronique, Peter Somogyi, and J. Paul Bolam. 1997. “Cellular, Subcellular, and Subsynaptic Distribution of AMPA-Type Glutamate Receptor Subunits in the Neostriatum of the Rat.” *The Journal of Neuroscience* 17 (2): 819–33. https://doi.org/10.1523/JNEUROSCI.17-02-00819.1997.

Betzig, Eric, George H. Patterson, Rachid Sougrat, O. Wolf Lindwasser, Scott Olenych, Juan S. Bonifacino, Michael W. Davidson, Jennifer Lippincott-Schwartz, and Harald F. Hess. 2006. “Imaging Intracellular Fluorescent Proteins at Nanometer Resolution.” *Science* 313 (5793): 1642–45. https://doi.org/10.1126/science.1127344.

Bi, Guo-qiang, and Mu-ming Poo. 1998. “Synaptic Modifications in Cultured Hippocampal Neurons: Dependence on Spike Timing, Synaptic Strength, and Postsynaptic Cell Type.” *Journal of Neuroscience* 18 (24): 10464–72. https://doi.org/10.1523/JNEUROSCI.18-24-10464.1998.

Biederer, Thomas, Pascal S. Kaeser, and Thomas A. Blanpied. 2017a. “Transcellular Nanoalignment of Synaptic Function.” *Neuron* 96 (3): 680–96. https://doi.org/10.1016/j.neuron.2017.10.006.

Blanpied, Thomas A., Derek B. Scott, and Michael D. Ehlers. 2002. “Dynamics and Regulation of Clathrin Coats at Specialized Endocytic Zones of Dendrites and Spines.” *Neuron* 36 (3): 435–49. https://doi.org/10.1016/s0896-6273(02)00979-0.

Boehm, Jannic, Myoung-Goo Kang, Richard C. Johnson, Jose Esteban, Richard L. Huganir, and Roberto Malinow. 2006. “Synaptic Incorporation of AMPA Receptors during LTP Is Controlled by a PKC Phosphorylation Site on GluR1.” *Neuron* 51 (2): 213–25. https://doi.org/10.1016/j.neuron.2006.06.013.

Bowie, D., and M. L. Mayer. 1995. “Inward Rectification of Both AMPA and Kainate Subtype Glutamate Receptors Generated by Polyamine-Mediated Ion Channel Block.” *Neuron* 15 (2): 453–62. https://doi.org/10.1016/0896-6273(95)90049-7.

Boyden, Edward S., Feng Zhang, Ernst Bamberg, Georg Nagel, and Karl Deisseroth. 2005. “Millisecond-Timescale, Genetically Targeted Optical Control of Neural Activity.” *Nature Neuroscience* 8 (9): 1263–68. https://doi.org/10.1038/nn1525.

Brodsky, Frances M. 2012. “Diversity of Clathrin Function: New Tricks for an Old Protein.” *Annual Review of Cell and Developmental Biology* 28: 309–36. https://doi.org/10.1146/annurev-cellbio-101011-155716.

Burger, P. M., E. Mehl, P. L. Cameron, P. R. Maycox, M. Baumert, F. Lottspeich, P. De Camilli, and R. Jahn. 1989. “Synaptic Vesicles Immunoisolated from Rat Cerebral Cortex Contain High Levels of Glutamate.” *Neuron* 3 (6): 715–20. https://doi.org/10.1016/0896-6273(89)90240-7.

Bykov, Yury S., Mirko Cortese, John A. G. Briggs, and Ralf Bartenschlager. 2016. “Correlative Light and Electron Microscopy Methods for the Study of Virus-Cell Interactions.” *FEBS Letters* 590 (13): 1877–95. https://doi.org/10.1002/1873-3468.12153.

Caporale, Natalia, and Yang Dan. 2008. “Spike Timing-Dependent Plasticity: A Hebbian Learning Rule.” *Annual Review of Neuroscience* 31: 25–46. https://doi.org/10.1146/annurev.neuro.31.060407.125639.

Carroll, Reed C., Eric C. Beattie, Houhui Xia, Christian Lüscher, Yoram Altschuler, Roger A. Nicoll, Robert C. Malenka, and Mark von Zastrow. 1999. “Dynamin-Dependent Endocytosis of Ionotropic Glutamate Receptors.” *Proceedings of the National Academy of Sciences of the United States of America* 96 (24): 14112–17.

Casanova, G., F. Nolin, L. Wortham, D. Ploton, V. Banchet, and J. Michel. 2016. “Shrinkage of Freeze-Dried Cryosections of Cells: Investigations by EFTEM and Cryo-CLEM.” *Micron (Oxford, England: 1993)* 88 (September): 77–83. https://doi.org/10.1016/j.micron.2016.06.005.

Catterall, William A. 2011. “Voltage-Gated Calcium Channels.” *Cold Spring Harbor Perspectives in Biology* 3 (8). https://doi.org/10.1101/cshperspect.a003947.

Chazot, Paul L., and F. Anne Stephenson. 1997. “Biochemical Evidence for the Existence of a Pool of Unassembled C2 Exon-Containing NR1 Subunits of the Mammalian Forebrain NMDA Receptor.” *Journal of Neurochemistry* 68 (2): 507–16. https://doi.org/10.1046/j.1471-4159.1997.68020507.x.

Chen, Xiaobing, Jonathan M. Levy, Austin Hou, Christine Winters, Rita Azzam, Alioscka A. Sousa, Richard D. Leapman, Roger A. Nicoll, and Thomas S. Reese. 2015. “PSD-95 Family MAGUKs Are Essential for Anchoring AMPA and NMDA Receptor Complexes at the Postsynaptic Density.” *Proceedings of the National Academy of Sciences* 112 (50): E6983–92. https://doi.org/10.1073/pnas.1517045112.

Chen, Xiaobing, Christine Winters, Rita Azzam, Xiang Li, James A. Galbraith, Richard D. Leapman, and Thomas S. Reese. 2008a. “Organization of the Core Structure of the

Postsynaptic Density." *Proceedings of the National Academy of Sciences* 105 (11): 4453–58. https://doi.org/10.1073/pnas.0800897105.
Cheng, Dongmei, Casper C. Hoogenraad, John Rush, Elizabeth Ramm, Max A. Schlager, Duc M. Duong, Ping Xu, et al. 2006. "Relative and Absolute Quantification of Postsynaptic Density Proteome Isolated from Rat Forebrain and Cerebellum*S." *Molecular & Cellular Proteomics* 5 (6): 1158–70. https://doi.org/10.1074/mcp.D500009-MCP200.
Chung, ChiHye, Barbara Barylko, Jeremy Leitz, Xinran Liu, and Ege T. Kavalali. 2010. "Acute Dynamin Inhibition Dissects Synaptic Vesicle Recycling Pathways That Drive Spontaneous and Evoked Neurotransmission." *The Journal of Neuroscience: The Official Journal of the Society for Neuroscience* 30 (4): 1363–76. https://doi.org/10.1523/JNEUROSCI.3427-09.2010.
Chung, Hee Jung, Yan Hua Huang, Lit-Fui Lau, and Richard L. Huganir. 2004. "Regulation of the NMDA Receptor Complex and Trafficking by Activity-Dependent Phosphorylation of the NR2B Subunit PDZ Ligand." *Journal of Neuroscience* 24 (45): 10248–59. https://doi.org/10.1523/JNEUROSCI.0546-04.2004.
Clements, J. D., R. A. Lester, G. Tong, C. E. Jahr, and G. L. Westbrook. 1992. "The Time Course of Glutamate in the Synaptic Cleft." *Science* 258 (5087): 1498–1501. https://doi.org/10.1126/science.1359647.
Colquhoun, D, P Jonas, and B Sakmann. 1992. "Action of Brief Pulses of Glutamate on AMPA/Kainate Receptors in Patches from Different Neurones of Rat Hippocampal Slices." *The Journal of Physiology* 458 (December): 261–87.
DeGiorgis, Joseph A., James A. Galbraith, Ayse Dosemeci, Xiaobing Chen, and Thomas S. Reese. 2006. "Distribution of the Scaffolding Proteins PSD-95, PSD-93, and SAP97 in Isolated PSDs." *Brain Cell Biology* 35 (4): 239–50. https://doi.org/10.1007/s11068-007-9017-0.
Delint-Ramirez, Ilse, Esperanza Fernández, Alex Bayés, Emese Kicsi, Noboru H. Komiyama, and Seth G. N. Grant. 2010. "In Vivo Composition of NMDA Receptor Signaling Complexes Differs between Membrane Subdomains and Is Modulated by PSD-95 And PSD-93." *Journal of Neuroscience* 30 (24): 8162–70. https://doi.org/10.1523/JNEUROSCI.1792-10.2010.
Denk, Winfried, and Heinz Horstmann. 2004a. "Serial Block-Face Scanning Electron Microscopy to Reconstruct Three-Dimensional Tissue Nanostructure." *PLOS Biology* 2 (11): e329. https://doi.org/10.1371/journal.pbio.0020329.
Dingledine, R., K. Borges, D. Bowie, and S. F. Traynelis. 1999a. "The Glutamate Receptor Ion Channels." *Pharmacological Reviews* 51 (1): 7–61.
Dubochet, Jacques. 2007. "The Physics of Rapid Cooling and Its Implications for Cryoimmobilization of Cells." *Methods in Cell Biology* 79: 7–21. https://doi.org/10.1016/S0091-679X(06)79001-X.
Ehlers, Michael D. 2003. "Activity Level Controls Postsynaptic Composition and Signaling via the Ubiquitin-Proteasome System." *Nature Neuroscience* 6 (3): 231–42. https://doi.org/10.1038/nn1013.
Ermolyuk, Yaroslav S., Felicity G. Alder, Rainer Surges, Ivan Y. Pavlov, Yulia Timofeeva, Dimitri M. Kullmann, and Kirill E. Volynski. 2013. "Differential Triggering of Spontaneous Glutamate Release by P/Q-, N- and R-Type Ca2+ Channels." *Nature Neuroscience* 16 (12): 1754–63. https://doi.org/10.1038/nn.3563.
Erreger, Kevin, Shashank M. Dravid, Tue G. Banke, David J. A. Wyllie, and Stephen F. Traynelis. 2005. "Subunit-Specific Gating Controls Rat NR1/NR2A and NR1/NR2B NMDA Channel Kinetics and Synaptic Signalling Profiles." *The Journal of Physiology* 563 (Pt 2): 345–58. https://doi.org/10.1113/jphysiol.2004.080028.
Erreger, Kevin, Matthew T. Geballe, Shashank M. Dravid, James P. Snyder, David J. A. Wyllie, and Stephen F. Traynelis. 2005. "Mechanism of Partial Agonism at NMDA Receptors for

a Conformationally Restricted Glutamate Analog." *Journal of Neuroscience* 25 (34): 7858–66. https://doi.org/10.1523/JNEUROSCI.1613-05.2005.
Espinosa, Felipe, and Ege T. Kavalali. 2009. "NMDA Receptor Activation by Spontaneous Glutamatergic Neurotransmission." *Journal of Neurophysiology* 101 (5): 2290–96. https://doi.org/10.1152/jn.90754.2008.
Esteban, José A., Song-Hai Shi, Christopher Wilson, Mutsuo Nuriya, Richard L. Huganir, and Roberto Malinow. 2003. "PKA Phosphorylation of AMPA Receptor Subunits Controls Synaptic Trafficking Underlying Plasticity." *Nature Neuroscience* 6 (2): 136–43. https://doi.org/10.1038/nn997.
Farina, Anthony N., Katherine Y. Blain, Tomohiko Maruo, Witek Kwiatkowski, Senyon Choe, and Terunaga Nakagawa. 2011a. "Separation of Domain Contacts Is Required for Heterotetrameric Assembly of Functional NMDA Receptors." *Journal of Neuroscience* 31 (10): 3565–79. https://doi.org/10.1523/JNEUROSCI.6041-10.2011.
Farley, MM, MT Swulius, and MN Waxham. 2015. "Electron Tomographic Structure and Protein Composition of Isolated Rat Cerebellar, Hippocampal and Cortical Postsynaptic Densities." *Neuroscience* 304 (September): 286–301. https://doi.org/10.1016/j.neuroscience.2015.07.062.
Fiuza, Maria, Christine M. Rostosky, Gabrielle T. Parkinson, Alexei M. Bygrave, Nagaraj Halemani, Marcio Baptista, Ira Milosevic, and Jonathan G. Hanley. 2017. "PICK1 Regulates AMPA Receptor Endocytosis via Direct Interactions with AP2 α-Appendage and Dynamin." *The Journal of Cell Biology* 216 (10): 3323–38. https://doi.org/10.1083/jcb.201701034.
Frank, James Allen, Henri G. Franquelim, Petra Schwille, and Dirk Trauner. 2016. "Optical Control of Lipid Rafts with Photoswitchable Ceramides." *Journal of the American Chemical Society* 138 (39): 12981–86. https://doi.org/10.1021/jacs.6b07278.
Fredj, Naila Ben, and Juan Burrone. 2009. "A Resting Pool of Vesicles Is Responsible for Spontaneous Vesicle Fusion at the Synapse." *Nature Neuroscience* 12 (6): 751–58. https://doi.org/10.1038/nn.2317.
Fukata, Yuko, Anastassios V. Tzingounis, Jonathan C. Trinidad, Masaki Fukata, Alma L. Burlingame, Roger A. Nicoll, and David S. Bredt. 2005. "Molecular Constituents of Neuronal AMPA Receptors." *Journal of Cell Biology* 169 (3): 399–404. https://doi.org/10.1083/jcb.200501121.
Fukazawa, Yugo, and Ryuichi Shigemoto. 2012. "Intra-Synapse-Type and Inter-Synapse-Type Relationships between Synaptic Size and AMPAR Expression." *Current Opinion in Neurobiology* 22 (3): 446–52. https://doi.org/10.1016/j.conb.2012.01.006.
Gan, Quan, Catherine L Salussolia, and Lonnie P Wollmuth. 2015. "Assembly of AMPA Receptors: Mechanisms and Regulation." *The Journal of Physiology* 593 (Pt 1): 39–48. https://doi.org/10.1113/jphysiol.2014.273755.
Goncalves, Julia, Tomas M. Bartol, Côme Camus, Florian Levet, Ana Paula Menegolla, Terrence J. Sejnowski, Jean-Baptiste Sibarita, Michel Vivaudou, Daniel Choquet, and Eric Hosy. 2020. "Nanoscale Co-Organization and Coactivation of AMPAR, NMDAR, and MGluR at Excitatory Synapses." *Proceedings of the National Academy of Sciences* 117 (25): 14503–11. https://doi.org/10.1073/pnas.1922563117.
Goodman, Lucy, David Baddeley, Wojciech Ambroziak, Clarissa L. Waites, Craig C. Garner, Christian Soeller, and Johanna M. Montgomery. 2017. "N-Terminal SAP97 Isoforms Differentially Regulate Synaptic Structure and Postsynaptic Surface Pools of AMPA Receptors." *Hippocampus* 27 (6): 668–82. https://doi.org/10.1002/hipo.22723.
Grauel, M. Katharina, Marta Maglione, Suneel Reddy-Alla, Claudia G. Willmes, Marisa M. Brockmann, Thorsten Trimbuch, Tanja Rosenmund, et al. 2016. "RIM-Binding Protein 2 Regulates Release Probability by Fine-Tuning Calcium Channel Localization at Murine

Hippocampal Synapses." *Proceedings of the National Academy of Sciences* 113 (41): 11615–20. https://doi.org/10.1073/pnas.1605256113.
Greger, Ingo H, Latika Khatri, and Edward B Ziff. 2002a. "RNA Editing at Arg607 Controls AMPA Receptor Exit from the Endoplasmic Reticulum." *Neuron* 34 (5): 759–72. https://doi.org/10.1016/S0896-6273(02)00693-1.
Greger, Ingo H., Jake F. Watson, and Stuart G. Cull-Candy. 2017. "Structural and Functional Architecture of AMPA-Type Glutamate Receptors and Their Auxiliary Proteins." *Neuron* 94 (4): 713–30. https://doi.org/10.1016/j.neuron.2017.04.009.
Guillaud, Laurent, Mitsutoshi Setou, and Nobutaka Hirokawa. 2003. "KIF17 Dynamics and Regulation of NR2B Trafficking in Hippocampal Neurons." *Journal of Neuroscience* 23 (1): 131–40. https://doi.org/10.1523/JNEUROSCI.23-01-00131.2003.
Haas, Kalina T, Benjamin Compans, Mathieu Letellier, Thomas M Bartol, Dolors Grillo-Bosch, Terrence J Sejnowski, Matthieu Sainlos, Daniel Choquet, Olivier Thoumine, and Eric Hosy. 2018. "Pre-Post Synaptic Alignment through Neuroligin-1 Tunes Synaptic Transmission Efficiency." Edited by Gary L Westbrook. *ELife* 7 (July): e31755. https://doi.org/10.7554/eLife.31755.
Hagler, D. J., and Y. Goda. 2001. "Properties of Synchronous and Asynchronous Release during Pulse Train Depression in Cultured Hippocampal Neurons." *Journal of Neurophysiology* 85 (6): 2324–34. https://doi.org/10.1152/jn.2001.85.6.2324.
Hainfeld, J. F., W. Liu, C. M. Halsey, P. Freimuth, and R. D. Powell. 1999. "Ni-NTA-Gold Clusters Target His-Tagged Proteins." *Journal of Structural Biology* 127 (2): 185–98. https://doi.org/10.1006/jsbi.1999.4149.
Hanley, Jonathan G. 2018. "The Regulation of AMPA Receptor Endocytosis by Dynamic Protein-Protein Interactions." *Frontiers in Cellular Neuroscience* 12 (October). https://doi.org/10.3389/fncel.2018.00362.
Hansen, Kasper B., Hiro Furukawa, and Stephen F. Traynelis. 2010a. "Control of Assembly and Function of Glutamate Receptors by the Amino-Terminal Domain." *Molecular Pharmacology* 78 (4): 535–49. https://doi.org/10.1124/mol.110.067157.
Harnett, Mark T., Judit K. Makara, Nelson Spruston, William L. Kath, and Jeffrey C. Magee. 2012. "Synaptic Amplification by Dendritic Spines Enhances Input Cooperativity." *Nature* 491 (7425): 599–602. https://doi.org/10.1038/nature11554.
Haucke, Volker, and Gilbert Di Paolo. 2007. "Lipids and Lipid Modifications in the Regulation of Membrane Traffic." *Current Opinion in Cell Biology* 19 (4): 426–35. https://doi.org/10.1016/j.ceb.2007.06.003.
Hayashi, Takashi, Gavin Rumbaugh, and Richard L. Huganir. 2005. "Differential Regulation of AMPA Receptor Subunit Trafficking by Palmitoylation of Two Distinct Sites." *Neuron* 47 (5): 709–23. https://doi.org/10.1016/j.neuron.2005.06.035.
Hayashi, Y., S. H. Shi, J. A. Esteban, A. Piccini, J. C. Poncer, and R. Malinow. 2000. "Driving AMPA Receptors into Synapses by LTP and CaMKII: Requirement for GluR1 and PDZ Domain Interaction." *Science (New York, N.Y.)* 287 (5461): 2262–67. https://doi.org/10.1126/science.287.5461.2262.
Hebert, Daniel N., and Maurizio Molinari. 2007. "In and out of the ER: Protein Folding, Quality Control, Degradation, and Related Human Diseases." *Physiological Reviews* 87 (4): 1377–1408. https://doi.org/10.1152/physrev.00050.2006.
Herguedas, Beatriz, James Krieger, and Ingo H. Greger. 2013. "Receptor Heteromeric Assembly-How It Works and Why It Matters: The Case of Ionotropic Glutamate Receptors." *Progress in Molecular Biology and Translational Science* 117: 361–86. https://doi.org/10.1016/B978-0-12-386931-9.00013-1.
Hessler, Neal A., Aneil M. Shirke, and Roberto Malinow. 1993. "The Probability of Transmitter Release at a Mammalian Central Synapse." *Nature* 366 (6455): 569–72. https://doi.org/10.1038/366569a0.

Heuser, J. E., and T. S. Reese. 1973. “Evidence for Recycling of Synaptic Vesicle Membrane during Transmitter Release at the Frog Neuromuscular Junction.” *The Journal of Cell Biology* 57 (2): 315–44. https://doi.org/10.1083/jcb.57.2.315.

Heuser, J E, and T S Reese. 1981. “Structural Changes after Transmitter Release at the Frog Neuromuscular Junction.” *Journal of Cell Biology* 88 (3): 564–80. https://doi.org/10.1083/jcb.88.3.564.

Heuser, J. E., T. S. Reese, M. J. Dennis, Y. Jan, L. Jan, and L. Evans. 1979. “Synaptic Vesicle Exocytosis Captured by Quick Freezing and Correlated with Quantal Transmitter Release.” *The Journal of Cell Biology* 81 (2): 275–300. https://doi.org/10.1083/jcb.81.2.275.

Hodgkin, A. L., and A. F. Huxley. 1939. “Action Potentials Recorded from Inside a Nerve Fibre.” *Nature* 144 (3651): 710–11. https://doi.org/10.1038/144710a0.

Hollmann, M., M. Hartley, and S. Heinemann. 1991. “Ca2+ Permeability of KA-AMPA--Gated Glutamate Receptor Channels Depends on Subunit Composition.” *Science (New York, N.Y.)* 252 (5007): 851–53. https://doi.org/10.1126/science.1709304.

Hollmann, Michael, Anne O’Shea-Greenfield, Scott W. Rogers, and Stephen Heinemann. 1989. “Cloning by Functional Expression of a Member of the Glutamate Receptor Family.” *Nature* 342 (6250): 643–48. https://doi.org/10.1038/342643a0.

Holmes, W R. 1995. “Modeling the Effect of Glutamate Diffusion and Uptake on NMDA and Non-NMDA Receptor Saturation.” *Biophysical Journal* 69 (5): 1734–47.

Holzinger, Andreas, and Kathrin Blaas. 2016. “Actin-Dynamics in Plant Cells: The Function of Actin-Perturbing Substances: Jasplakinolide, Chondramides, Phalloidin, Cytochalasins, and Latrunculins.” *Methods in Molecular Biology (Clifton, N.J.)* 1365: 243–61. https://doi.org/10.1007/978-1-4939-3124-8_13.

Horak, Martin, Kai Chang, and Robert J. Wenthold. 2008. “Masking of the Endoplasmic Reticulum Retention Signals during Assembly of the NMDA Receptor.” *Journal of Neuroscience* 28 (13): 3500–3509. https://doi.org/10.1523/JNEUROSCI.5239-07.2008.

Horak, Martin, Ronald S. Petralia, Martina Kaniakova, and Nathalie Sans. 2014. “ER to Synapse Trafficking of NMDA Receptors.” *Frontiers in Cellular Neuroscience* 8 (November). https://doi.org/10.3389/fncel.2014.00394.

Horak, Martin, and Robert J. Wenthold. 2009. “Different Roles of C-Terminal Cassettes in the Trafficking of Full-Length NR1 Subunits to the Cell Surface.” *Journal of Biological Chemistry* 284 (15): 9683–91. https://doi.org/10.1074/jbc.M807050200.

Hruska, Martin, Nathan Henderson, Sylvain J. Le Marchand, Haani Jafri, and Matthew B. Dalva. 2018. “Synaptic Nanomodules Underlie the Organization and Plasticity of Spine Synapses.” *Nature Neuroscience* 21 (5): 671–82. https://doi.org/10.1038/s41593-018-0138-9.

Huganir, Richard L., and Roger A. Nicoll. 2013. “AMPARs and Synaptic Plasticity: The Last 25 Years.” *Neuron* 80 (3): 704–17. https://doi.org/10.1016/j.neuron.2013.10.025.

Huh, Kyung-Hye, and Robert J. Wenthold. 1999. “Turnover Analysis of Glutamate Receptors Identifies a Rapidly Degraded Pool of the N-Methyl-d-Aspartate Receptor Subunit, NR1, in Cultured Cerebellar Granule Cells.” *Journal of Biological Chemistry* 274 (1): 151–57. https://doi.org/10.1074/jbc.274.1.151.

Hunt, C. A., L. J. Schenker, and M. B. Kennedy. 1996. “PSD-95 Is Associated with the Postsynaptic Density and Not with the Presynaptic Membrane at Forebrain Synapses.” *Journal of Neuroscience* 16 (4): 1380–88. https://doi.org/10.1523/JNEUROSCI.16-04-01380.1996.

Idevall-Hagren, Olof, Eamonn J. Dickson, Bertil Hille, Derek K. Toomre, and Pietro De Camilli. 2012. “Optogenetic Control of Phosphoinositide Metabolism.” *Proceedings of the National Academy of Sciences* 109 (35): E2316–23. https://doi.org/10.1073/pnas.1211305109.

Ishikawa, Taro, Yoshinori Sahara, and Tomoyuki Takahashi. 2002. “A Single Packet of Transmitter Does Not Saturate Postsynaptic Glutamate Receptors.” *Neuron* 34 (4): 613–21. https://doi.org/10.1016/S0896-6273(02)00692-X.
Jang, Seil, Hyejin Lee, and Eunjoon Kim. 2017. “Synaptic Adhesion Molecules and Excitatory Synaptic Transmission.” *Current Opinion in Neurobiology* 45 (August): 45–50. https://doi.org/10.1016/j.conb.2017.03.005.
Jiang, Jianxiong, Vishnu Suppiramaniam, and Marie W. Wooten. 2006. “Posttranslational Modifications and Receptor-Associated Proteins in AMPA Receptor Trafficking and Synaptic Plasticity.” *Neuro-Signals* 15 (5): 266–82. https://doi.org/10.1159/000105517.
Jonas, P, G Major, and B Sakmann. 1993. “Quantal Components of Unitary EPSCs at the Mossy Fibre Synapse on CA3 Pyramidal Cells of Rat Hippocampus.” *The Journal of Physiology* 472 (December): 615–63.
Kaeser, Pascal S., and Wade G. Regehr. 2014. “Molecular Mechanisms for Synchronous, Asynchronous, and Spontaneous Neurotransmitter Release.” *Annual Review of Physiology* 76: 333–63. https://doi.org/10.1146/annurev-physiol-021113-170338.
Kaeser and Regehr. 2017. “The Readily Releasable Pool of Synaptic Vesicles.” *Current Opinion in Neurobiology* 43 (April): 63–70. https://doi.org/10.1016/j.conb.2016.12.012.
Kastning, Kathrin, Viktoria Kukhtina, Josef T. Kittler, Guojun Chen, Arndt Pechstein, Sven Enders, Sang Hyoung Lee, Morgan Sheng, Zhen Yan, and Volker Haucke. 2007. “Molecular Determinants for the Interaction between AMPA Receptors and the Clathrin Adaptor Complex AP-2.” *Proceedings of the National Academy of Sciences* 104 (8): 2991–96. https://doi.org/10.1073/pnas.0611170104.
Kauer, J. A., R. C. Malenka, and R. A. Nicoll. 1988. “A Persistent Postsynaptic Modification Mediates Long-Term Potentiation in the Hippocampus.” *Neuron* 1 (10): 911–17. https://doi.org/10.1016/0896-6273(88)90148-1.
Kavalali, Ege T. 2015. “The Mechanisms and Functions of Spontaneous Neurotransmitter Release.” *Nature Reviews. Neuroscience* 16 (1): 5–16. https://doi.org/10.1038/nrn3875.
Kenny, Anna V., Sarah L. Cousins, Leonor Pinho, and F. Anne Stephenson. 2009. “The Integrity of the Glycine Co-Agonist Binding Site of N-Methyl-d-Aspartate Receptors Is a Functional Quality Control Checkpoint for Cell Surface Delivery.” *Journal of Biological Chemistry* 284 (1): 324–33. https://doi.org/10.1074/jbc.M804023200.
Kharazia, V. N., and R. J. Weinberg. 1997a. “Tangential Synaptic Distribution of NMDA and AMPA Receptors in Rat Neocortex.” *Neuroscience Letters* 238 (1–2): 41–44. https://doi.org/10.1016/s0304-3940(97)00846-x.
Kinney, Justin P., Josef Spacek, Thomas M. Bartol, Chandrajit L. Bajaj, Kristen M. Harris, and Terrence J. Sejnowski. 2013. “Extracellular Sheets and Tunnels Modulate Glutamate Diffusion in Hippocampal Neuropil.” *The Journal of Comparative Neurology* 521 (2): 448–64. https://doi.org/10.1002/cne.23181.
Knott, Graham, Herschel Marchman, David Wall, and Ben Lich. 2008. “Serial Section Scanning Electron Microscopy of Adult Brain Tissue Using Focused Ion Beam Milling.” *Journal of Neuroscience* 28 (12): 2959–64. https://doi.org/10.1523/JNEUROSCI.3189-07.2008.
Kobayashi, Shouhei, Masaaki Iwamoto, and Tokuko Haraguchi. 2016. “Live Correlative Light-Electron Microscopy to Observe Molecular Dynamics in High Resolution.” *Microscopy (Oxford, England)* 65 (4): 296–308. https://doi.org/10.1093/jmicro/dfw024.
Kopec, Charles D., Bo Li, Wei Wei, Jannic Boehm, and Roberto Malinow. 2006. “Glutamate Receptor Exocytosis and Spine Enlargement during Chemically Induced Long-Term Potentiation.” *The Journal of Neuroscience: The Official Journal of the Society for Neuroscience* 26 (7): 2000–2009. https://doi.org/10.1523/JNEUROSCI.3918-05.2006.
Kornau, H. C., L. T. Schenker, M. B. Kennedy, and P. H. Seeburg. 1995. “Domain Interaction between NMDA Receptor Subunits and the Postsynaptic Density Protein PSD-95.”

Science (New York, N.Y.) 269 (5231): 1737–40. https://doi.org/10.1126/science.7569905.
Kornau, Hans-Christian, Peter H Seeburg, and Mary B Kennedy. 1997. “Interaction of Ion Channels and Receptors with PDZ Domain Proteins.” *Current Opinion in Neurobiology* 7 (3): 368–73. https://doi.org/10.1016/S0959-4388(97)80064-5.
Kramer, Richard H., Doris L. Fortin, and Dirk Trauner. 2009. “New Photochemical Tools for Controlling Neuronal Activity.” *Current Opinion in Neurobiology* 19 (5): 544–52. https://doi.org/10.1016/j.conb.2009.09.004.
Kukulski, Wanda, Martin Schorb, Marko Kaksonen, and John A. G. Briggs. 2012. “Plasma Membrane Reshaping during Endocytosis Is Revealed by Time-Resolved Electron Tomography.” *Cell* 150 (3): 508–20. https://doi.org/10.1016/j.cell.2012.05.046.
Kukulski, Wanda, Martin Schorb, Sonja Welsch, Andrea Picco, Marko Kaksonen, and John A.G. Briggs. 2011. “Correlated Fluorescence and 3D Electron Microscopy with High Sensitivity and Spatial Precision.” *Journal of Cell Biology* 192 (1): 111–19. https://doi.org/10.1083/jcb.201009037.
Kusick, Grant F., Morven Chin, Sumana Raychaudhuri, Kristina Lippmann, Kadidia P. Adula, Edward J. Hujber, Thien Vu, M. Wayne Davis, Erik M. Jorgensen, and Shigeki Watanabe. 2020. “Synaptic Vesicles Transiently Dock to Refill Release Sites.” *Nature Neuroscience* 23 (11): 1329–38. https://doi.org/10.1038/s41593-020-00716-1.
Lavezzari, Gabriela, Jennifer McCallum, Colleen M. Dewey, and Katherine W. Roche. 2004. “Subunit-Specific Regulation of NMDA Receptor Endocytosis.” *Journal of Neuroscience* 24 (28): 6383–91. https://doi.org/10.1523/JNEUROSCI.1890-04.2004.
Lee, H. K., K. Kameyama, R. L. Huganir, and M. F. Bear. 1998. “NMDA Induces Long-Term Synaptic Depression and Dephosphorylation of the GluR1 Subunit of AMPA Receptors in Hippocampus.” *Neuron* 21 (5): 1151–62. https://doi.org/10.1016/s0896-6273(00)80632-7.
Lee, Sang Hyoung, Alyson Simonetta, and Morgan Sheng. 2004. “Subunit Rules Governing the Sorting of Internalized AMPA Receptors in Hippocampal Neurons.” *Neuron* 43 (2): 221–36. https://doi.org/10.1016/j.neuron.2004.06.015.
Li, Dong, Lin Shao, Bi-Chang Chen, Xi Zhang, Mingshu Zhang, Brian Moses, Daniel E. Milkie, et al. 2015. “Extended-Resolution Structured Illumination Imaging of Endocytic and Cytoskeletal Dynamics.” *Science* 349 (6251). https://doi.org/10.1126/science.aab3500.
Li, Tuo P., Yu Song, Harold D. MacGillavry, Thomas A. Blanpied, and Sridhar Raghavachari. 2016. “Protein Crowding within the Postsynaptic Density Can Impede the Escape of Membrane Proteins.” *The Journal of Neuroscience* 36 (15): 4276–95. https://doi.org/10.1523/JNEUROSCI.3154-15.2016.
Lin, Da–Ting, Yuichi Makino, Kamal Sharma, Takashi Hayashi, Rachael Neve, Kogo Takamiya, and Richard L. Huganir. 2009. “Regulation of AMPA Receptor Extrasynaptic Insertion by 4.1N, Phosphorylation and Palmitoylation.” *Nature Neuroscience* 12 (7): 879–87. https://doi.org/10.1038/nn.2351.
Lisé, Marie-France, Tak Pan Wong, Alex Trinh, Rochelle M. Hines, Lidong Liu, Rujun Kang, Dustin J. Hines, et al. 2006. “Involvement of Myosin Vb in Glutamate Receptor Trafficking.” *The Journal of Biological Chemistry* 281 (6): 3669–78. https://doi.org/10.1074/jbc.M511725200.
Lisman, John E., Sridhar Raghavachari, and Richard W. Tsien. 2007. “The Sequence of Events That Underlie Quantal Transmission at Central Glutamatergic Synapses.” *Nature Reviews. Neuroscience* 8 (8): 597–609. https://doi.org/10.1038/nrn2191.
Lisman, John, and Sridhar Raghavachari. 2006. “A Unified Model of the Presynaptic and Postsynaptic Changes During LTP at CA1 Synapses.” *Science’s STKE* 2006 (356): re11–re11. https://doi.org/10.1126/stke.3562006re11.

Lisman, John, Ryohei Yasuda, and Sridhar Raghavachari. 2012. “Mechanisms of CaMKII Action in Long-Term Potentiation.” *Nature Reviews Neuroscience* 13 (3): 169–82. https://doi.org/10.1038/nrn3192.

Liu, G., S. Choi, and R. W. Tsien. 1999. “Variability of Neurotransmitter Concentration and Nonsaturation of Postsynaptic AMPA Receptors at Synapses in Hippocampal Cultures and Slices.” *Neuron* 22 (2): 395–409. https://doi.org/10.1016/s0896-6273(00)81099-5.

Lois, Carlos, Elizabeth J. Hong, Shirley Pease, Eric J. Brown, and David Baltimore. 2002. “Germline Transmission and Tissue-Specific Expression of Transgenes Delivered by Lentiviral Vectors.” *Science (New York, N.Y.)* 295 (5556): 868–72. https://doi.org/10.1126/science.1067081.

Lomeli, H., J. Mosbacher, T. Melcher, T. Hoger, Geiger, T. Kuner, H. Monyer, M. Higuchi, A. Bach, and P. H. Seeburg. 1994. “Control of Kinetic Properties of AMPA Receptor Channels by Nuclear RNA Editing.” *Science* 266 (5191): 1709–13. https://doi.org/10.1126/science.7992055.

Los, Georgyi V., Lance P. Encell, Mark G. McDougall, Danette D. Hartzell, Natasha Karassina, Chad Zimprich, Monika G. Wood, et al. 2008. “HaloTag: A Novel Protein Labeling Technology for Cell Imaging and Protein Analysis.” *ACS Chemical Biology* 3 (6): 373–82. https://doi.org/10.1021/cb800025k.

Lu, Jiuyi, Thomas D. Helton, Thomas A. Blanpied, Bence Rácz, Thomas M. Newpher, Richard J. Weinberg, and Michael D. Ehlers. 2007. “Postsynaptic Positioning of Endocytic Zones and AMPA Receptor Cycling by Physical Coupling of Dynamin-3 to Homer.” *Neuron* 55 (6): 874–89. https://doi.org/10.1016/j.neuron.2007.06.041.

Lu, Wen, Weiqing Fang, Jian Li, Bin Zhang, Qian Yang, Xunyi Yan, Lin Peng, et al. 2015. “Phosphorylation of Tyrosine 1070 at the GluN2B Subunit Is Regulated by Synaptic Activity and Critical for Surface Expression of N-Methyl-d-Aspartate (NMDA) Receptors.” *The Journal of Biological Chemistry* 290 (38): 22945–54. https://doi.org/10.1074/jbc.M115.663450.

Lüscher, Christian, and Robert C. Malenka. 2012. “NMDA Receptor-Dependent Long-Term Potentiation and Long-Term Depression (LTP/LTD).” *Cold Spring Harbor Perspectives in Biology* 4 (6). https://doi.org/10.1101/cshperspect.a005710.

Lüscher, Christian, Houhui Xia, Eric C Beattie, Reed C Carroll, Mark von Zastrow, Robert C Malenka, and Roger A Nicoll. 1999. “Role of AMPA Receptor Cycling in Synaptic Transmission and Plasticity.” *Neuron* 24 (3): 649–58. https://doi.org/10.1016/S0896-6273(00)81119-8.

MacGillavry, Harold D., Yu Song, Sridhar Raghavachari, and Thomas A. Blanpied. 2013a. “Nanoscale Scaffolding Domains within the Postsynaptic Density Concentrate Synaptic AMPA Receptors.” *Neuron* 78 (4): 615–22. https://doi.org/10.1016/j.neuron.2013.03.009.

Mainen, Z. F., J. Joerges, J. R. Huguenard, and T. J. Sejnowski. 1995. “A Model of Spike Initiation in Neocortical Pyramidal Neurons.” *Neuron* 15 (6): 1427–39. https://doi.org/10.1016/0896-6273(95)90020-9.

Malenka, R. C. 1994. “Synaptic Plasticity in the Hippocampus: LTP and LTD.” *Cell* 78 (4): 535–38. https://doi.org/10.1016/0092-8674(94)90517-7.

Malinow, R., and J. P. Miller. 1986. “Postsynaptic Hyperpolarization during Conditioning Reversibly Blocks Induction of Long-Term Potentiation.” *Nature* 320 (6062): 529–30. https://doi.org/10.1038/320529a0.

Man, H. Y., J. W. Lin, W. H. Ju, G. Ahmadian, L. Liu, L. E. Becker, M. Sheng, and Y. T. Wang. 2000. “Regulation of AMPA Receptor-Mediated Synaptic Transmission by Clathrin-Dependent Receptor Internalization.” *Neuron* 25 (3): 649–62. https://doi.org/10.1016/s0896-6273(00)81067-3.

Masugi-Tokita, Miwako, and Ryuichi Shigemoto. 2007. “High-Resolution Quantitative Visualization of Glutamate and GABA Receptors at Central Synapses.” *Current Opinion in Neurobiology* 17 (3): 387–93. https://doi.org/10.1016/j.conb.2007.04.012.

Masugi-Tokita, Miwako, Etsuko Tarusawa, Masahiko Watanabe, Elek Molnár, Kazushi Fujimoto, and Ryuichi Shigemoto. 2007a. “Number and Density of AMPA Receptors in Individual Synapses in the Rat Cerebellum as Revealed by SDS-Digested Freeze-Fracture Replica Labeling.” *The Journal of Neuroscience: The Official Journal of the Society for Neuroscience* 27 (8): 2135–44. https://doi.org/10.1523/JNEUROSCI.2861-06.2007.

Matsuda, Shinji, Wataru Kakegawa, Timotheus Budisantoso, Toshihiro Nomura, Kazuhisa Kohda, and Michisuke Yuzaki. 2013. “Stargazin Regulates AMPA Receptor Trafficking through Adaptor Protein Complexes during Long-Term Depression.” *Nature Communications* 4 (1): 2759. https://doi.org/10.1038/ncomms3759.

Matsuzaki, M., G. C. Ellis-Davies, T. Nemoto, Y. Miyashita, M. Iino, and H. Kasai. 2001. “Dendritic Spine Geometry Is Critical for AMPA Receptor Expression in Hippocampal CA1 Pyramidal Neurons.” *Nature Neuroscience* 4 (11): 1086–92. https://doi.org/10.1038/nn736.

Mayer, M. L., G. L. Westbrook, and P. B. Guthrie. 1984. “Voltage-Dependent Block by Mg2+ of NMDA Responses in Spinal Cord Neurones.” *Nature* 309 (5965): 261–63. https://doi.org/10.1038/309261a0.

McAllister, A. Kimberley, and Charles F. Stevens. 2000. “Nonsaturation of AMPA and NMDA Receptors at Hippocampal Synapses.” *Proceedings of the National Academy of Sciences* 97 (11): 6173–78. https://doi.org/10.1073/pnas.100126497.

McGlade-McCulloh, Ellen, Hideyuki Yamamoto, Soon-Eng Tan, Debra A. Brickey, and Thomas R. Soderling. 1993. “Phosphorylation and Regulation of Glutamate Receptors by Calcium/Calmodulin-Dependent Protein Kinase II.” *Nature* 362 (6421): 640–42. https://doi.org/10.1038/362640a0.

McIlhinney, R. A. Jeffrey, Beatrice Le Bourdellès, Elek Molnár, Nicolas Tricaud, Peter Streit, and Paul J Whiting. 1998. “Assembly Intracellular Targeting and Cell Surface Expression of the Human N-Methyl-d-Aspartate Receptor Subunits NR1a and NR2A in Transfected Cells.” *Neuropharmacology* 37 (10): 1355–67. https://doi.org/10.1016/S0028-3908(98)00121-X.

Mok, Hyejung, Hyewon Shin, Seho Kim, Jae-Ran Lee, Jiyoung Yoon, and Eunjoon Kim. 2002. “Association of the Kinesin Superfamily Motor Protein KIF1Balpha with Postsynaptic Density-95 (PSD-95), Synapse-Associated Protein-97, and Synaptic Scaffolding Molecule PSD-95/Discs Large/Zona Occludens-1 Proteins.” *The Journal of Neuroscience: The Official Journal of the Society for Neuroscience* 22 (13): 5253–58. https://doi.org/20026553.

Mukherjee, S., R. N. Ghosh, and F. R. Maxfield. 1997. “Endocytosis.” *Physiological Reviews* 77 (3): 759–803. https://doi.org/10.1152/physrev.1997.77.3.759.

Mulkey, R. M., S. Endo, S. Shenolikar, and R. C. Malenka. 1994. “Involvement of a Calcineurin/Inhibitor-1 Phosphatase Cascade in Hippocampal Long-Term Depression.” *Nature* 369 (6480): 486–88. https://doi.org/10.1038/369486a0.

Mulkey, Rosel M., and Robert C. Malenka. 1992. “Mechanisms Underlying Induction of Homosynaptic Long-Term Depression in Area CA1 of the Hippocampus.” *Neuron* 9 (5): 967–75. https://doi.org/10.1016/0896-6273(92)90248-C.

Müller-Reichert, Thomas, Martin Srayko, Anthony Hyman, Eileen T. O’Toole, and Kent McDonald. 2007. “Correlative Light and Electron Microscopy of Early Caenorhabditis Elegans Embryos in Mitosis.” *Methods in Cell Biology* 79: 101–19. https://doi.org/10.1016/S0091-679X(06)79004-5.

Nagel, Georg, Martin Brauner, Jana F. Liewald, Nona Adeishvili, Ernst Bamberg, and Alexander Gottschalk. 2005. “Light Activation of Channelrhodopsin-2 in Excitable Cells of

Caenorhabditis Elegans Triggers Rapid Behavioral Responses." *Current Biology: CB* 15 (24): 2279–84. https://doi.org/10.1016/j.cub.2005.11.032.
Nagel, Georg, Doris Ollig, Markus Fuhrmann, Suneel Kateriya, Anna Maria Musti, Ernst Bamberg, and Peter Hegemann. 2002. "Channelrhodopsin-1: A Light-Gated Proton Channel in Green Algae." *Science* 296 (5577): 2395–98. https://doi.org/10.1126/science.1072068.
Nagel, Georg, Tanjef Szellas, Wolfram Huhn, Suneel Kateriya, Nona Adeishvili, Peter Berthold, Doris Ollig, Peter Hegemann, and Ernst Bamberg. 2003. "Channelrhodopsin-2, a Directly Light-Gated Cation-Selective Membrane Channel." *Proceedings of the National Academy of Sciences* 100 (24): 13940–45. https://doi.org/10.1073/pnas.1936192100.
Nahum-Levy, R, D Lipinski, S Shavit, and M Benveniste. 2001. "Desensitization of NMDA Receptor Channels Is Modulated by Glutamate Agonists." *Biophysical Journal* 80 (5): 2152–66.
Nair, Deepak, Eric Hosy, Jennifer D. Petersen, Audrey Constals, Gregory Giannone, Daniel Choquet, and Jean-Baptiste Sibarita. 2013a. "Super-Resolution Imaging Reveals That AMPA Receptors Inside Synapses Are Dynamically Organized in Nanodomains Regulated by PSD95." *Journal of Neuroscience* 33 (32): 13204–24. https://doi.org/10.1523/JNEUROSCI.2381-12.2013.
Niu, Jacqueline, Manu Ben Johny, Ivy E. Dick, and Takanari Inoue. 2016. "Following Optogenetic Dimerizers and Quantitative Prospects." *Biophysical Journal* 111 (6): 1132–40. https://doi.org/10.1016/j.bpj.2016.07.040.
Nowak, L., P. Bregestovski, P. Ascher, A. Herbet, and A. Prochiantz. 1984. "Magnesium Gates Glutamate-Activated Channels in Mouse Central Neurones." *Nature* 307 (5950): 462–65. https://doi.org/10.1038/307462a0.
Nusser, Z., R. Lujan, G. Laube, J. D. Roberts, E. Molnar, and P. Somogyi. 1998. "Cell Type and Pathway Dependence of Synaptic AMPA Receptor Number and Variability in the Hippocampus." *Neuron* 21 (3): 545–59. https://doi.org/10.1016/s0896-6273(00)80565-6.
Nusser, Z., E. Mulvihill, P. Streit, and P. Somogyi. 1994a. "Subsynaptic Segregation of Metabotropic and Ionotropic Glutamate Receptors as Revealed by Immunogold Localization." *Neuroscience* 61 (3): 421–27. https://doi.org/10.1016/0306-4522(94)90421-9.
Nusser, Zoltan, Rafael Lujan, Gregor Laube, J. David B Roberts, Elek Molnar, and Peter Somogyi. 1998. "Cell Type and Pathway Dependence of Synaptic AMPA Receptor Number and Variability in the Hippocampus." *Neuron* 21 (3): 545–59. https://doi.org/10.1016/S0896-6273(00)80565-6.
Orth, Angela, Daniel Tapken, and Michael Hollmann. 2013. "The Delta Subfamily of Glutamate Receptors: Characterization of Receptor Chimeras and Mutants." *The European Journal of Neuroscience* 37 (10): 1620–30. https://doi.org/10.1111/ejn.12193.
Osterweil, Emily, David G. Wells, and Mark S. Mooseker. 2005. "A Role for Myosin VI in Postsynaptic Structure and Glutamate Receptor Endocytosis." *Journal of Cell Biology* 168 (2): 329–38. https://doi.org/10.1083/jcb.200410091.
Palmer, Claire L., Wonil Lim, Peter G.R. Hastie, Marie Toward, Viktor I. Korolchuk, Stephen A. Burbidge, George Banting, Graham L. Collingridge, John. T.R. Isaac, and Jeremy M. Henley. 2005. "Hippocalcin Functions as a Calcium Sensor in Hippocampal LTD." *Neuron* 47 (4): 487–94. https://doi.org/10.1016/j.neuron.2005.06.014.
Palmer, Lucy M., and Greg J. Stuart. 2009. "Membrane Potential Changes in Dendritic Spines during Action Potentials and Synaptic Input." *Journal of Neuroscience* 29 (21): 6897–6903. https://doi.org/10.1523/JNEUROSCI.5847-08.2009.
Park, Joongkyu, Andrés E. Chávez, Yann S. Mineur, Megumi Morimoto-Tomita, Stefano Lutzu, Kwang S. Kim, Marina R. Picciotto, Pablo E. Castillo, and Susumu Tomita. 2016.

"CaMKII Phosphorylation of TARPγ-8 Is a Mediator of LTP and Learning and Memory." *Neuron* 92 (1): 75–83. https://doi.org/10.1016/j.neuron.2016.09.002.
Patneau, DK, and ML Mayer. 1990. "Structure-Activity Relationships for Amino Acid Transmitter Candidates Acting at N-Methyl-D-Aspartate and Quisqualate Receptors." *The Journal of Neuroscience* 10 (7): 2385–99. https://doi.org/10.1523/JNEUROSCI.10-07-02385.1990.
Patriarchi, Tommaso, Olivia R Buonarati, and Johannes W Hell. 2018. "Postsynaptic Localization and Regulation of AMPA Receptors and Cav1.2 by B2 Adrenergic Receptor/PKA and Ca2+/CaMKII Signaling." *The EMBO Journal* 37 (20). https://doi.org/10.15252/embj.201899771.
Pei, Weimin, Zhen Huang, Congzhou Wang, Yan Han, Jae Seon Park, and Li Niu. 2009. "Flip and Flop: A Molecular Determinant for AMPA Receptor Channel Opening." *Biochemistry* 48 (17): 3767–77. https://doi.org/10.1021/bi8015907.
Pérez-Otaño, Isabel, and Michael D. Ehlers. 2005. "Homeostatic Plasticity and NMDA Receptor Trafficking." *Trends in Neurosciences* 28 (5): 229–38. https://doi.org/10.1016/j.tins.2005.03.004.
Petralia, Ronald S., Rana A. Al-Hallaq, and Robert J. Wenthold. 2009. "Trafficking and Targeting of NMDA Receptors." In *Biology of the NMDA Receptor*, edited by Antonius M. Van Dongen. Frontiers in Neuroscience. Boca Raton (FL): CRC Press/Taylor & Francis. http://www.ncbi.nlm.nih.gov/books/NBK5290/.
Pick, Joseph E., Latika Khatri, Matheus F. Sathler, and Edward B. Ziff. 2017. "MGluR Long-Term Depression Regulates GluA2 Association with COPII Vesicles and Exit from the Endoplasmic Reticulum." *The EMBO Journal* 36 (2): 232–44. https://doi.org/10.15252/embj.201694526.
Pick, Joseph E, and Edward B Ziff. 2018. "Regulation of AMPA Receptor Trafficking and Exit from the Endoplasmic Reticulum." *Molecular and Cellular Neurosciences* 91 (September): 3–9. https://doi.org/10.1016/j.mcn.2018.03.004.
Popratiloff, A., R. J. Weinberg, and A. Rustioni. 1996. "AMPA Receptor Subunits Underlying Terminals of Fine-Caliber Primary Afferent Fibers." *Journal of Neuroscience* 16 (10): 3363–72. https://doi.org/10.1523/JNEUROSCI.16-10-03363.1996.
Purves, Dale, George J. Augustine, David Fitzpatrick, Lawrence C. Katz, Anthony-Samuel LaMantia, James O. McNamara, and S. Mark Williams. 2001. "Two Families of Postsynaptic Receptors." *Neuroscience. 2nd Edition*. https://www.ncbi.nlm.nih.gov/books/NBK10855/.
Racca, C., F. A. Stephenson, P. Streit, J. D. Roberts, and P. Somogyi. 2000. "NMDA Receptor Content of Synapses in Stratum Radiatum of the Hippocampal CA1 Area." *The Journal of Neuroscience: The Official Journal of the Society for Neuroscience* 20 (7): 2512–22.
Rácz, Bence, Thomas A. Blanpied, Michael D. Ehlers, and Richard J. Weinberg. 2004. "Lateral Organization of Endocytic Machinery in Dendritic Spines." *Nature Neuroscience* 7 (9): 917–18. https://doi.org/10.1038/nn1303.
Raghavachari, Sridhar, and John E. Lisman. 2004a. "Properties of Quantal Transmission at CA1 Synapses." *Journal of Neurophysiology* 92 (4): 2456–67. https://doi.org/10.1152/jn.00258.2004.
Redemann, Stefanie, and Thomas Müller-Reichert. 2013. "Correlative Light and Electron Microscopy for the Analysis of Cell Division." *Journal of Microscopy* 251 (2): 109–12. https://doi.org/10.1111/jmi.12056.
Rosenmund, C., J. D. Clements, and G. L. Westbrook. 1993a. "Nonuniform Probability of Glutamate Release at a Hippocampal Synapse." *Science* 262 (5134): 754–57. https://doi.org/10.1126/science.7901909.
Rosenmund, C., A. Feltz, and G. L. Westbrook. 1995. "Synaptic NMDA Receptor Channels Have a Low Open Probability." *The Journal of Neuroscience: The Official Journal of the Society for Neuroscience* 15 (4): 2788–95.

Rubio, M. E., and R. J. Wenthold. 1999. “Calnexin and the Immunoglobulin Binding Protein (BiP) Coimmunoprecipitate with AMPA Receptors.” *Journal of Neurochemistry* 73 (3): 942–48. https://doi.org/10.1046/j.1471-4159.1999.0730942.x.

Rubio, Maria E, and Robert J Wenthold. 1997. “Glutamate Receptors Are Selectively Targeted to Postsynaptic Sites in Neurons.” *Neuron* 18 (6): 939–50. https://doi.org/10.1016/S0896-6273(00)80333-5.

Rudolph, Stephanie, Ming-Chi Tsai, Henrique von Gersdorff, and Jacques I. Wadiche. 2015. “The Ubiquitous Nature of Multivesicular Release.” *Trends in Neurosciences* 38 (7): 428–38. https://doi.org/10.1016/j.tins.2015.05.008.

Saglietti, Laura, Caroline Dequidt, Kinga Kamieniarz, Marie-Claude Rousset, Pamela Valnegri, Olivier Thoumine, Francesca Beretta, et al. 2007. “Extracellular Interactions between GluR2 and N-Cadherin in Spine Regulation.” *Neuron* 54 (3): 461–77. https://doi.org/10.1016/j.neuron.2007.04.012.

Saheki, Yasunori, and Pietro De Camilli. 2012. “Synaptic Vesicle Endocytosis.” *Cold Spring Harbor Perspectives in Biology* 4 (9). https://doi.org/10.1101/cshperspect.a005645.

Salavessa, Laura, and Nathalie Sauvonnet. 2021. “Stoichiometry of ReceptorsReceptors at the Plasma MembranePlasma Membrane During Their EndocytosisEndocytosis Using Total Internal Reflection Fluorescent (TIRF) MicroscopyMicroscopy Live Imaging and Single-Molecule Tracking.” In *Exocytosis and Endocytosis: Methods and Protocols*, edited by Florence Niedergang, Nicolas Vitale, and Stéphane Gasman, 3–17. Methods in Molecular Biology. New York, NY: Springer US. https://doi.org/10.1007/978-1-0716-1044-2_1.

Sans, N., C. Racca, R. S. Petralia, Y. X. Wang, J. McCallum, and R. J. Wenthold. 2001. “Synapse-Associated Protein 97 Selectively Associates with a Subset of AMPA Receptors Early in Their Biosynthetic Pathway.” *The Journal of Neuroscience: The Official Journal of the Society for Neuroscience* 21 (19): 7506–16.

Sans, Nathalie, Philip Y. Wang, Quansheng Du, Ronald S. Petralia, Ya-Xian Wang, Sajan Nakka, Joe B. Blumer, Ian G. Macara, and Robert J. Wenthold. 2005. “MPins Modulates PSD-95 and SAP102 Trafficking and Influences NMDA Receptor Surface Expression.” *Nature Cell Biology* 7 (12): 1179–90. https://doi.org/10.1038/ncb1325.

Santamaria, Fidel, Jossina Gonzalez, George J. Augustine, and Sridhar Raghavachari. 2010. “Quantifying the Effects of Elastic Collisions and Non-Covalent Binding on Glutamate Receptor Trafficking in the Post-Synaptic Density.” *PLOS Computational Biology* 6 (5): e1000780. https://doi.org/10.1371/journal.pcbi.1000780.

Santucci, David M., and Sridhar Raghavachari. 2008. “The Effects of NR2 Subunit-Dependent NMDA Receptor Kinetics on Synaptic Transmission and CaMKII Activation.” *PLoS Computational Biology* 4 (10). https://doi.org/10.1371/journal.pcbi.1000208.

Sanz-Clemente, Antonio, Roger A. Nicoll, and Katherine W. Roche. 2013. “Diversity in NMDA Receptor Composition: Many Regulators, Many Consequences.” *The Neuroscientist : A Review Journal Bringing Neurobiology, Neurology and Psychiatry* 19 (1): 62–75. https://doi.org/10.1177/1073858411435129.

Sara, Yildirim, Manjot Bal, Megumi Adachi, Lisa M. Monteggia, and Ege T. Kavalali. 2011. “Use-Dependent AMPA Receptor Block Reveals Segregation of Spontaneous and Evoked Glutamatergic Neurotransmission.” *Journal of Neuroscience* 31 (14): 5378–82. https://doi.org/10.1523/JNEUROSCI.5234-10.2011.

Sara, Yildirim, Tuhin Virmani, Ferenc Deák, Xinran Liu, and Ege T. Kavalali. 2005. “An Isolated Pool of Vesicles Recycles at Rest and Drives Spontaneous Neurotransmission.” *Neuron* 45 (4): 563–73. https://doi.org/10.1016/j.neuron.2004.12.056.

Sato, Ken, and Akihiko Nakano. 2007. “Mechanisms of COPII Vesicle Formation and Protein Sorting.” *FEBS Letters* 581 (11): 2076–82. https://doi.org/10.1016/j.febslet.2007.01.091.

Scheefhals, Nicky, and Harold D. MacGillavry. 2018. “Functional Organization of Postsynaptic Glutamate Receptors.” *Molecular and Cellular Neuroscience*, Membrane Trafficking and Cytoskeletal Dynamics in Neuronal Function, 91 (September): 82–94. https://doi.org/10.1016/j.mcn.2018.05.002.

Schnell, Eric, Max Sizemore, Siavash Karimzadegan, Lu Chen, David S. Bredt, and Roger A. Nicoll. 2002. “Direct Interactions between PSD-95 and Stargazin Control Synaptic AMPA Receptor Number.” *Proceedings of the National Academy of Sciences of the United States of America* 99 (21): 13902–7. https://doi.org/10.1073/pnas.172511199.

Schüler, Thomas, Ivana Mesic, Christian Madry, Ingo Bartholomäus, and Bodo Laube. 2008a. “Formation of NR1/NR2 and NR1/NR3 Heterodimers Constitutes the Initial Step in N-Methyl-D-Aspartate Receptor Assembly.” *Journal of Biological Chemistry* 283 (1): 37–46. https://doi.org/10.1074/jbc.M703539200.

Scott, Derek B., Thomas A. Blanpied, Geoffrey T. Swanson, Chi Zhang, and Michael D. Ehlers. 2001. “An NMDA Receptor ER Retention Signal Regulated by Phosphorylation and Alternative Splicing.” *Journal of Neuroscience* 21 (9): 3063–72. https://doi.org/10.1523/JNEUROSCI.21-09-03063.2001.

Seeburg, P. H., N. Burnashev, G. Köhr, T. Kuner, R. Sprengel, and H. Monyer. 1995. “The NMDA Receptor Channel: Molecular Design of a Coincidence Detector.” *Recent Progress in Hormone Research* 50: 19–34. https://doi.org/10.1016/b978-0-12-571150-0.50006-8.

Sergey, Gorelick, Korneev Denis, Handley Ava, Gervinskas Gediminas, Oorschot Viola, Kaluza Owen L, Law Ruby H.p, et al. 2018. “Oxygen Plasma Focused Ion Beam Scanning Electron Microscopy for Biological Samples.” *BioRxiv*, October, 457820. https://doi.org/10.1101/457820.

Setou, Mitsutoshi, Dae-Hyung Seog, Yosuke Tanaka, Yoshimitsu Kanai, Yosuke Takei, Masahiko Kawagishi, and Nobutaka Hirokawa. 2002. “Glutamate-Receptor-Interacting Protein GRIP1 Directly Steers Kinesin to Dendrites.” *Nature* 417 (6884): 83–87. https://doi.org/10.1038/nature743.

Shepherd, Jason D., and Richard L. Huganir. 2007. “The Cell Biology of Synaptic Plasticity: AMPA Receptor Trafficking.” *Annual Review of Cell and Developmental Biology* 23: 613–43. https://doi.org/10.1146/annurev.cellbio.23.090506.123516.

Shi, S., Y. Hayashi, J. A. Esteban, and R. Malinow. 2001. “Subunit-Specific Rules Governing AMPA Receptor Trafficking to Synapses in Hippocampal Pyramidal Neurons.” *Cell* 105 (3): 331–43. https://doi.org/10.1016/s0092-8674(01)00321-x.

Shin, Hyewon, Michael Wyszynski, Kyung-Hye Huh, Juli G. Valtschanoff, Jae-Ran Lee, Jaewon Ko, Michel Streuli, Richard J. Weinberg, Morgan Sheng, and Eunjoon Kim. 2003a. “Association of the Kinesin Motor KIF1A with the Multimodular Protein Liprin-Alpha.” *The Journal of Biological Chemistry* 278 (13): 11393–401. https://doi.org/10.1074/jbc.M211874200.

Sinnen, Brooke L., Aaron B. Bowen, Jeffrey S. Forte, Brian G. Hiester, Kevin C. Crosby, Emily S. Gibson, Mark L. Dell’Acqua, and Matthew J. Kennedy. 2017. “Optogenetic Control of Synaptic Composition and Function.” *Neuron* 93 (3): 646-660.e5. https://doi.org/10.1016/j.neuron.2016.12.037.

Sjollema, Klaas A., Ulrike Schnell, Jeroen Kuipers, Ruby Kalicharan, and Ben N. G. Giepmans. 2012. “Correlated Light Microscopy and Electron Microscopy.” *Methods in Cell Biology* 111: 157–73. https://doi.org/10.1016/B978-0-12-416026-2.00009-1.

Sommer, Bernd, Martin Köhler, Rolf Sprengel, and Peter H. Seeburg. 1991. “RNA Editing in Brain Controls a Determinant of Ion Flow in Glutamate-Gated Channels.” *Cell* 67 (1): 11–19. https://doi.org/10.1016/0092-8674(91)90568-J.

Standley, S., K. W. Roche, J. McCallum, N. Sans, and R. J. Wenthold. 2000. “PDZ Domain Suppression of an ER Retention Signal in NMDA Receptor NR1 Splice Variants.” *Neuron* 28 (3): 887–98. https://doi.org/10.1016/s0896-6273(00)00161-6.
Start, R D, C M Layton, S S Cross, and J H Smith. 1992. “Reassessment of the Rate of Fixative Diffusion.” *Journal of Clinical Pathology* 45 (12): 1120–21.
Steinbrecht, Rudolf A., and Karl Zierold, eds. 1987. *Cryotechniques in Biological Electron Microscopy*. Berlin Heidelberg: Springer-Verlag. https://doi.org/10.1007/978-3-642-72815-0.
Stephenson, F. Anne, Sarah L. Cousins, and Anna V. Kenny. 2008. “Assembly and Forward Trafficking of NMDA Receptors (Review).” *Molecular Membrane Biology* 25 (4): 311–20. https://doi.org/10.1080/09687680801971367.
Südhof, Thomas C. 2013. “Neurotransmitter Release: The Last Millisecond in the Life of a Synaptic Vesicle.” *Neuron* 80 (3): 675–90. https://doi.org/10.1016/j.neuron.2013.10.022.
Swanwick, Catherine Croft, Marietta E. Shapiro, Zhaohong Yi, Kai Chang, and Robert J. Wenthold. 2009. “NMDA Receptors Interact with Flotillin-1 and -2, Lipid Raft-Associated Proteins.” *FEBS Letters* 583 (8): 1226–30. https://doi.org/10.1016/j.febslet.2009.03.017.
Takumi, Y., V. Ramírez-León, P. Laake, E. Rinvik, and O. P. Ottersen. 1999. “Different Modes of Expression of AMPA and NMDA Receptors in Hippocampal Synapses.” *Nature Neuroscience* 2 (7): 618–24. https://doi.org/10.1038/10172.
Tanaka, Jun-ichi, Masanori Matsuzaki, Etsuko Tarusawa, Akiko Momiyama, Elek Molnar, Haruo Kasai, and Ryuichi Shigemoto. 2005. “Number and Density of AMPA Receptors in Single Synapses in Immature Cerebellum.” *Journal of Neuroscience* 25 (4): 799–807. https://doi.org/10.1523/JNEUROSCI.4256-04.2005.
Tang, Ai-Hui, Haiwen Chen, Tuo P. Li, Sarah R. Metzbower, Harold D. MacGillavry, and Thomas A. Blanpied. 2016. “A Trans-Synaptic Nanocolumn Aligns Neurotransmitter Release to Receptors.” *Nature* 536 (7615): 210–14. https://doi.org/10.1038/nature19058.
Tang, C. M., M. Dichter, and M. Morad. 1989. “Quisqualate Activates a Rapidly Inactivating High Conductance Ionic Channel in Hippocampal Neurons.” *Science (New York, N.Y.)* 243 (4897): 1474–77. https://doi.org/10.1126/science.2467378.
Tarusawa, Etsuko, Ko Matsui, Timotheus Budisantoso, Elek Molnár, Masahiko Watanabe, Minoru Matsui, Yugo Fukazawa, and Ryuichi Shigemoto. 2009. “Input-Specific Intrasynaptic Arrangements of Ionotropic Glutamate Receptors and Their Impact on Postsynaptic Responses.” *Journal of Neuroscience* 29 (41): 12896–908. https://doi.org/10.1523/JNEUROSCI.6160-08.2009.
Tomita, Susumu, Roger A. Nicoll, and David S. Bredt. 2001. “PDZ Protein Interactions Regulating Glutamate Receptor Function and Plasticity.” *The Journal of Cell Biology* 153 (5): 19–24.
Tomita, Susumu, Valentin Stein, Tim J. Stocker, Roger A. Nicoll, and David S. Bredt. 2005. “Bidirectional Synaptic Plasticity Regulated by Phosphorylation of Stargazin-like TARPs.” *Neuron* 45 (2): 269–77. https://doi.org/10.1016/j.neuron.2005.01.009.
Tong, G., and C. E. Jahr. 1994. “Multivesicular Release from Excitatory Synapses of Cultured Hippocampal Neurons.” *Neuron* 12 (1): 51–59. https://doi.org/10.1016/0896-6273(94)90151-1.
Trussell, Laurence O., and Gerald D. Fischbach. 1989. “Glutamate Receptor Desensitization and Its Role in Synaptic Transmission.” *Neuron* 3 (2): 209–18. https://doi.org/10.1016/0896-6273(89)90034-2.
Uteshev, V V, and P S Pennefather. 1996. “A Mathematical Description of Miniature Postsynaptic Current Generation at Central Nervous System Synapses.” *Biophysical Journal* 71 (3): 1256–66.
Valtschanoff, J. G., A. Burette, M. A. Davare, A. S. Leonard, J. W. Hell, and R. J. Weinberg. 2000. “SAP97 Concentrates at the Postsynaptic Density in Cerebral Cortex.” *The*

European Journal of Neuroscience 12 (10): 3605–14. https://doi.org/10.1046/j.1460-9568.2000.00256.x.
Vargas-Caballero, Mariana, and Hugh P. C. Robinson. 2004. “Fast and Slow Voltage-Dependent Dynamics of Magnesium Block in the NMDA Receptor: The Asymmetric Trapping Block Model.” *Journal of Neuroscience* 24 (27): 6171–80. https://doi.org/10.1523/JNEUROSCI.1380-04.2004.
von Kleist, Lisa, Wiebke Stahlschmidt, Haydar Bulut, Kira Gromova, Dmytro Puchkov, Mark J. Robertson, Kylie A. MacGregor, et al. 2011. “Role of the Clathrin Terminal Domain in Regulating Coated Pit Dynamics Revealed by Small Molecule Inhibition.” *Cell* 146 (3): 471–84. https://doi.org/10.1016/j.cell.2011.06.025.
Wahl, L. M., C. Pouzat, and K. J. Stratford. 1996. “Monte Carlo Simulation of Fast Excitatory Synaptic Transmission at a Hippocampal Synapse.” *Journal of Neurophysiology* 75 (2): 597–608. https://doi.org/10.1152/jn.1996.75.2.597.
Wang, Xinxin, Leonard Benjamin Hills, and Yina Hsing Huang. 2015. “Lipid and Protein Co-Regulation of PI3K Effectors Akt and Itk in Lymphocytes.” *Frontiers in Immunology* 6. https://doi.org/10.3389/fimmu.2015.00117.
Wang, Y. T., and D. J. Linden. 2000. “Expression of Cerebellar Long-Term Depression Requires Postsynaptic Clathrin-Mediated Endocytosis.” *Neuron* 25 (3): 635–47. https://doi.org/10.1016/s0896-6273(00)81066-1.
Watanabe, Shigeki. 2016. “Flash-and-Freeze: Coordinating Optogenetic Stimulation with Rapid Freezing to Visualize Membrane Dynamics at Synapses with Millisecond Resolution.” *Frontiers in Synaptic Neuroscience* 8: 24. https://doi.org/10.3389/fnsyn.2016.00024.
Watanabe, Shigeki, Qiang Liu, M Wayne Davis, Gunther Hollopeter, Nikita Thomas, Nels B Jorgensen, and Erik M Jorgensen. 2013a. “Ultrafast Endocytosis at Caenorhabditis Elegans Neuromuscular Junctions.” Edited by Eve Marder. *ELife* 2 (September): e00723. https://doi.org/10.7554/eLife.00723.
Watanabe, Shigeki, Benjamin R. Rost, Marcial Camacho-Pérez, M. Wayne Davis, Berit Söhl-Kielczynski, Christian Rosenmund, and Erik M. Jorgensen. 2013a. “Ultrafast Endocytosis at Mouse Hippocampal Synapses.” *Nature* 504 (7479): 242–47. https://doi.org/10.1038/nature12809.
Watanabe, Shigeki, Thorsten Trimbuch, Marcial Camacho-Pérez, Benjamin R. Rost, Bettina Brokowski, Berit Söhl-Kielczynski, Annegret Felies, M. Wayne Davis, Christian Rosenmund, and Erik M. Jorgensen. 2014a. “Clathrin Regenerates Synaptic Vesicles from Endosomes.” *Nature* 515 (7526): 228–33. https://doi.org/10.1038/nature13846.
Weigert, Roberto. 2014. “Imaging the Dynamics of Endocytosis in Live Mammalian Tissues.” *Cold Spring Harbor Perspectives in Biology* 6 (4): a017012. https://doi.org/10.1101/cshperspect.a017012.
Weitzman, Matthew, and Klaus M. Hahn. 2014. “Optogenetic Approaches to Cell Migration and Beyond.” *Current Opinion in Cell Biology* 30 (October): 112–20. https://doi.org/10.1016/j.ceb.2014.08.004.
Wenzel, Eva M., Andrew Morton, Katrin Ebert, Oliver Welzel, Johannes Kornhuber, Michael A. Cousin, and Teja W. Groemer. 2012. “Key Physiological Parameters Dictate Triggering of Activity-Dependent Bulk Endocytosis in Hippocampal Synapses.” *PLOS ONE* 7 (6): e38188. https://doi.org/10.1371/journal.pone.0038188.
Williams, Megan E., Joris de Wit, and Anirvan Ghosh. 2010. “Molecular Mechanisms of Synaptic Specificity in Developing Neural Circuits.” *Neuron* 68 (1): 9–18. https://doi.org/10.1016/j.neuron.2010.09.007.
Xie, X., J. S. Liaw, M. Baudry, and T. W. Berger. 1997. “Novel Expression Mechanism for Synaptic Potentiation: Alignment of Presynaptic Release Site and Postsynaptic Receptor.” *Proceedings of the National Academy of Sciences of the United States of America* 94 (13): 6983–88. https://doi.org/10.1073/pnas.94.13.6983.

Xu-Friedman, Matthew A., and Wade G. Regehr. 2004. “Structural Contributions to Short-Term Synaptic Plasticity.” *Physiological Reviews* 84 (1): 69–85. https://doi.org/10.1152/physrev.00016.2003.

Yadav, Roopali, Shashank M. Dravid, Hongjie Yuan, and Stephen F. Traynelis. 2017. “AMPA Receptors: Molecular Biology and Pharmacology☆.” In *Reference Module in Neuroscience and Biobehavioral Psychology*. Elsevier. https://doi.org/10.1016/B978-0-12-809324-5.02325-7.

Zheng, Kaiyu, Thomas P. Jensen, Leonid P. Savtchenko, James A. Levitt, Klaus Suhling, and Dmitri A. Rusakov. 2017. “Nanoscale Diffusion in the Synaptic Cleft and beyond Measured with Time-Resolved Fluorescence Anisotropy Imaging.” *Scientific Reports* 7 (1): 42022. https://doi.org/10.1038/srep42022.